DIRECTED EVOLUTION OF PHOSPHOTRIESTERASE FOR DETOXIFICATION OF THE NERVE AGENT VX

A Dissertation

by

EMAN MOHAMED GHANEM

Submitted to the Office of Graduate Studies of
Texas A&M University
in partial fulfillment of the requirements for the degree

DOCTOR OF PHILOSOPHY

August 2006

Major Subject: Chemistry

DIRECTED EVOLUTION OF PHOSPHOTRIESTERASE FOR DETOXIFICATION OF THE NERVE AGENT VX

A Dissertation

by

EMAN MOHAMED GHANEM

Submitted to the Office of Graduate Studies of
Texas A&M University
in partial fulfillment of the requirements for the degree

DOCTOR OF PHILOSOPHY

Approved by:

Chair of Committee, Frank M. Raushel
Committee Members, Paul Fitzpatrick
Paul A. Lindahl
Marcetta Y. Darensbourg
Head of Department, Emile A. Schweikert

August 2006

Major Subject: Chemistry

ABSTRACT

Directed Evolution of Phosphotriesterase for Detoxification of the

Nerve Agent VX. (August 2006)

Eman Mohamed Ghanem, B.S., Ain Shams University; M.S., Eastern Illinois University

Chair of Advisory Committee: Dr. Frank M. Raushel

Phosphotriesterase (PTE) isolated from the soil bacterium *Flavobacterium sp*. is a member of the amidohydrolase superfamily. PTE catalyzes the hydrolysis of a broad spectrum of organophosphate triesters including the insecticide paraoxon, and the chemical warfare agents; GF, sarin, and soman. In addition, PTE has been shown to catalytically hydrolyze the lethal nerve agent, VX. However, the rate of VX hydrolysis is significantly slower. PTE was subjected to directed evolution studies to identify variants with enhanced activity towards VX hydrolysis. First generation libraries targeted amino acid residues in the substrate binding site. The H254A mutation displayed a 4-fold enhancement in k_{cat} and a 2-fold enhancement in k_{cat}/K_m over wild type PTE. The double mutant H254Q/H257F was isolated from the second generation libraries and displayed a 10-fold enhancement in k_{cat} and a 3-fold enhancement in k_{cat}/K_m. In addition, H254Q/H257F displayed a 9-fold enhancement in k_{cat}/K_m for the hydrolysis of the VX analog, demeton-S.

An *in vivo* selection approach utilizing organophosphate triesters as the sole phosphorus source is discussed. The selection is based on co-expressing PTE with the phosphodiesterase (GpdQ) from *E. aerogenes*. Substrate specificity of GpdQ was

investigated using a small library of structurally diverse organophosphate diesters and phosphonate monoesters. Results obtained from the *in vivo* growth assays showed that GpdQ enabled *E. coli* to utilize various organophosphate diesters and phosphonate monoesters as the sole phosphorus source. Cells co-expressing PTE and GpdQ were tested for their ability to utilize two different organophosphate triesters as the sole phosphorus source. The results from this experiment indicate that the growth rate is limited by the phosphotriesterase activity.

Protein translocation to the periplasm was proven advantageous for *in vivo* selection since it overcomes the limitation of intercellular delivery of the substrate of interest. Translocation of PTE to the periplasmic space of *E. coli* was examined. Two signal peptides were tested; the native leader peptide from *Flavobacterium sp.* and the signal sequence of alkaline phosphatase. The results obtained from cellular fractionation indicated that neither signal peptides were able to translocate PTE to the periplasm and that the protein remained in the cytoplasm.

ACKNOWLEDGEMENTS

I would like to thank my research advisor, Dr. Frank Raushel, for his guidance and advice throughout my graduate career. I would also like to express my appreciation to my committee members: Dr. Paul Fitzpatrick, Dr. Paul Lindahl, Dr. Marcetta Darensbourg, and former member Dr. Victoria DeRose. I thank Dr. Ryland Young and his group members for their help and advice. I would also like to thank my former advisor, Dr. Robert Standaert, for every thing that he taught me. Thanks to my family and my sincere friends for their continuous support.

TABLE OF CONTENTS

CHAPTER Page

LIST OF TABLES

TABLE Page

LIST OF FIGURES

FIGURE Page

FIGURE Page

CHAPTER I

INTRODUCTION

Organophosphate triesters have been employed in the agricultural industry as pesticides and insecticides for several decades. Approximately 60 million pounds of various organophosphates are applied annually to agriculture crops in the US. The most toxic organophosphorus compounds known are the lethal nerve agents, tabun (GA), sarin (GB), soman (GD), and VX as shown in Scheme 1.1. The toxicity of these compounds is due primarily to the practically irreversible inhibition of acetylcholine esterase (AchE), the enzyme responsible for hydrolysis of the neurotransmitter acetylcholine (Ecobichon, 2001). Enzymes that are capable of hydrolyzing and detoxifying such agents are of significant utility.

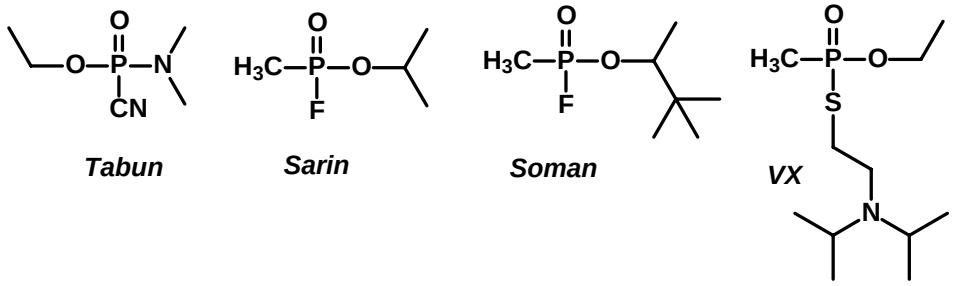

Scheme 1.1. Structure of organophosphate nerve agents

This dissertation follows the style of Toxicology and Applied Pharmacology.

Several organophosphate degrading enzymes have been isolated and characterized. The best characterized among them is the phosphotriesterase (PTE) that was initially isolated from the soil bacterium *Flavobacterium sp.* strain ATCC 27551 identified in Philippines (Raushel and Holden, 2000). The *opd* (organophosphate degrading) gene encoding the active hydrolase was located on an extrachromosomal plasmid.

The gene for the bacterial phosphotriesterase was subcloned into several expression systems, including *Escherichia coli* (Dumas et al., 1989), insect cells (Dumas et al., 1990a) and *in vitro* compartmentalization (Griffiths and Tawfik, 2003). The natural substrate for PTE remains unknown. However, the purified enzyme is capable of hydrolyzing the insecticide paraoxon at a rate that approaches the diffusion-controlled limit as presented in Scheme 2.2. The turnover number of the zinc-substituted PTE for paraoxon hydrolysis is 2100 s^{-1}, while the corresponding value for k_{cat}/K_m is 4 x 10^7 $M^{-1}s^{-1}$. Since the synthesis of paraoxon was first reported in 1950 (Schrader, 1950), it is remarkable that PTE could have evolved to such a catalytic efficiency over a relatively short period of time. PTE also possesses the ability to catalyze the hydrolysis of a wide spectrum of organophosphate insecticides including parathion, methyl-parathion, fensulfothion, among others (Dumas et al., 1989). In addition, PTE is capable of hydrolyzing the nerve agents sarin, soman, and VX, but the catalytic efficiency for these substrates are significantly lower than the less toxic insecticides (Dumas et al., 1990b; Kolakowski et al., 1997).

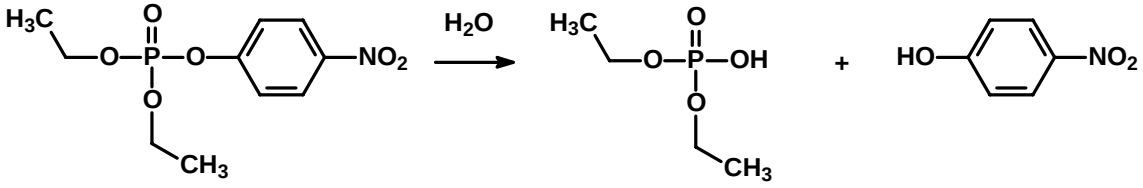

Scheme 1.2. Hydrolysis of paraoxon by PTE.

Three Dimensional Structure of Phosphotriesterase

Phosphotriesterase is a member of the amidohydrolase superfamily (Holm and Sander, 1997), which also includes urease (Jabri et al., 1995) and dihydroorotase (Thoden et al., 2001) among others. Members of this superfamily utilize one or two divalent metal ions to activate a hydrolytic water molecule for a nucleophilic attack at tetrahedral phosphorus or trigonal carbon centers. PTE is a homodimeric metalloprotein with a molecular weight of ~36 kDa/monomer (Benning et al., 1994). A high resolution X-ray structure has been solved for the bacterial PTE (Benning et al., 2001). The active site of the native enzyme contains two zinc ions per monomer. Incubation of PTE with various metal chelators such as EDTA and 1,10-phenanthroline renders the enzyme inactive (Omburo et al., 1992). The enzyme retains catalytic activity when the native Zn^{2+} is replaced by Co^{2+}, Cd^{2+}, Ni^{2+}, or Mn^{2+} (Omburo et al., 1992).

Like other members of the amidohydrolase superfamily, PTE adopts a TIM-barrel $(\alpha\beta)_8$-fold where the binuclear metal center is located at the C-terminal end of the β-barrel (Figure 1.1). The more buried metal ion in the active site, also known as the α-metal, is ligated to His-55, His-57, and Asp-301. The more solvent exposed metal ion (β-metal) is coordinated by His-201, His-230, and a water molecule. The two metal ions are bridged by the carboxylated Lys-169 and a water/hydroxide molecule, which is the apparent nucleophilic species during the hydrolysis reaction (Figure 1.2).

The X-ray structure of phosphotriesterase bound with the prochiral substrate analog, diethyl 4-methylbenzylphosphonate, revealed the presence of three subsites for substrate binding: the *small*, *large* and *leaving* group pockets accommodate the three substituents attached to the phosphorus center (Vanhooke et al., 1996). The *large* subsite contains residues His-254, His-257, Leu-271, and Met-317. The *small* binding pocket is defined by the residues, Gly-60, Leu-303, Ser-308, and Ile-106. The hydrophobic leaving group pocket contains the residues Phe-306, Phe-132, Trp-131, and Tyr-309 (Figure 1.3). It has been shown that the side chains of these twelve residues dictate the substrate and stereo-selectivity of PTE.

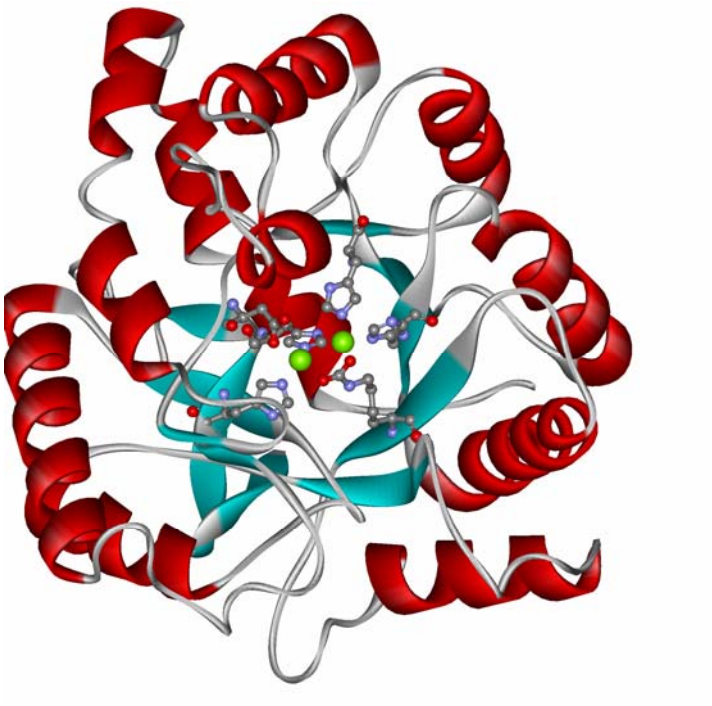

Figure 1.1. The crystal structure of phosphotriesterase featuring a TIM barrel fold. Coordinates take from PDB file 1HZY.

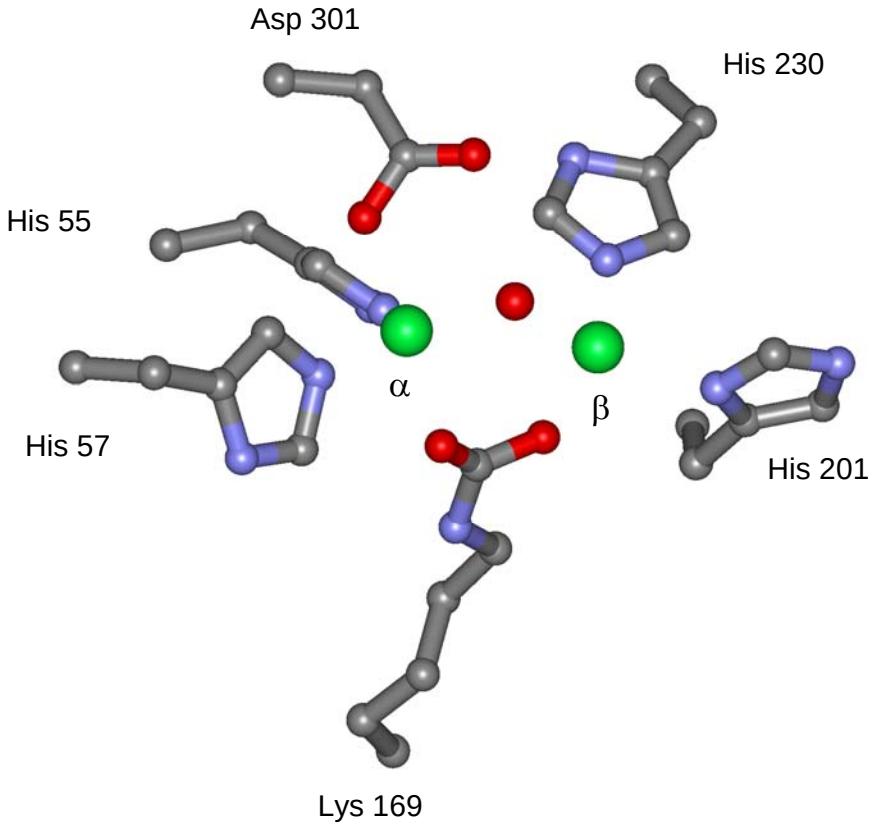

Figure 1.2. Binuclear metal center of Phosphotriesterase representing the α and β metals bridged by the catalytic solvent molecule. Coordinates taken from PDB file 1HZY.

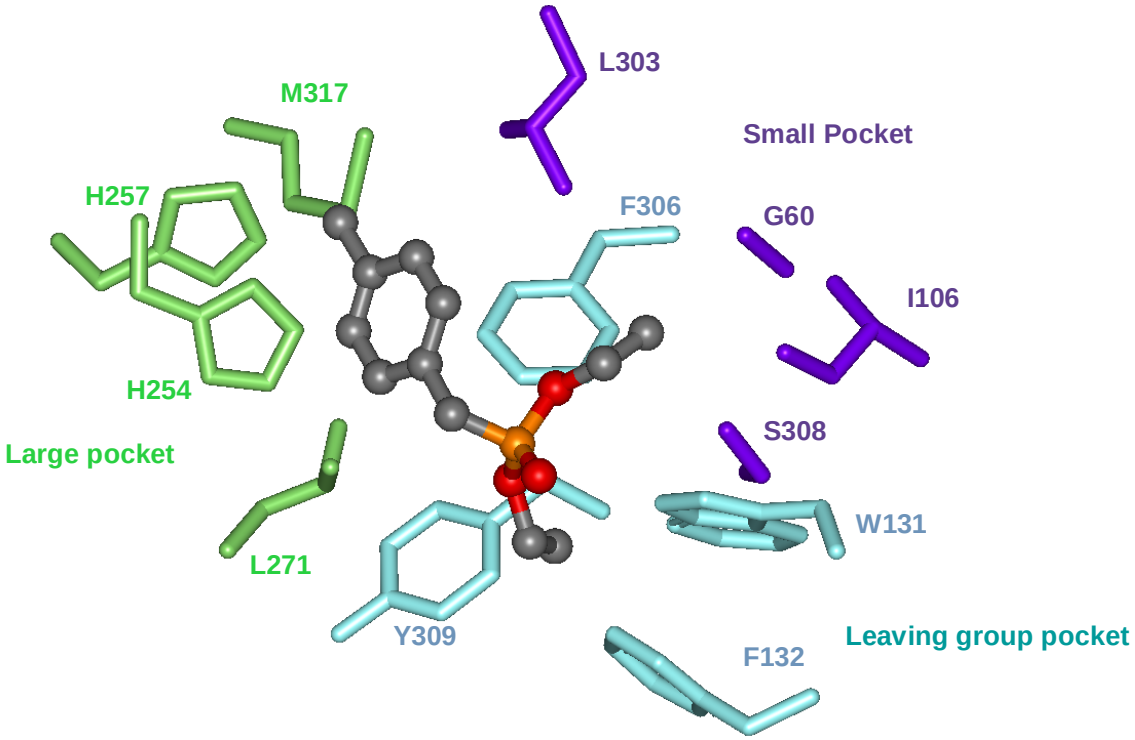

Figure 1.3. The substrate binding site of phosphotriesterase bound to the inhibitor diethyl 4-methylbenzyl phosphonate. Residues in the *small* binding pocket are Gly60, Ile106, Ser308, and Leu303. The *large* binding pocket is defined by residues His254, His257, Met317, and Leu271. Residues in the *leaving group* pocket are Phe132, Trp131, Phe306 and Tyr309. Coordinates taken from PDB file 1DPM.

Reaction Mechanism

The catalytic mechanism for the hydrolysis of organophosphate triesters has been extensively studied. The proposed mechanism of the bacterial PTE is presented in Figure 1.4. The pH-rate profiles for the hydrolysis of paraoxon indicate that a single group must be deprotonated with a pK_a of ~6.1 (Donarski et al., 1989). The ionization observed in the pH-rate profiles must be associated with the enzyme since the substrate does not ionize in this pH range. In addition, it has been demonstrated that the kinetic pK_a is dependent on the identity of the divalent cation bound to the enzyme (Aubert et al., 2004). These results are consistent with the utilization of a bridging hydroxide between the two divalent metal ions as the nucleophile during substrate turnover.

The reactivity of the bridging hydroxyl is apparently enhanced by proton transfer to Asp-301. Nucleophilic attack of the activated hydroxyl at the phosphorus center occurs with the expulsion of the leaving group. His-254 is currently believed to assist the reaction by the shuttling of the proton from Asp-301 to the bulk solvent and away from the active site (Aubert et al., 2004). Theoretical studies have suggested that Tyr-309 could stabilize the *p*-nitrophenol leaving group through a hydrogen bonding interaction (Koca et al., 2001). However, the mutation of Tyr-309 to a phenylalanine did not significantly affect the hydrolysis of organophosphate triesters by PTE and thus this potential interaction does not contribute to substrate turnover (Aubert et al., 2004).

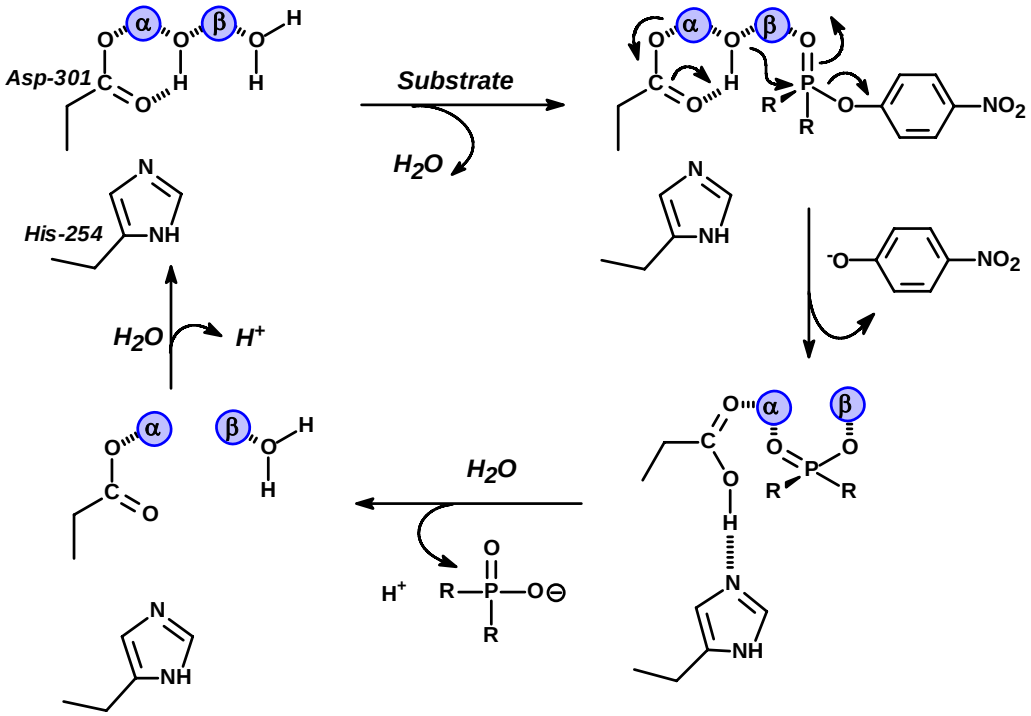

Figure 1.4. The proposed catalytic mechanism for the hydrolysis of paraoxon by bacterial phosphotriesterase.

The chiral insecticide *O*-ethyl *O*-*p*-nitrophenyl phenylphosphonothioate (EPN) was utilized to determine the net stereochemistry at the phosphorus center during organophosphate hydrolysis by PTE. It was determined that hydrolysis of the S_P-enantiomer of EPN by PTE results in the formation of the S_P-enantiomer of the corresponding thiophosphonic acid (Lewis et al., 1988). This result demonstrates that the reaction proceeds via an S_N2-like mechanism with a net inversion of stereochemistry at the phosphorus center. Therefore the reaction mechanism does not involve the formation of a phosphorylated enzyme intermediate. The X-ray structure of PTE bound to the sarin analog, diisopropyl methyl phosphonate, has provided evidence for the proposed orientation of the substrate in the active site. In this complex, the distance between the phosphoryl oxygen of the substrate and the more solvent exposed metal ion (β-metal) was 2.5 Å (Benning et al., 2000). These results support the role of the β-metal to polarize the phosphoryl oxygen bond and enhance the electrophilicity of the phosphorus center.

Substrate and Stereochemical Specificity

Although paraoxon is the best substrate known for PTE, the substrate specificity is very broad and covers a wide range of organophosphates, thiophosphates and phosphorothiolates. For substrates with different leaving groups, the catalytic efficiency and the rate limiting step are dependent on the pK_a of the leaving group (Hong and Raushel, 1996). The substrate specificity of PTE was probed using a small library of paraoxon analogs as illustrated in Scheme 1.3. All combinations of methyl, ethyl,

isopropyl and phenyl groups were substituted for the substituents **X** and **Y,** resulting in 16 potential organophosphate substrates. All of these paraoxon analogs were found to be substrates for PTE with turnover values ranging from 18,000 s^{-1} for dimethyl *p*-nitrophenyl phosphate to 220 s^{-1} for the diisopropyl *p*-nitrophenyl phosphate (Hong and Raushel, 1999a). The most interesting feature that emerged from this study was the inherent stereoselectivity of PTE. The enzyme was found to preferentially hydrolyze the S_P-enantiomer within a racemic mixture of chiral organophosphate triesters (Lewis et al., 1988; Hong and Raushel, 1999b). The stereoselectivity was more pronounced for the methyl isopropyl *p*-nitrophenyl phosphate, for which the efficiency of hydrolyzing the S_P-enantiomer was 100-fold greater than for the corresponding R_P-enantiomer (Hong and Raushel, 1999a). This catalytic property is of significant interest since the toxicity of most organophosphate nerve agents is dependent on the stereochemistry at the phosphorus center (Benschop and De Jong, 1988). From the crystal structure of PTE with a bound substrate analog, it was demonstrated that the substituents attached to the phosphorus center bind in a specific orientation within the active site, which is apparently dictated by the space available within the various subsites (Vanhooke et al., 1996). In all cases, the preferred stereoisomer is the one with the bulkier group represented by **Y** and the smaller group represented by **X**.

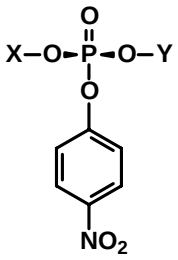

Scheme 1.3. Template used to probe the substrate specificity of PTE

When these paraoxon analogs were screened for their ability to inactivate AChE, the R_P-enantiomer was always a more potent inhibitor of AChE than the corresponding S_P-enantiomer (Hong and Raushel, 1999a; Hong and Raushel, 1999b). From a comparison of the absolute configuration of the nerve agent sarin and methyl diisopropyl *p*-nitrophenol phosphate, it was predicted that PTE would preferentially hydrolyze the less toxic R_P-enantiomer of sarin over the more toxic S_P-enantiomer. The same trend in relative stereoselectivity was obtained for the hydrolysis of chiral organophosphates with a thiolate leaving group. When a racemic mixture of the insecticide acephate was subjected to hydrolysis by PTE, the rate of hydrolysis of the S_P-enantiomer was significantly higher than the R_P-enantiomer (Chae et al., 1994). However, the overall rates of hydrolysis of the P-S bond are substantially slower than the rates reported for the cleavage of P-O and P-F bonds (Chae et al., 1994).

Inactivation of Acetylcholinesterase

Acetylcholinesterase (AChE) is a remarkably efficient serine hydrolase. It catalyzes the hydrolysis of the neurotransmitter acetylcholine (ACh) at cholinergic synapses (Figure 1.5). The hydrolysis reaction is initiated by the nucleophilic attack of Ser-200 on the carbonyl center of ACh to form an acetylated enzyme intermediate that is coupled with the release of the first product, choline. The free enzyme is regenerated by hydrolysis of the acetylated-enzyme intermediate and release of the second product, acetate. In the presence of organophosphates, the active site Ser-200 is phosphorylated to form a phosphorylated enzyme intermediate. In this case, the hydrolysis of the phosphorylated-enzyme intermediate is very slow. If AChE is not reactivated by an oxime nucleophile such as 2-PAM, the phosphorylated enzyme intermediate can undergo a base-assisted dealkylation reaction resulting in formation of "aged" AChE that is permanently inactivated (Millard et al., 1999). The half-time for aging is dependent on the nerve agent bound to the active site, pH and ionic strength (Berman and Decker, 1986).

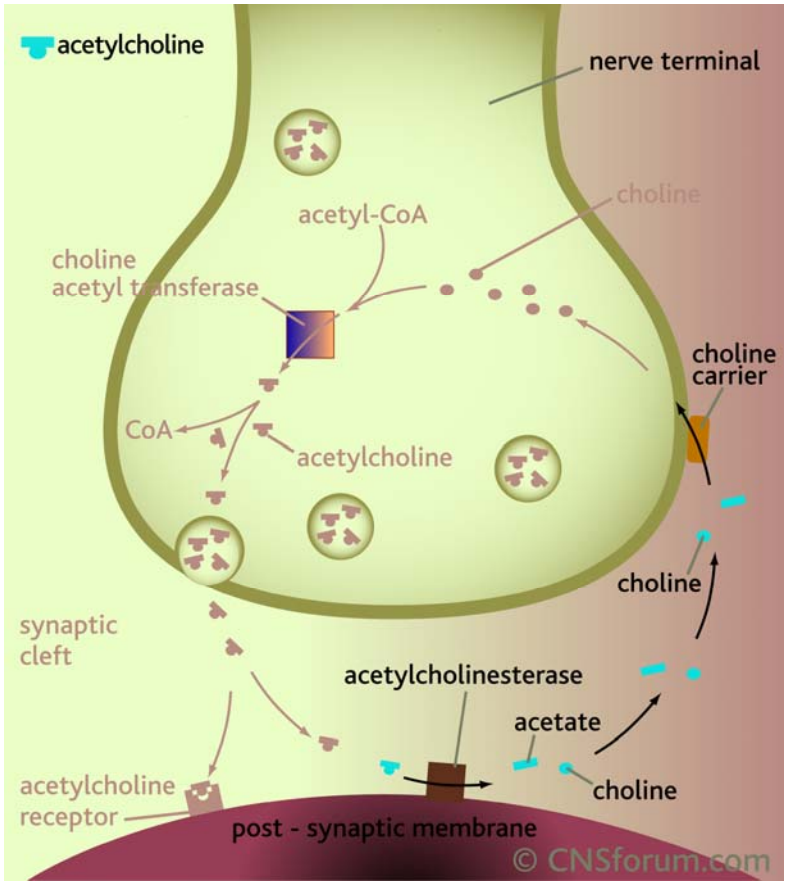

Figure 1.5. Acetylcholinesterase-catalyzed hydrolysis of acetylcholine at the cholinergic synapses. Figure is available at the CNSforum web site at the following web address (http://www.cnsforum.com/imagebank/item/rcpt_sys_ACH_esterase/default.aspx).

The toxicity of nerve agents is dependent on the stereochemistry at the phosphorus center. Since sarin and VX have a single chiral center there are two stereoisomers in the racemic mixture (see Scheme 1.4). However, in soman there is an additional stereogenic center within the pinacolyl group and thus soman consists of a mixture of four stereoisomers. Although the racemic mixture of soman is a potent inhibitor of AChE, studies with mice have indicated that the two S_P-diastereomers of soman are 100-fold more toxic than the corresponding R_P-enantiomers (Benschop et al., 1984). A similar trend has been observed for sarin and VX where the S_P-enantiomer is a more potent AChE inhibitor than the R_P-enantiomer. Table 1.1 lists the toxicity of individual isomers of sarin, soman and VX in terms of LD_{50} values and rate constants for the inhibition of AChE (Benschop and De Jong, 1988).

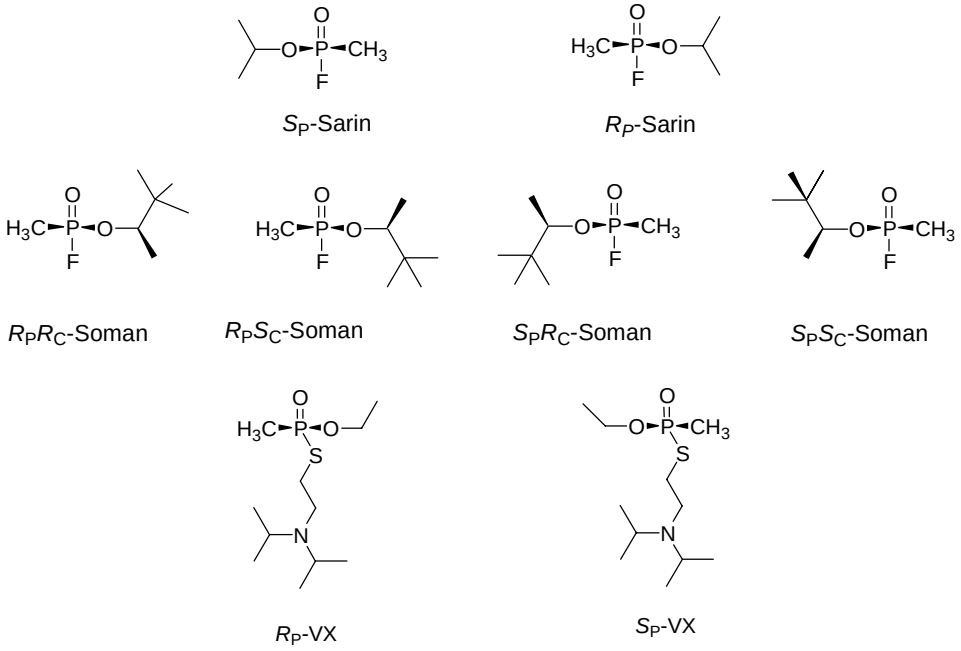

Scheme 1.4. Individual stereoisomers of the verve agents sarin, soman, and VX.

Table 1.1. Toxicity of individual stereoisomers of organophosphate nerve agents from scheme 1.4 (Benschop et al., 1988).

Nerve Agent Stereoisomer	LD_{50} (Mouse) μg/kg	Inhibition Rate Constant ($M^{-1}min^{-1}$)
R_P-sarin		$<3 \times 10^3$
S_P-sarin	41	1.4×10^7
R_PR_C-soman	>5000	$<5 \times 10^3$
R_PS_C-soman	>2000	$<5 \times 10^3$
S_PR_C-soman	99	2.8×10^8
S_PS_C-soman	38	1.8×10^8
R_P-VX	165	2×10^6
S_P-VX	12.6	4×10^8

Other Organophosphate Hydrolyzing Enzymes

Another group of enzymes involved in the detoxification of chemical warfare agents is the squid-type DFPases that have the ability to hydrolyze diisopropylfluorophosphate (DFP), sarin, soman, tabun, but not VX. The crystal structure of the DFPase from *Loligo vulgaris* shows that the protein exists as a monomer and adopts a 6-fold β-propeller-like motif (Scharff et al., 2001). DFPase contains high and low affinity Ca^{2+} binding sites that have been suggested to be involved in the hydrolytic reaction. DFPase is very efficient for the detoxification of DFP with a k_{cat}/K_m value of 1.3×10^6 $M^{-1}s^{-1}$ (Hartleib and Rüterjans, 2001).

An organophosphorus acid anhydrolase (OpaA) from *Alteromonas* sp. JD6.5 was cloned and sequenced at the Edgewood Research, Development, and Engineering Center (Cheng et al., 1996). The natural function of OpaA has been proposed to be a dipeptidase that catalyzes the hydrolysis of dipeptides with a proline residue at the C-terminus (Cheng et al., 1996). OpaA also displays catalytic activity with organophosphate triesters including the nerve agents sarin and soman. Unlike PTE, OpaA is unable to hydrolyze the nerve agent VX (Cheng et al., 1999). The stereoselectivity of OpaA was surveyed with the same library of paraoxon analogs that has been used for PTE. Like PTE, OpaA preferentially hydrolyzes the S_P-enantiomers of the organophosphate triesters shown in Scheme 1.3**,** although the overall catalytic efficiency is significantly lower than for PTE (Hill et al., 2000). Similarly, OpaA displays a stereoselective preference toward the hydrolysis of the least toxic R_P-enantiomers of sarin and soman analogs (Hill et al., 2001).

Another prolidase that was identified as an enzyme capable of degrading organophosphates is the *E. coli* aminopeptidase P (PepP). PepP is a metalloprotein that requires two Mn^{2+} cations for catalysis. The enzyme functions as a tetramer that adopts a "pita-bread" fold similar to methionine aminopeptidase and creatinase (Wilce et al., 1998). The ability of PepP to hydrolyze organophosphate triesters was probed with a small library of racemic paraoxon analogs. The highest rates were observed for the substrates containing the substituents methyl-isopropyl and methyl-isobutyl (Jao et al., 2004).

PTE-Catalyzed Detoxification of Organophosphorus Compounds

Currently, decontamination of organophosphates relies on bleach treatment, alkaline hydrolysis, or incineration. In all cases, the conditions are harsh and the byproducts can be toxic. Therefore, efforts have been directed toward enzyme-catalyzed decontamination and bioremediation. The use of bio-scavengers, such as the exogenous administration of acetyl cholinesterase (Saxena et al., 1997) or human butyryl cholinesterase (Raveh, et al., 1997) has proven affective for protection against organophosphate poisoning. These reagents exert their function by binding to the nerve agents and preventing them from reaching their target. The disadvantage associated with this approach is the large amount of scavenger required for optimum protection, since these enzymes have a binding stoichiometry of unity. Therefore, attention has been drawn to enzymes that can catalytically hydrolyze organophosphate nerve agents.

Due to a broad substrate specificity and stereoselectivity, PTE is a promising candidate for *in vivo* and *in vitro* detoxification of organophosphate nerve agents. Animal studies in mice showed that intravenous injection with 1.5 IU (paraoxonase activity of 1.5 μmol/min) of PTE before or immediately after the administration of paraoxon protected brain AChE activity against inhibition by paraoxon (Kaliste-Korhonen et al., 1993). When PTE was injected 10 minutes before administration of paraoxon, the concentration required to decrease the activity of brain AChE to 40% of the control was increased from 0.5 mg paraoxon/Kg to 20 mg paraoxon/Kg (Kaliste-Korhonen et al., 1993).

The slower rates of sarin, soman, and DFP hydrolysis by PTE were reflected in the *in vivo* study. In the case of DFP exposure, PTE treatment protected slightly the activity of brain AChE, but not the serum AChE (Tuovinen et al., 1994). However, when the two Zn^{2+} ions in the binuclear metal center were replaced by Co^{2+}, the protection of AChE against DFP inhibition was enhanced (Tuovinen et al., 1996a). The total plasma paraoxon hydrolyzing activity for the Co^{2+}-reconstituted PTE was approximately 10-fold higher than the Zn^{2+}-enzyme. The intravenous injection of 6.9 μg PTE/g 10 minutes after exposure to 1.8 mg DFP/kg retained AChE activity of 90% of the control for up to 6 hours, which was better than the protection effect of the carbamate, eptastigmine (Tuovinen et al., 1996b). If the same dose of PTE was injected 30 minutes after exposure, the protection of AChE dropped to 40% after 6 hours and 15% after 24 hours (Tuovinen et al., 1996c). These data are similar to the protection

rates obtained for eptastigmine. Therefore, it was concluded that PTE treatment is much more effective during the first few minutes after exposure.

PTE pretreatment did not significantly protect brain or serum AChE against sarin or soman toxicity (Tuovinen et al., 1994). However, it increased the sarin dose required to induce inactivation of AChE. A relatively high dose of PTE (104 U/g body weight) increased the LD_{50} of sarin toxicity from 1.4 mg/kg to 4.7 mg/kg (Tuovinen et al., 1999). When the same dose of PTE was combined with 0.09 mg/kg body weight of the carbamate, physositigmine, the LD_{50} was further increased to 6.0 mg/kg (Tuovinen et al., 1999). When PTE was incubated *in vitro* with mouse serum that was treated with paraoxon, the AChE activity was recovered from 25-31% to 76-100 % of control activity in 24 hours (Tuovinen et al., 1994). The overall results from animal studies indicated that PTE-pretreated animals can tolerate 50-fold higher doses of paraoxon than the untreated animals.

The biological distribution of PTE using [^{125}I] labeling indicated that the enzyme was found in the liver, kidney, and lungs, but not in the nervous system. This suggests that PTE hydrolyzes organophosphates in circulation before reaching the nervous system (Tuovinen et al., 1996a). The *in vivo* therapeutic application of PTE is restricted by its half-life in plasma, which was reported to be approximately 5 hours (Tuovinen et al., 1996a). To overcome this limitation, attempts have been made to encapsulate PTE in biodegradable carriers. PTE was successfully encapsulated within murine erythrocytes by hypotonic dialysis (Pei et al., 1994) and within sterically stable liposomes (Petrikovics et al., 1999) to antagonize paraoxon toxicity.

Altering Substrate Specificity and Directed Evolution of PTE

PTE has been subjected to several rational design and directed evolution studies to optimize the active site for enhanced detoxification of organophosphates and the related organophosphonate nerve agents. The stereo-specificity displayed by PTE initiated a series of investigations to reshape the substrate binding site by utilizing site directed mutagenesis for *enhanced*, *relaxed* or *reversed* stereoselectivity. The first set of experiments was based on the mutation of all residues that define the hydrophobic substrate binding site to alanine, and a subsequent investigation of the impact of these alterations on the stereoselectivity of PTE. For the residue Gly-60, which is located in the *small* binding pocket, mutation to alanine significantly *enhanced* the substrate stereoselectivity (Chen-Goodspeed et al., 2001a). For example, the ratio for hydrolysis of the chiral methyl phenyl *p*-nitrophenyl phosphate by wild type PTE is 90 in favor of the S_P-enantiomer over the R_P-enantiomer (Hong and Raushel, 1999a). The G60A mutant of PTE displayed a 100-fold reduction in k_{cat}/K_m for the R_P-enantiomer and therefore, the ratio of stereoselectivity was *enhanced* to 13,000 in favor of the S_P-enantiomer (Chen-Goodspeed et al., 2001a). Mutations of the *large* subsite residues, His-245, His-257, Leu-271 and Met-317 to alanine had no impact on the stereospecificity. These data suggest that the substrate specificity is mainly dictated by the steric constraints within the *small* binding pocket (Chen-Goodspeed et al., 2001a).

These studies were further extended to include other mutations that can reconstruct the active site of PTE. The mutation I106G in the *small* subsite *relaxed* the stereoselectivity for hydrolysis of chiral methyl phenyl *p*-nitrophenyl phosphate from

90:1 to 1.7:1 (Chen-Goodspeed, et al., 2001b). This result was achieved by increasing the k_{cat}/K_m for the hydrolysis of the R_P-enantiomer 100-fold over the wild type enzyme. The stereoselectivity was *reversed* by simultaneously enlarging the *small* subsite and shrinking the *large* subsite. While the wild type enzyme prefers the S_P-enantiomer of methyl phenyl *p*-nitrophenyl phosphate by a factor of 90, the mutant I106G/F132G/H257Y/S308G prefers the R_P-enantiomer by a factor of 190. The same mutant displays a preference for the R_P-enantiomer of chiral ethyl phenyl *p*-nitrophenyl phosphate over the S_P-enantiomer with a ratio of 80:1 (Chen-Goodspeed, et al., 2001b). A novel application based on these findings was to utilize PTE variants with enhanced and reversed stereospecificity for efficient synthesis of chiral organophosphate triesters. The mutants G60A and I106A/F132A/H257Y were successfully used to kinetically resolve racemic mixtures of chiral paraoxon analogs with an enantiomeric excess of approximately 95-99 % (Wu et al., 2000).

PTE is of interest owing to its ability to catalytically hydrolyze the nerve agents sarin, soman and VX. Since these agents are not readily available for research use, analogs have been synthesized to help screen for optimized variants of PTE toward the detoxification of organophosphonates (Figure 1.6). For sarin and soman, chromogenic analogs were obtained by substituting the fluoride leaving group with a *p*-nitrophenyl group. For VX, prochiral analogs were synthesized with slight modifications in the thiolate leaving group. The toxicity of these analogs was assessed in terms of minimum effective concentration (MEC) using a simple and cost efficient bioassay in *Hydra attenuata* (Lum et al., 2003). The individual toxicity of sarin, soman and VX was

reflected in the toxicity of their analogs with two of the VX analogs being the most toxic (Table 1.2). For the chiral sarin analogs, the S_P-enantiomer was approximately 4 orders of magnitude more toxic than the R_P-enantiomer (Lum et al., 2003).

Very promising and interesting results were obtained when the chiral sarin and soman analogs were used to evaluate the potential of PTE for stereoselective detoxification of nerve agents. As expected from previous stereoselectivity profiles, wild type PTE preferentially hydrolyzes the least toxic R_P-enantiomer of the sarin analog 10-fold better than the more toxic S_P-enantiomer. This preference was reversed by the mutant I106A/F132A/H257Y, which showed an enhanced rate of hydrolysis of the S_P-enantiomer by a factor of 30 (Li et al., 2001). A similar trend was observed for the soman analogs. These data clearly demonstrate that the active site of PTE can be manipulated for optimum decontamination and decomposition of the neurotoxins, sarin and soman.

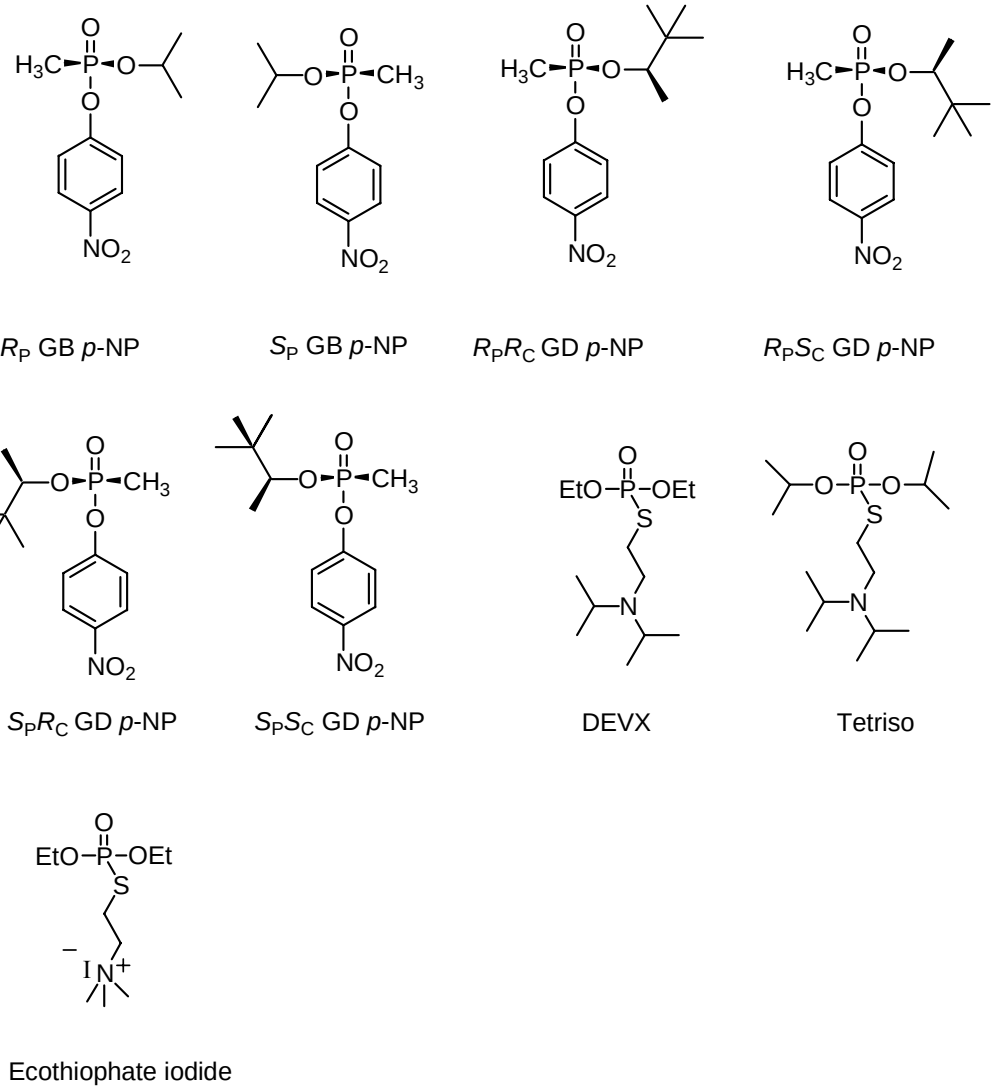

Figure 1.6. Structures of synthetic analogs of the nerve agents sarin, soman, and VX.

Table 1.2. Toxicity of organophosphate analogs that appear in Figure 1.6 (Lum, et al., 2003).

Compound	MEC $_{92th}$ (mg/L)
p-nitrophenol	9.4×10^{1}
paraoxon	2.5×10^{1}
(Rp)-GB *p*-NP	1.0×10^{2}
(Rp/Sp)-GB *p*-NP	2.0×10^{-2}
(Sp)-GB *p*-NP	1.3×10^{-2}
(RpRc/RpSc/SpRc/SpSc)-GD *p*-NP	2.5×10^{-4}
(SpRc/SpSc)-GD *p*-NP	2.0×10^{-4}
(SpSc)-GD *p*-NP	8.5×10^{-5}
Ecothiophate iodide	1.0×10^{-4}
Diethyl VX	3.0×10^{-6}
Tetriso	3.1×10^{-6}

A semi-rational approach was taken to expand the search for PTE mutants with enhanced activity for the hydrolysis of chemical warfare agents. The active site residues were randomly mutated by saturation mutagenesis and variants were screened using a crude cell assay. Screening with the most toxic *p*-nitrophenyl soman analog resulted in the isolation and identification of the mutant H254G/H257W/L303T which has a rate enhancement of approximately 3 orders of magnitude over the wild type enzyme (Hill et al., 2003). It was noted from the mutagenesis experiments on PTE that the large subsite residue, His-257, is significant for modifying the substrate specificity. Another PTE homolog (opdA) was recently isolated from *Agrobacterium radiobacter* P 230 (Horne et al., 2002) that shares a 90% sequence identity with PTE from *P. diminuta.* The major difference between PTE and *opd*A is the presence of Arg and Tyr at positions 254 and 257 respectively instead of His in PTE. In a directed evolution study, the *opd* gene was shuffled in a search for enhanced variants for methyl parathion hydrolysis. The mutation H257Y was found in all isolates that displayed higher activities (Cho et al., 2002). The highest activity was obtained by introducing 7 different mutations, with only the mutation H257Y located in the active site. The large subsite was target for a rational design experiment that led to the identification of the mutant H254R/H257L, which had 20-fold enhancement over wild type for the VX analog demeton-S (Di Sioudi et al., 1999).

Potential Applications

The current methods for the detoxification of organophosphorus compounds are harmful and possess serious environmental consequences. Therefore, utilizing enzymes for the detection and decontamination of organophosphate agents has received considerable attention. PTE has been recognized as a potential candidate for extending the process of organophosphate detoxification. The insecticides paraoxon and parathion were successfully hydrolyzed by PTE that was immobilized on a trityl agarose matrix (Caldwell and Raushel, 1991a). The immobilization resulted in a relative increase in the stability of PTE and the maximum efficiency of the system was about 40%, relative to the free enzyme. The immobilized enzyme exhibited a similar kinetic profile to the free enzyme with a 3-fold higher K_m for paraoxon (Caldwell and Raushel, 1991a). Since immobilization of PTE on trityl agarose was based on hydrophobic interactions, the use of organic solvents to solubilize the pesticides was problematic and weakened the interaction between the enzyme and the solid support. This limitation was overcome by covalently immobilizing PTE on nylon tubing, powder, and membranes (Caldwell and Raushel, 1991b). In this case, methanol was used as a solvent at a concentration up to 40% with no adverse effect on the activity of PTE, which allowed hydrolysis of very high substrate concentrations. The amount of PTE immobilized was dependent on the surface area of the membrane and was limited to 390 U for a 48 cm^2 nylon 66 membrane. This amount was significantly increased to 9000 units for a 2000 cm^2 nylon 6 membrane. The catalytic efficiency of the 11 U nylon 66 membrane reactor in the presence of 0%, 10%, and 40% methanol were reduced to 4% of the soluble enzyme

activity under the same reaction conditions (Caldwell and Raushel, 1991b). This low efficiency could be attributed to the internal diffusional effect since hydrolysis of paraoxon by soluble PTE achieves the diffusion control limits. PTE immobilized on nylon powder (240 U/ 750 mg nylon 11 powder), was stable for as long as 20 months at 5 °C. A reactor of 900 PTE units immobilized onto 2.5 g of the nylon 11 powder could hydrolyze 18.3 mM paraoxon in 30% methanol at a rate of 76 μmol/min (Caldwell and Raushel, 1991b).

Another study to develop a delivery method for use of PTE in the decontamination of organophosphates involved incorporating PTE within fire fighting foams. Foams containing PTE displayed high capacity for surface decontamination. A 1.2 cm foam height containing 11.4 nM PTE could detoxify a surface contaminated with 1.15 μmol paraoxon/cm^2 with 43% conversion (LeJeune and Russell, 1999). When the foam height was increased to 3.0 cm, the conversion was enhanced to 70%. To test the ability of PTE foams to decontaminate soil, two sand columns were contaminated with 2.3 μmol/g paraoxon. While soluble PTE was applied to one column, an equal amount of enzyme activity was immobilized onto the foam and applied to the second column. By analyzing the products, it was determined that the column treated with the PTE foam had a 85% conversion in 1 hour, while the column treated with soluble PTE displayed less than 50% conversion (LeJeune and Russell, 1999). In addition, nanocomposites of PTE adsorbed on isocyanatopropyl-silica and poly hydroxymethylsiloxane (PHOMS) were shown to be effective in detoxifying liquid and gas phase organophosphates (Gill and Ballesteros, 2000).

The extensive use of organophosphates necessitated the need to develop devices for early detection and quantification of organophosphates in contaminated areas. AChE inhibition based biosensors have been used to monitor organophosphate exposure. Although, AChE-biosensors are very sensitive, they are not selective since AChE is inhibited by a wide range of compounds including carbamates. In addition, AChE sensors are based on very complicated procedures and cannot be regenerated because of irreversible inhibition. PTE-based devices were developed based on the products of the hydrolysis reaction. For example, the hydrolysis of paraoxon by PTE releases two protons and a chromophoric leaving group, which can be utilized for the design of potentiometric and optical biosensors, respectively. To develop a PTE based potentiometric biosensor, a pH glass electrode was modified by immobilizing purified PTE. Concentrations of paraoxon, parathion, and methyl parathion as low as 2 μM were detected using a 500-unit PTE electrode (Mulchandani et al., 1999a). Based on the same principle, a PTE potentiometric biosensor was developed by immobilizing recombinant *E. coli* cells harboring the *opd* gene instead of purified protein (Rainina et al., 1996). A fluorescent biosensor was developed based on the change of pH resulting from hydrolysis of organophosphates by using fluorescein isothiocyanate (FITC) modified PTE. The FITC-PTE was adsorbed on polymethyl methacrylate beads, and the decrease in the fluorescent intensity of FITC was measured as the enzymatic hydrolysis proceeds (Roger et al., 1999). A broad scope of organophosphates could be detected by this methodology including parathion, diazinon, methylparathion and coumaphos.

A fiber-optic enzyme biosensor (FOEB) of PTE was designed based on the reaction products that can be detected spectrophotometrically. The biosensor contained a monochromator with a wavelength cutoff of 400 nm (for the *p*-nitrophenol leaving group of paraoxon and parathion) and a cutoff of 348 nm for the hydrolysis product of coumaphos (Mulchandani et al., 1999b). PTE was immobilized by covalent cross-linking with glutaraldehyde on a 0.45 μm pore size nylon membrane. The detection limit for this FOEB was 2 μM paraoxon, which is comparable to the potentiometeric biosensors.

Despite their great potential, the detection limit of PTE biosensors was much higher than the AChE-based devices. An amperometric biosensor was developed based on electrochemical oxidation of the *p*-nitrophenol (*p*NP) released from PTE-catalyzed hydrolysis (Mulchandani et al., 1999c). The electrode was composed of purified PTE immobilized onto a printed carbon surface. The oxidation current was directly proportional to the level of *p*NP released. Unlike the potentiometric and optical biosensors, the detection limits for this device were significantly low, 0.7 nM and 0.9 nM for methyl parathion and paraoxon respectively (Mulchandani et al., 1999c). The same principle was applied to develop a microbial amperometric biosensor based on the immobilization of whole cells expressing PTE anchored to the outer membrane by fusion to the ice nucleation protein from *Pseudomonas syringae* (Mulchandani et al., 2001). It was determined that the microbial biosensor offered sufficient selectivity and that other cellular or environmental chemicals did not interfere with the sensor detection.

This technology provides a cost efficient, simple, reliable and rapid detection of organophosphate pesticides and nerve agents.

CHAPTER II

EVOLUTION OF PHOSPHOTRIESTERASE FOR EFFICIENT DETOXIFICATION OF THE NERVE AGENT VX

Introduction

Historical Background

Among the known lethal chemical warfare agents, the V-type agents are the most toxic nerve agents known. Their discovery started in the 1950's when Dr. Ranajit Ghosh, a chemist at the Plant Protection Laboratories of the British firm Imperial Chemical Industries (ICI), was investigating a class of organophosphate compounds (organophosphate esters of substituted aminoethanethiols) as potential agricultural pesticides. In 1954, the ICI released the compound Amiton® (**1** in Scheme 2.1) to the market as an effective pesticide. Amiton, also known as VG, was shortly withdrawn after its release for its extreme toxicity. Consequently, the CW British facility at Porton Down adopted the technology and started producing the new class of nerve agent, V-class, for military use. The best known agent in this class is VX (**2**). When the Russians took on the synthesis of V-agents, they synthesized a derivative of VX and called it Russian-VX (RVX), also known as V-gas (**3**). The US started producing and stockpiling VX in 1961 (Organization for the Prohibition of Chemical Weapons, OPCW).

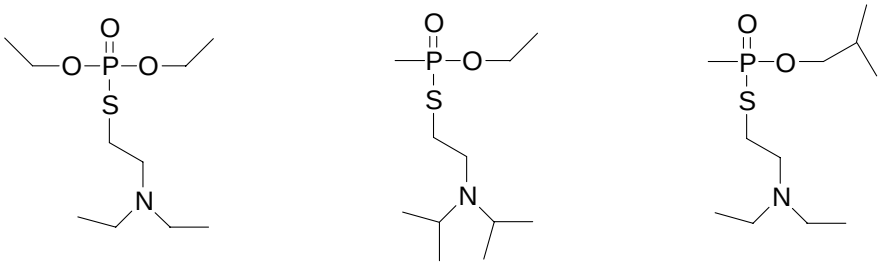

Amiton (1) VX (2) Russian-VX (3)

Scheme 2.1. Chemical Structures of the V-series nerve agents.

The V-series agents are known to be more lethal and persistent than the G-class agents (sarin and soman). However, the irreversible inhibition of acetylcholinesterase (aging) caused by VX occurs with a significantly longer half-life of approximately 2 days compared to a half-life of 1-10 minutes in case of soman. Due to the serious environmental and health risks associated with organophosphates, efforts have been devoted to the biodegradation and bioremediation of this series of compounds.

Among enzymes that catalytically hydrolyze organophosphate triesters, the phosphotriesterase from *Flavobacterium sp.* (PTE) is the only enzyme known to catalyze the hydrolysis of organophosphono thiolates such as the lethal nerve agents VX and R-VX (Kolakowski et al., 1997). However, the catalytic efficiency is significantly lower. For example, the k_{cat}/K_m values for paraoxon and VX hydrolysis by PTE are 6×10^6 $M^{-1}s^{-1}$ and 45 $M^{-1}s^{-1}$, respectively.

Protein Engineering

Protein engineering has been widely used to create novel enzymes with enhanced activity, stability and/or substrate specificity. Two approaches are currently available; rational design, and directed evolution. Rational design involves precise changes in the amino acid sequence using site directed mutagenesis (SDM). This technique is mainly based on a good understanding of protein structure, function, and mechanism. Unlike rational design, directed evolution does not require detailed knowledge of the protein structure. Molecular diversity is achieved by multiple rounds of random mutagenesis or recombination of a target gene followed by screening or selection for desired variants. Error-prone PCR (ep-PCR), DNA shuffling, saturation mutagenesis, and *E.coli* mutator strains are among the different strategies for *in vitro* evolution.

EP-PCR reaction utilizes an "error-prone" DNA polymerase. *Taq* polymerase is the most commonly used enzyme for this purpose. In addition, the reaction mixture contains manganese chloride instead of magnesium chloride (Cadwell et al., 1992). Manganese chloride was shown to have a significant mutagenic effect on several polymerases (Beckman et al., 1985). The overall error rate is 1-2 base substitutions for each generation. EP-PCR was successfully combined with saturation mutagenesis to evolve a bacterial lipase from *P. aeruginosa*. Six rounds of random mutagenesis resulted in an enzyme with a 25-fold enhancement in enantioselectivity over wild type (Liebeton et al., 2000).

DNA shuffling as a technique for *in vitro* evolution via gene reassembly was developed by W. P. Stemmer in Maxygen, Inc. (Stemmer, 1994). In this method, a

population of genes containing beneficial mutations are randomly digested by DNase I into a pool of 10-50 nucleotide fragments. The fragments then are self-primed, based on homology, using PCR. Not only does DNA shuffling accelerate the process of molecular breeding, it also provides a very flexible technique that can be applied for a single gene shuffling (Stemmer, 1994), homologous genes shuffling, "family shuffling" (Crameri et al., 1998), or whole-genome shuffling (Zhang et al., 2002).

In this chapter, PTE is subjected to directed evolution experiments by employing the semi-rational design approach in an attempt to engineer the substrate binding site for enhanced degradation of synthetic analogs of the nerve agent VX (Scheme 2.2). Since the Amiton analog, diisopropyl amiton (DEVX **4**) is more structurally related to the nerve agent VX, this investigation will be more focused on the hydrolysis of this substrate.

Diisopropyl amiton (DEVX)
(4)

Demeton-S
(5)

Scheme 2.2. The structures of VX analogs used in this study.

Materials and Methods

Materials

QuickChange® site directed mutagenesis kit was purchased from Stratagene. *E. coli* BL21-DEIII, XL1-Blue cells and the Bugbuster cell lysis reagent were purchased

from Novagen. Wizard-Plus SV miniprep DNA Purification System was obtained from Promega. All restriction enzymes and T4 DNA ligase were obtained from New England Biolabs. Demeton-S was purchased from Chem. Service. The VX analog, diisopropyl amiton (DEVX) was synthesized in our laboratory by Dr. Yingchun Li. The medium copy number expression vector, pZA32-luc (Figure 2.1), was a gift from Dr. Ryland Young, Department of Biochemistry & Biophysics. Oligonucleotides were synthesized by the Integrated DNA Technologies (IDT). DNA sequencing was performed in the Gene Technologies Lab. (GTL), Texas A&M University. All other materials were purchased from Sigma.

Construction of Single Substitution Libraries

The plasmid, pJames, served as the template for constructing the single substitution libraries. Twelve libraries targeting amino acid residues that define the substrate binding site of PTE were created using the Quick Change site directed mutagenesis technique. Oligonucleotides containing the degenerate codon NNS at a specific site were used to eliminate two stop codons, TGA and TAA. PCR products were transformed in *E. coli* XL1-blue electro-competent cells for DNA sequencing. Colony forming units (CFU's) obtained from each library were sequenced until all mutagenesis possibilities were identified for each position, resulting in a combinatorial library of 228 plasmids in addition to wild type.

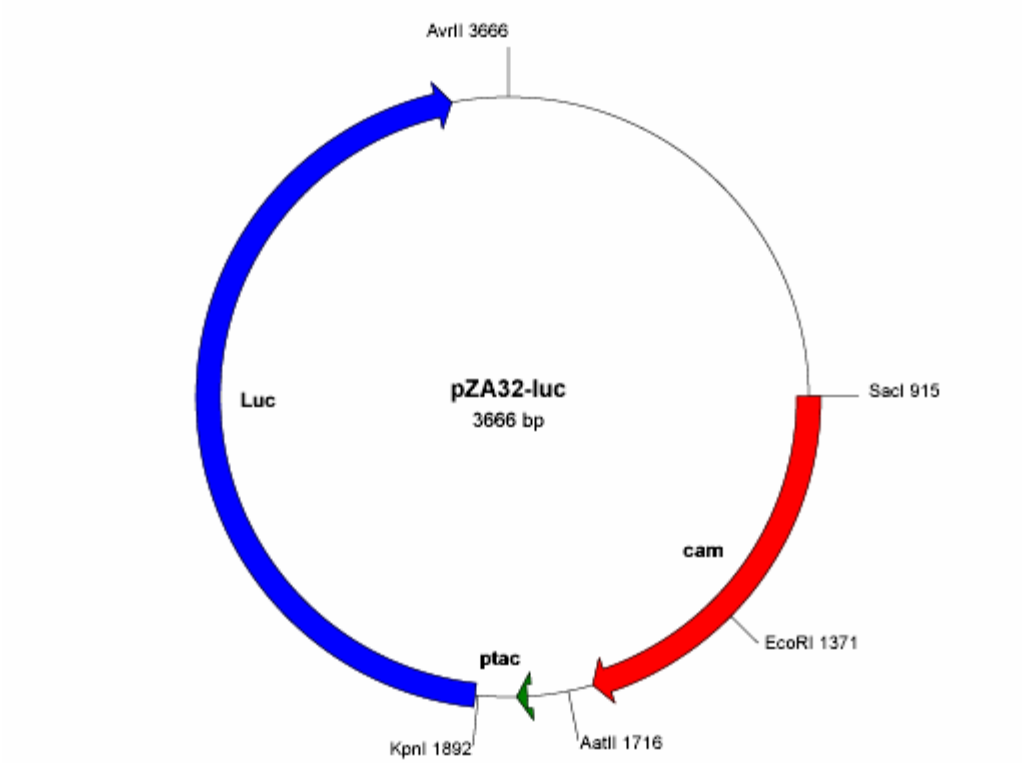

Figure 2.1. A map of the pZA32-Luc plasmid showing the chloramphenicol resistance gene and the *ptac* promoter. The *opd* gene was inserted between the *KpnI* and *AvrII* restriction sites.

Construction of Third Generation Libraries in the H254Q/H257F Template

Libraries in the H254Q/H257F parent were constructed as described above. Due to the inconsistency in protein expression associated with the high copy number pBS(+) vector, the plasmid pZA32-QF served as the template for the subsequent libraries. To construct pZA32-QF, the *opd* gene was amplified from the plasmid pJK01 using the primers pJK01-5'-*Kpn I*, 5'-CGCGCCGGGTACCATGTCGATCGGCACAGGCGATCGG, and pJK01-3'-*Avr II*, 5'- CCGGGTACCCCTAGGTCATCATCATGACGCCCGCAAGGTC. The 1000 bp PCR product was purified, digested with *Kpn I* and *Avr II* and ligated in the chloramphenicol resistant plasmid pZA32-Luc resulting in the construct pZA32-opd. The double mutation H254Q/H257F was constructed in pZA32-opd using Quick Change mutagenesis resulting in the construct PZA32-QF, which was utilized to randomize the remaining 10 residues in the substrate binding pocket of PTE.

Kinetics Measurements

All kinetic measurements and screening were performed on a SPECTRAmax-340 plate reader (Molecular Devices Inc, Sunnyvale CA). For the paraoxon assays, release of *p*-nitrophenol (ε_{400} = 17,000 $M^{-1}cm^{-1}$) was monitored at pH 9.0. For the VX analogs, the DTNB reaction (Ellman Assay) was utilized, and the formation of the thiol anion (ε_{412} = 14,150 $M^{-1}cm^{-1}$) was monitored at pH 8.0 (Scheme 2.3).

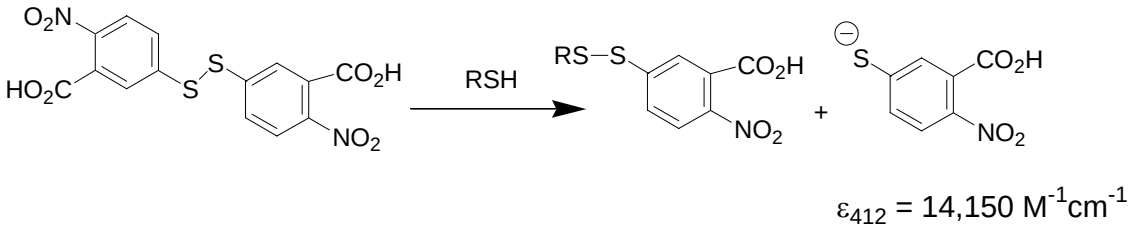

Scheme 2.3. Detection of free thiols using the DTNB reagent.

Kinetic parameters were obtained by fitting the data to equation 1 where *v* is the initial velocity, V_{max} is the maximal velocity, S is substrate concentration, and K_m is the Michaelis constant.

$$v = V_{max}\,[S]/K_m + [S] \qquad (1)$$

Growth Conditions

Single colonies obtained from transforming the mutagenesis product were inoculated in 96-deep well growth blocks containing 0.75 mL super broth (SB) supplemented with 0.5 mM $CoCl_2$, and 0.1 mg/mL ampicillin or 25μg/mL chloramphenicol. The culture blocks were incubated for 30-36 hours at 30 °C, shaking at 250 rpm. In the case of single substitution libraries, each block contained two copies of each variant and controls, therefore, 12 libraries were grown in a total of 6 growth blocks. In addition to PTE variants, each block included a set of standards with known catalytic parameters. Standards used are wild type, H254A, H254Q/H257F, I106A/F132A/H257Y (AAY), H254G/H257W/L303T (GWT), and BL21-DEIII cells.

Screening

The culture was diluted 10-fold with MQ water and cell density was measured spectrophotometrically at 600 nm. The OD_{600} for 10-fold diluted culture ranged from 0.5-0.7. The paraoxon screen contained 10 μL diluted culture, 0.1 mM substrate, 50 mM CHES buffer, pH 9.0, and 2.0 % (v/v) Bugbuster. The release of *p*-nitrophenol was monitored spectrophotometrically at 25 °C. The final conditions for the DEVX (**4**) screen were 50 μL diluted culture, 0.2 mM substrate, 50 mM HEPES buffer, pH 8.0, 0.3 mM DTNB, and 2 % (v/v) Bugbuster. Release of the thiolate anion is monitored spectrophotometrically at 412 nm. Since the rate of DEVX hydrolysis is very slow compared to paraoxon, the results from the DEVX screens are recorded in an end point format. The initial OD_{412} was subtracted from final OD_{412} after six-hour incubation at 25 °C. In all crude screens, rates were normalized to cell density.

Protein Purification

Wild type and mutants of PTE were expressed in *E. coli* BL21-DEIII cells and grown in terrific broth (TB) supplemented with 1.0 mM $CoCl_2$ and the appropriate antibiotic. After 24-hour incubation at 30 °C, protein expression was induced by the addition of 1.0 mM isopropyl-β-thiogalactoside (IPTG) and cells were grown for additional 36-40 hours. PTE was purified according to the previously published protocol (Omburo et al., 1992).

Results

Screening of the Double Substitution Library, H254X/H257X

The double substitution library, H254X/H257X was constructed by Dr. Craig Hill in an attempt to engineer the active site of PTE to enhance the catalytic efficiency towards the hydrolysis of *p*-nitrophenol analogs of the nerve agent soman (Hill et al., 2003). Twelve growth blocks were screened for the hydrolysis of paraoxon and the VX analog, DEVX. The standards included is this library were wild type in positions 19 & 22 and H254A in positions 43 & 46. Graphical representation of screening results for block 3 is shown in Figure 2.2. Two variants were isolated from this block for enhanced activity over wild type. They were identified as H254G/H257F and H254Q/H257F with the later being the highest. H254Q/H257F (QF) served as a template for subsequent rounds of random mutagenesis.

Single Substitution Libraries

Single substitution libraries were constructed for positions Gly60, Ile106, Leu303, Ser308, Trp131, Phe132, Phe306, Tyr309, His245, His257, Leu271, and Met317. All nineteen substitution possibilities at each position were identified by DNA sequencing and inoculated in 96-deep well culture blocks. Each block was screened with 0.1 mM paraoxon and 0.2 mM DEVX. Table 2.1 shows the distribution of the G60X and I106X libraries in the 96-deep well block. Figure 2.3A and B shows the screening results with paraoxon and DEVX, respectively.

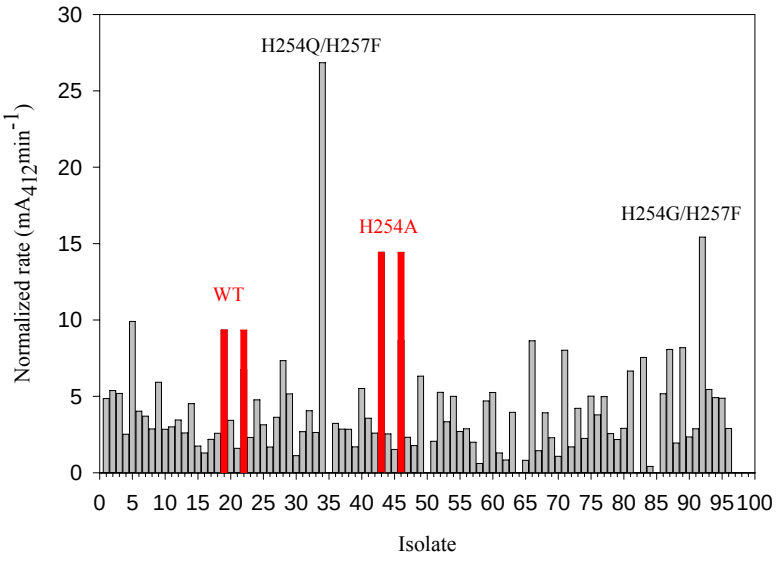

Figure 2.2. Screening results for block 3 of the H254X/H257X double substitution library. The library was screened with 0.2 mM DEVX (**4**).

Table 2.1. Positions of members of the G60X and I106X single substitution libraries. Standards (in red) were wild type, H254A, H254Q/H257 (QF), I106A/F132A/H257Y (AAY), H254G/H257W/L303T (GWT), and BL21 cells.

	1	2	3	4	5	6	7	8	9	10	11	12
A	1 G60A	9 G60F	17 G60K	25 G60P	33 G60S	41 G60Y	49 I106D	57 I106H	65 I106M	73 I106R	81 I106V	89
B	2 G60A	10 G60F	18 G60K	26 G60P	34 G60S	42 G60Y	50 I106D	58 I106H	66 I106M	74 I106R	82 I106V	90
C	3 G60C	11 WT	19 G60L	27 H254A	35 G60T	43 QF	51 I106E	59 AAY	67 I106N	75 GWT	83 I106W	91 BL21
D	4 G60C	12 G60H	20 G60L	28 G60Q	36 G60T	44 I106A	52 I106E	60 I106K	68 I106N	76 I106S	84 I106W	92
E	5 G60D	13 G60H	21 G60M	29 G60Q	37 G60V	45 I106A	53 I106F	61 I106K	69 I106P	77 I106S	85 I106Y	93
F	6 G60D	14 WT	22 G60M	30 H254A	38 G60V	46 QF	54 I106F	62 AAY	70 I106P	78 GWT	86 I106Y	94 BL21
G	7 G60E	15 G60I	23 G60N	31 G60R	39 G60W	47 I106C	55 I106G	63 I106L	71 I106Q	79 I106T	87	95
H	8 G60E	16 G60I	24 G60N	32 G60R	40 G60W	48 I106C	56 I106G	64 I106L	72 I106Q	80 I106T	88	96

A

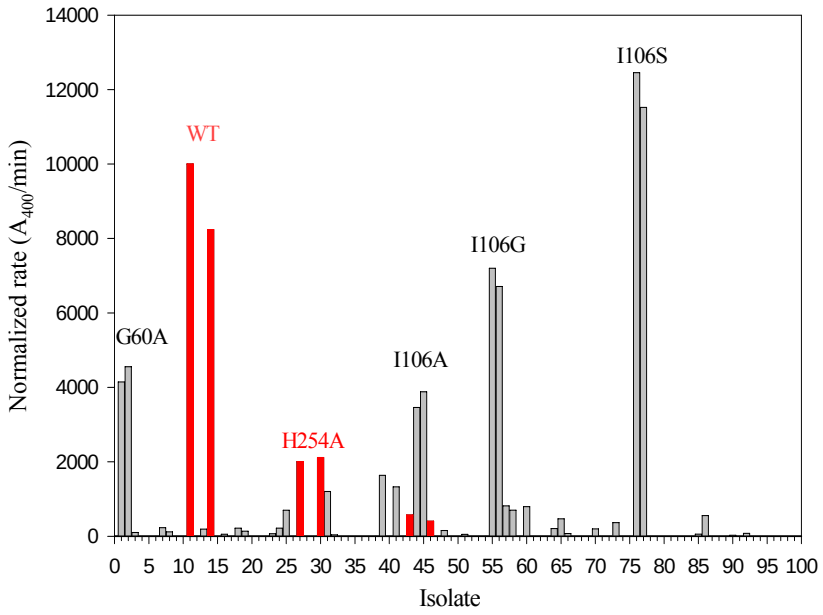

B

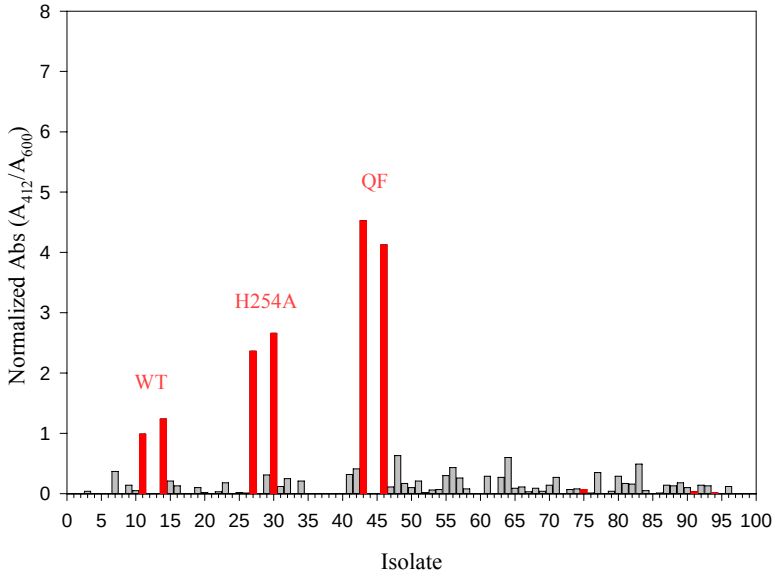

Figure 2.3. Results from the crude screen for the G60X and I106X single substitution libraries. The block was screened with paraoxon (A) and DEVX (B).

The relative paraoxonase activity profile obtained from the crude assay is comparable to the kinetic parameters for previously purified PTE mutants. For example, the k_{cat}/K_m ($M^{-1}s^{-1}$) values for wild type, G60A, I106A, and I106G are 6.4 x 10^7, 4.2 x 10^7, 3.8 x 10^7, and 5.5 x 10^7, respectively (Chen-Goodspeed et al., 2001a, 2001b). As can be observed from the screen, the order of activity is that G60A is similar to I106A, which is lower than I106G, which is less than wild type. The activity of I106S towards paraoxon hydrolysis was slightly higher that the wild type. Screening with DEVX did not show any enhancement compared to the standard, QF.

The block containing H254X and W131X single substitution libraries was similarly screened with paraoxon and DEVX. Table 2.2 shows the location of each variant relative to the controls. The screening results are shown in Figure 2.4A and B. The rate of the standard wild type was approximately 20% less than the average rate. Two variants had higher activity with paraoxon than the wild type; H254K and W131V. Purified W131A has a k_{cat}/K_m value of 8.3 x 10^6 $M^{-1}s^{-1}$, which is approximately 10-fold lower than wild type (Chen-Goodspeed et al., 2001a,b). However, on the screen, it appears to have similar activity to wild type. This could be due to different levels of protein expression in the growth blocks. The relative activities of controls toward DEVX hydrolysis were similar to the G60X, I106X block. In addition, the rate obtained for H254A in positions 1 and 2 was comparable to the rate obtained for the H254A control. None of the variants was higher than the control, QF with DEVX.

Table 2.2. Positions of members of the H254X and W131X single substitution libraries. Standards (in red) are wild type, H254A, H254Q/H257F (QF), I106A/F132A/H257Y (AAY), H254G/H257W/L303T (GWT), and BL21 cells.

	1	2	3	4	5	6	7	8	9	10	11	12
A	1 H254A	9 H254F	17 H254K	25 H254P	33 H254S	41 H254Y	49 W131D	57 W131H	65 W131L	73 W131Q	81 W131T	89
B	2 H254A	10 H254F	18 H254K	26 H254P	34 H254S	42 H254Y	50 W131D	58 W131H	66 W131L	74 W131Q	82 W131T	90
C	3 H254C	11 WT	19 H254L	27 H2554A	35 H254T	43 QF	51 W131E	59 AAY	67 W131M	75 GWT	83 W131V	91 BL21
D	4 H254C	12 H254G	20 H254L	28 H254Q	36 H254T	44 W131A	52 W131E	60 W131I	68 W131M	76 W131R	84 W131V	92
E	5 H254D	13 H254G	21 H254M	29 H254Q	37 H254V	45 W131A	53 W131F	61 W131I	69 W131N	77 W131R	85 W131Y	93
F	6 H254D	14 WT	22 H254M	30 H254A	38 H254V	46 QF	54 W131F	62 AAY	70 W11N	78 GWT	86 W131Y	94 BL21
G	7 H254E	15 H254I	23 H254N	31 H254R	39 H254W	47 W131C	55 W131G	63 W131K	71 W131P	79 W131S	87	95
H	8 H254E	16 H254I	24 H254N	32 H254R	40 H254W	48 W131C	56 W131G	64 W131K	72 W131P	80 W131S	88	96

A

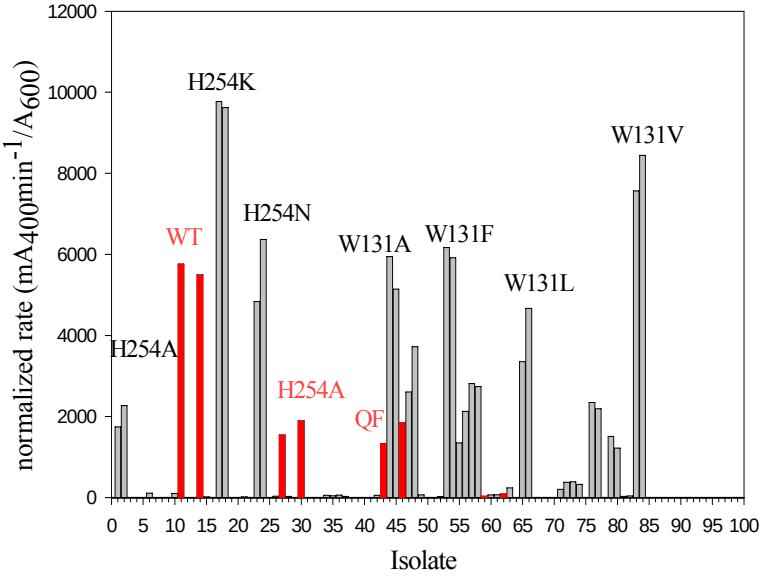

B

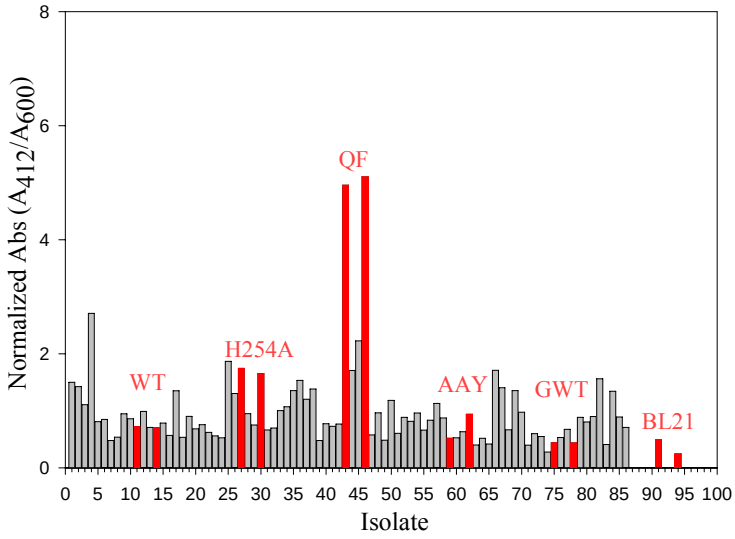

Figure 2.4. Results from the crude assay for the block containing the H254X and W131X single substitution libraries. The block was screened with paraoxon (A) and DEVX (B)

The block containing the single libraries H257X and Y309X was screened with paraoxon and DEVX. The locations of all variants and controls are shown in Table 2.3. The paraoxon screen showed comparable rates of the variants H257W, H257Y, and Y309A relative to the wild type standard (Figure 2.5A). The k_{cat}/K_m ($M^{-1}s^{-1}$) values for H257W, H257Y, and Y309A are 4.4 x 10^7, 6.4 x 10^7, and 6.1 X 10^6, respectively (Chen-Goodspeed et al., 2001a, 2001b). Although the k_{cat}/K_m value for Y309A is approximately 10-fold lower than the wild type, that rate difference seems smaller on the crude cell assay. The 10-fold decrease in activity of the mutant H257A (k_{cat}/K_m = 3.4 x 10^6) is also reflected in the paraoxon screen. In the DEVX crude cell assay, two variants were higher than the QF standard (Figure 2.5B). However, the activity of the controls in this plate with DEVX was lower in general than the rest of the plates. Both H257S and H257T were purified and the kinetic constants were determined to be lower than those for QF.

Screening results for the growth block containing the single substitution libraries L303X and M317X are shown in Figure 2.6. The positions of all variants relative to controls are shown in Table 2.4. The activity of the wild type and H254A standards with paraoxon was lower than expected. The k_{cat}/K_m value for paraoxon hydrolysis by the mutant L303A is 9.0 x 10^6 $M^{-1}s^{-1}$, which was reflected in approximately 10-fold lower activity on the crude assay compared to wild type. When screened with DEVX, the relative activity of the controls was reproducible. H254A remained higher than wild type, but lower than H254Q/H257F. The mutant L303F was slightly higher than wild type, but remained lower than the control H254Q/H257F.

Table 2.3. Positions of members of the H257X and Y309X single substitution libraries. Standards (in red) are wild type, H254A, H254Q/H257F (QF), I106A/F132A/H257Y (AAY), H254G/H257W/L303T (GWT), and BL21 cells.

	1	2	3	4	5	6	7	8	9	10	11	12
A	1 H257A	9 H257F	17 H257K	25 H257P	33 H257S	41 H257Y	49 Y309D	57 Y309H	65 Y309L	73 Y309Q	81 Y309T	89
B	2 H257A	10 H257F	18 H257K	26 H257P	34 H257S	42 H257Y	50 Y309D	58 Y309H	66 Y309L	74 Y309Q	82 Y309T	90
C	3 H257C	11 WT	19 H257L	27 H254A	35 H257T	43 QF	51 Y309E	59 AAY	67 Y309M	75 GWT	83 Y309V	91 BL21
D	4 H257C	12 H257G	20 H257L	28 H257Q	36 H257T	44 Y309A	52 Y309E	60 Y309I	68 Y309M	76 Y309R	84 Y309AV	92
E	5 H257D	13 H257G	21 H257M	29 H257Q	37 H257V	45 Y309A	53 Y309F	61 Y309I	69 Y309N	77 Y309R	85 Y309W	93
F	6 H257D	14 WT	22 H257M	30 H254A	38 H257V	46 QF	54 Y309F	62 AAY	70 Y309N	78 GWT	86 Y309W	94 BL21
G	7 H257E	15 H257I	23 H257N	31 H257R	39 H257W	47 Y309C	55 Y309G	63 Y309K	71 Y309P	79 Y309S	87	95
H	8 H257E	16 H257I	24 H257N	32 H257R	40 H257W	48 Y309C	56 Y309G	64 Y309K	72 Y309P	80 H257S	88	96

A

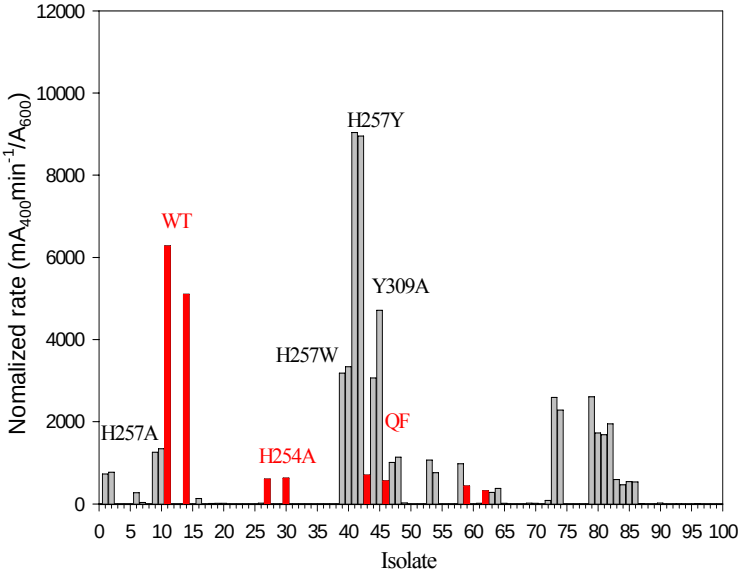

B

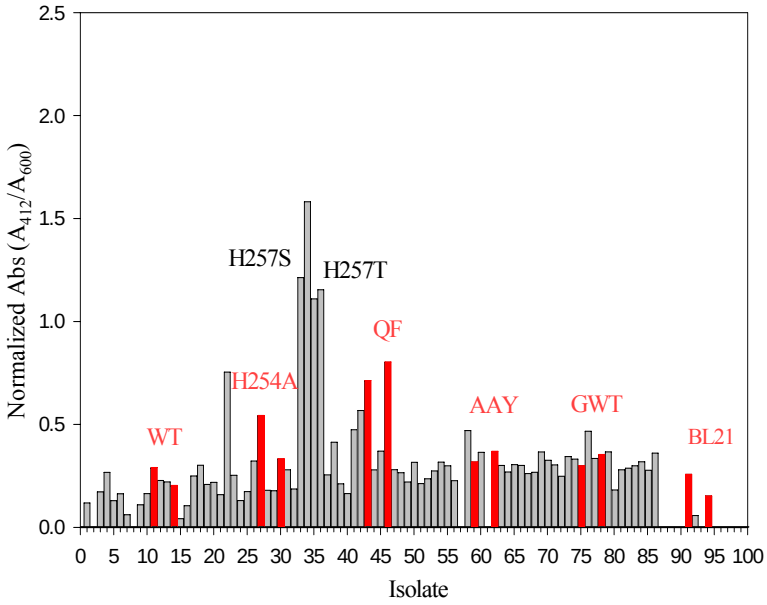

Figure 2.5. Results from the crude assay for the block containing the H257X and Y309X single substitution libraries. The block was screened with 0.1 mM paraoxon (A) and 0.2 mM DEVX (B)

Table 2.4. Positions of members of the L303X and M317X single substitution libraries. Standards (in red) are wild type, H254A, H254Q/H257F (QF), I106A/F132A/H257Y (AAY), H254G/H257W/L303T (GWT), and BL21 cells.

	1	2	3	4	5	6	7	8	9	10	11	12
A	1 L303A	9 L303F	17 L303I	25 L303P	33 L303S	41 L303Y	49 M317D	57 M317H	65 M317L	73 M317R	81 M317V	89
B	2 L303A	10 L303F	18 L303I	26 L303P	34 L303S	42 L303Y	50 M317D	58 M317H	66 M317L	74 M317R	82 M317V	90
C	3 L303C	11 WT	19 L303K	27 H2554A	35 L303T	43 QF	51 M317E	59 AAY	67 M317N	75 GWT	83 M317W	91 BL21
D	4 L303C	12 L303G	20 L303K	28 L303Q	36 L303T	44 M317A	52 M317E	60 M317I	68 M317N	76 M317S	84 M317W	92
E	5 L303D	13 L303G	21 L303M	29 L303Q	37 L303V	45 M317A	53 M317F	61 M317I	69 M317P	77 M317S	85 M317Y	93
F	6 L303D	14 WT	22 L303M	30 H254A	38 L303V	46 QF	54 M317F	62 AAY	70 M317P	78 GWT	86 M317Y	94 BL21
G	7 L303E	15 L303H	23 L303N	31 L303R	39 L303W	47 M317C	55 M317G	63 M317K	71 M317Q	79 M317T	87	95
H	8 L303E	16 L303H	24 L303N	32 L303R	40 L303W	48 M317C	56 M317G	64 M317K	72 M317Q	80 M317T	88	96

A

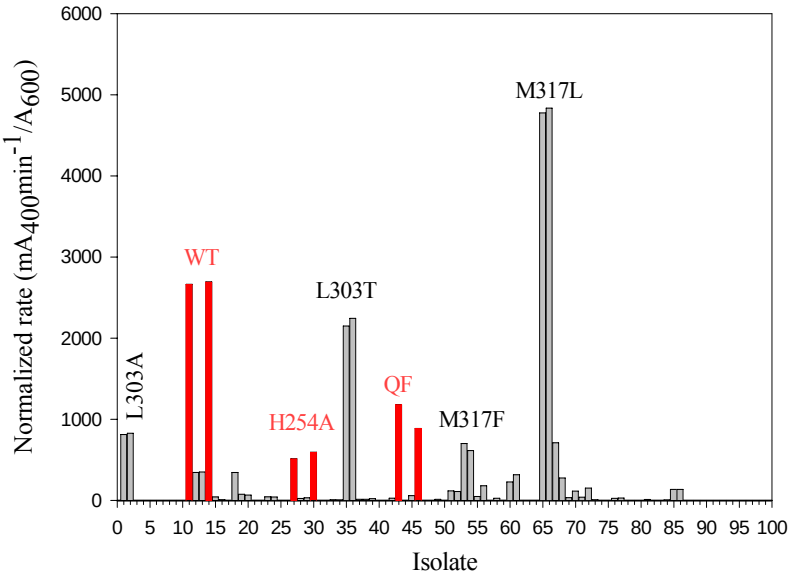

B

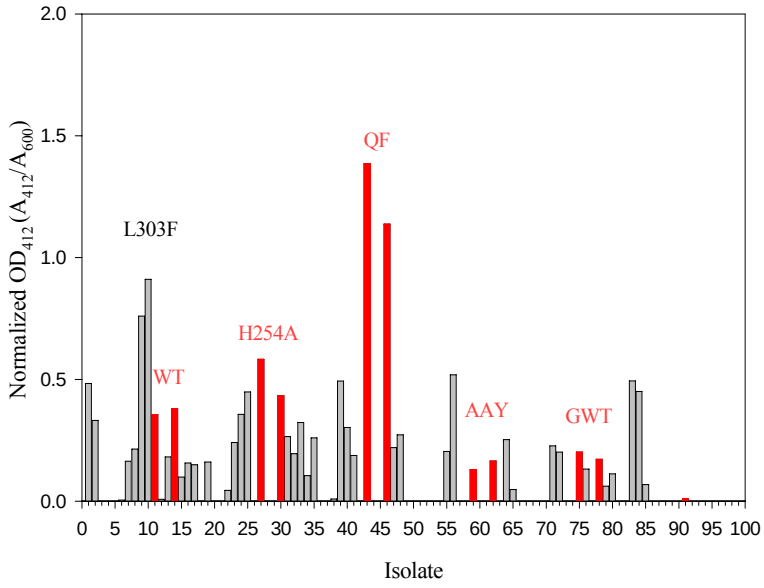

Figure 2.6. Results from the crude screen for the block containing the L303X and M317X single substitution libraries. The block was screened with 0.1 mM paraoxon (A) and 0.2 mM DEVX (B).

The block containing the F306X and L271X single substitution libraries was screened with paraoxon and DEVX as well. Shown in Table 2.5 and Figure 2.7, are the distribution of all variants and results for the crude screen, respectively. The activity of F306A, located in positions 1 and 2, was 34 $mA_{400}\,min^{-1}$, which is 300-fold lower than wild type (Figure 2.7A). This is consistent with the published k_{cat}/K_m value for purified F306A ($2.3 \times 10^5\ M^{-1}s^{-1}$), which is 280-fold lower than wild type (Chen-Goodspeed et al., 2001a, 2001b). However, some inconsistency in the crude assay was observed. For example, the activity of the variant L271A on the crude assay was 600 $mA_{400}min^{-1}$, which is 16-fold lower than wild type. The purified L271A has a k_{cat}/K_m of $1.2 \times 10^7\ M^{-1}s^{-1}$, which is only 5-fold lower than wild type. Also, no activity towards paraoxon hydrolysis was observed for the variants L271F and L271W, although the purified protein displayed a 2-fold decrease on k_{cat}/K_m compared to wild type. Screening with the VX analog, DEVX, did not result in any enhancements over the control H254Q/H257F (Figure 2.7B).

Table 2.5. Positions of members of the F306X and L271X single substitution libraries. Standards (in red) are wild type, H254A, H254Q/H257F (QF), I106A/F132A/H257Y (AAY), H254G/H257W/L303T (GWT), and BL21 cells.

	1	2	3	4	5	6	7	8	9	10	11	12
A	1 F306A	9 F306G	17 F306K	25 F306P	33 F306S	41 F306Y	49 L271D	57 L271H	65 L271M	73 L271R	81 L271V	89
B	2 F306A	10 F306G	18 F306K	26 F306P	34 F306S	42 F306Y	50 L271D	58 L271H	66 L271M	74 L271R	82 L271V	90
C	3 F306C	11 WT	19 F306L	27 H254A	35 F306T	43 QF	51 L271E	59 AAY	67 L271N	75 GWT	83 L271W	91 BL21
D	4 F306C	12 F306H	20 F306L	28 F306Q	36 F306T	44 L271A	52 L271E	60 L271I	68 L271N	76 L271S	84 L271W	92
E	5 F306D	13 F306H	21 F306M	29 F306Q	37 F306V	45 L271A	53 L271F	61 L271I	69 L271P	77 L271S	85 L271Y	93
F	6 F306D	14 WT	22 F306M	30 H254A	38 F306V	46 QF	54 L271F	62 AAY	70 L271P	78 GWT	86 L271Y	94 BL21
G	7 F306E	15 F306I	23 F306N	31 F306R	39 F306W	47 L271C	55 L271G	63 L271K	71 L271Q	79 L271T	87	95
H	8 F306E	16 F306I	24 F306N	32 F306R	40 F306W	48 L271C	56 L271G	64 L271K	72 L271Q	80 L271T	88	96

A

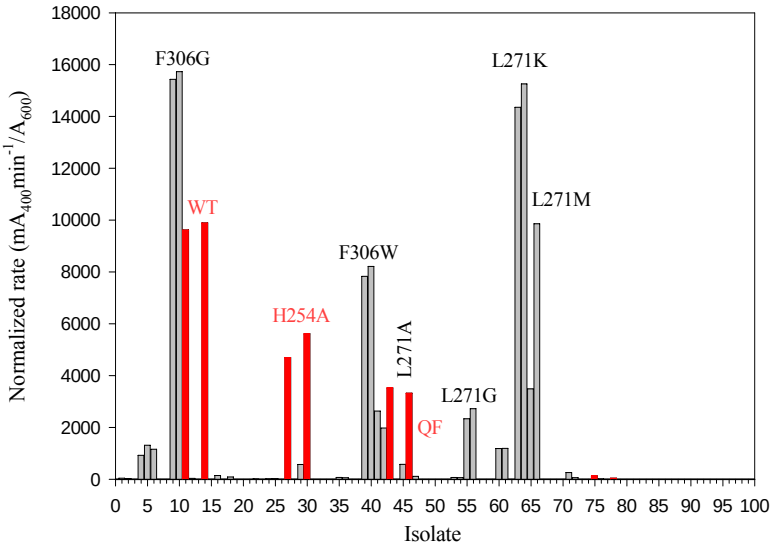

B

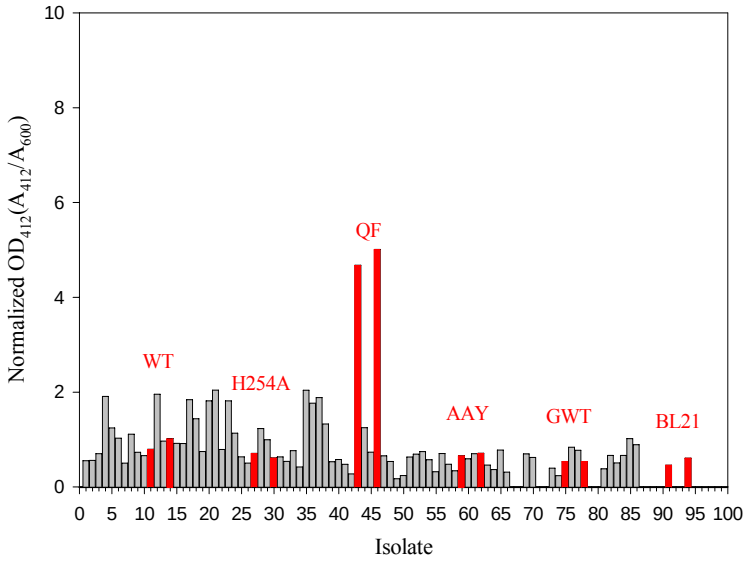

Figure 2.7. Results from the crude screen for the block containing the F306X and L271X single substitution libraries. The block was screened with 0.1 mM paraoxon (A) and 0.2 mM DEVX (B).

The sixth block contained the F132X and S308X single substitution libraries. The identities of all variants and results for the crude screen are shown in Table 2.6 and Figure 2.8, respectively. The paraoxon screen revealed slight variations compared to rates obtained using purified protein. For example, the published k_{cat}/K_m value for F132A is 3.4 x 10^7 $M^{-1}s^{-1}$, which is 2-fold lower than wild type (Chen-Goodspeed et al., 2001a, 2001b). However, the F132A variant on this plate was approximately 4-fold lower than wild type. The activity of F132G, S308A, and S308A relative to wild type was in agreement with the kinetic parameters for the purified protein. The relative activity towards DEVX hydrolysis for which the activity of H254A was greater than wild type, but less than H254Q/H257F was reproducible in this growth block (Figure 2.8B). The variants F132I, S308T, and S308K had a slightly higher activity compared to wild type, but were lower than QF.

Table 2.6. Positions of members of the F132X and S308X single substitution libraries. Standards (in red) are wild type, H254A, H254Q/H257F (QF), I106A/F132A/H257Y (AAY), H254G/H257W/L303T (GWT), and BL21 cells.

	1	2	3	4	5	6	7	8	9	10	11	12
A	1 F132A	9 F132G	17 F132K	25 F132P	33 F132S	41 F132Y	49 S308D	57 S308H	65 S308L	73 S308Q	81 S308V	89
B	2 F132A	10 F132G	18 F132K	26 F132P	34 F132S	42 F132Y	50 S308D	58 S308H	66 S308L	74 M317Q	82 S308V	90
C	3 F132C	11 WT	19 F132L	27 H254A	35 F132T	43 QF	51 S308E	59 AAY	67 S308M	75 GWT	83 S308W	91 BL21
D	4 F132C	12 F132H	20 F132L	28 F132Q	36 F132T	44 S308A	52 S308E	60 S308F	68 S308M	76 S308R	84 S308W	92
E	5 F132D	13 F132H	21 F132M	29 F132Q	37 F132V	45 S308A	53 S308F	61 S308I	69 S308N	77 S308R	85 S308Y	93
F	6 F132D	14 WT	22 F132M	30 H254A	38 F132V	46 QF	54 S308F	62 AAY	70 S308N	78 GWT	86 S308Y	94 BL21
G	7 F132E	15 F132I	23 F132N	31 F132R	39 F132W	47 S308C	55 S308G	63 S308K	71 S308P	79 S308T	87	95
H	8 F132E	16 F132I	24 F132N	32 F132R	40 F132W	48 S308C	56 S308G	64 S308K	72 S308P	80 S308T	88	96

A

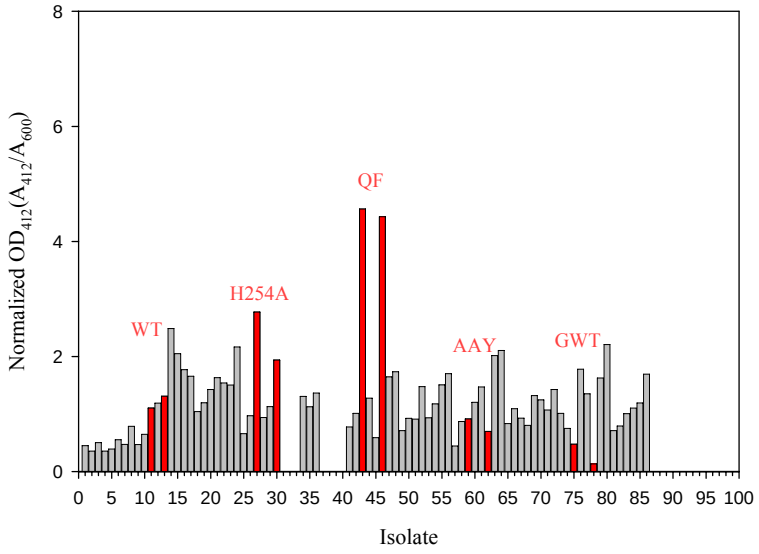

B

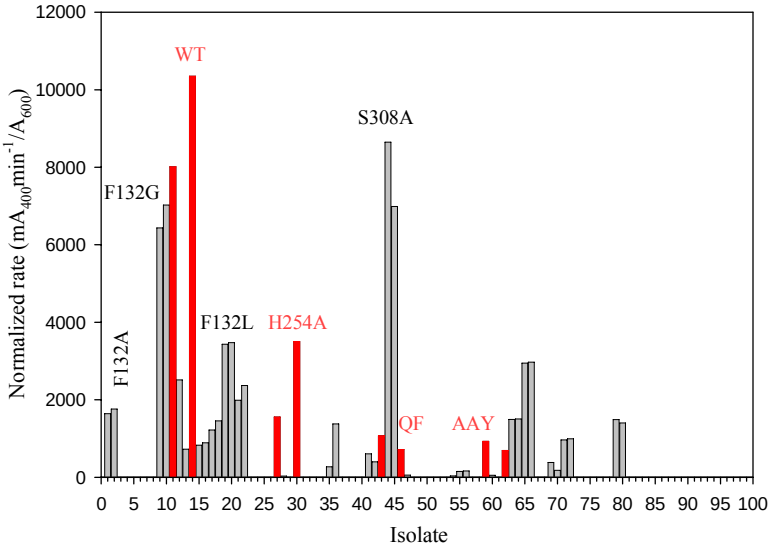

Figure 2.8. Results from the crude screen for the block containing the F132X and S308X single substitution libraries. The block was screened with 0.1 mM paraoxon (A) and 0.2 mM DEVX (B).

Screening of the Third Generation Libraries in the H254Q/H257F Template

Since H254Q/H257F (QF) displayed the most enhancement for DEVX hydrolysis compared to wild type, it was utilized as a parent for randomizing the remaining ten amino acid residues in the substrate binding pocket of PTE. Due to the observed inconsistency in levels of protein expression associated with the pBS+ vector, the *opd* gene was expressed in the medium copy number expression vector, pZA32-Luc. Consequently, the construct pZA32-QF was utilized as a template for the third generation libraries. Ten libraries were constructed; pZA32-QF/G60X, pZA32-QF/I106X, pZA32-QF/L271X, pZA32-QF/Y309X, pZA32-QF/F306X, pZA32-QF/W131X, pZA32-QF/F132X, pZA32-QF/L303X, pZA32-QF/M317X, and pZA32-QF/S308X. Four to six colony forming units (CFU's) were selected from each library and sequenced to confirm sample randomness (Table 2.7). Two growth blocks were screened for each library. The previously characterized standards, wild type and H254Q/H257F were included in positions 11 & 14 and 27 & 30, respectively.

Table 2.7. The identities of random colonies isolated from each single substitution library in the pZA32-QF template.

QF/W131X		QF/F132X		QF/Y309X		QF/G60X	
TGG	wild type	TTC	wild type	TAC	wild type	GGT	wild type
GAG	Glu	GGG	Gly	CTC	Leu	CTG	Leu
AGG	Arg	CTG	Leu	TCC	Ser	GGT	Gly
GCC	Ala	TAG	Stop	CAC	His	GGT	Gly
TAG	stop	ATC	Ile	TAC	Tyr	GCC	Ala
CCG	Pro	GGC	Gly	TTC	Phe		

QF/F306X		QF/I106X		QF/L271X		QF/L303X	
TTC	wild type	ATC	wild type	CTG	wild type	CTG	wild type
GGC	Gly	TCC	Ser	CTG	Leu	GTG	Glu
CAG	Gln	ATC	Ile	CTC	Leu	TCC	Ser
TTC	Phe	ACG	Thr	AAC	Asn	GTG	Val
GGC	Gly	TCG	Ser	AAG	Lys	GAC	Asp
CCG	Pro	GCA	Ala	GCG	Ala	CTG	Leu
CGC	Arg	TCC	Ser				

QFS308X		M317X	
AGC	wild type	ATG	wild type
CTC	Leu	TAC	Tyr
CAC	His	AGC	Ser
CCC	Pro	TAC	Tyr
AGC	Ser		
CAG	Gln		

.

The pZA32-QF/Y309X library was screened with 0.1 mM paraoxon and 0.2 mM DEVX. Figure 2.9A and B shows the DEVX screening results for block 1 and block 2, respectively. Standards are shown in red. Block 1 contained one copy of the wild type standard in position 14. Four variants were isolated from that block and sequenced because they displayed similar activity to the QF control. Sequencing results indicated that they are the template QF. Screening results from block 2 are shown in Figure 2.9B. In this plate the variant QF/Y309L in well number 40 and 87 was slightly higher than the QF control, while QF/Y309E had similar rate. In general, there were no significant enhancements towards DEVX hydrolysis compared to the controls.

Screening results for pZA32-QF/I106X are shown in Figure 2.10A and B. In block 1, several variants displayed enhancements over wild type. They were identified as QF/I106Q, QF/I106L, QF/I106S, and QF/I106P. The template QF was represented in this block at approximately 4% of the total population. Although the background was relatively high in block 2, the standard QF was easily distinguishable from the background.

A

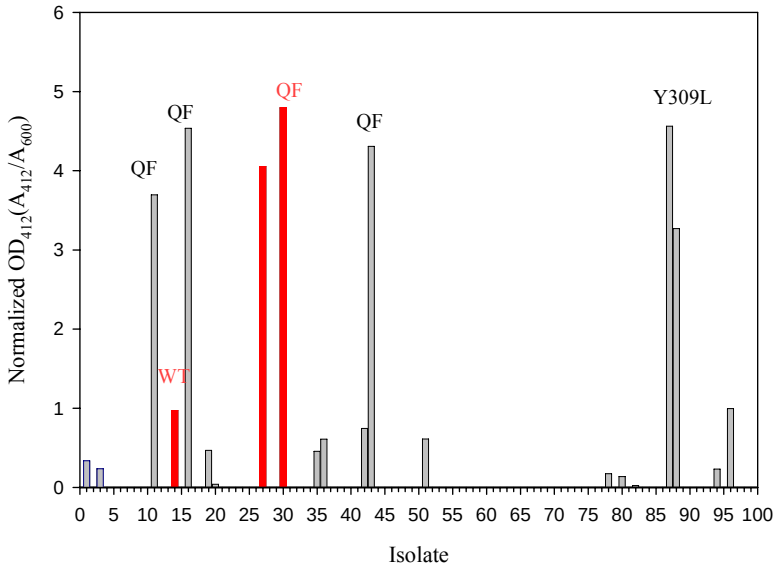

B

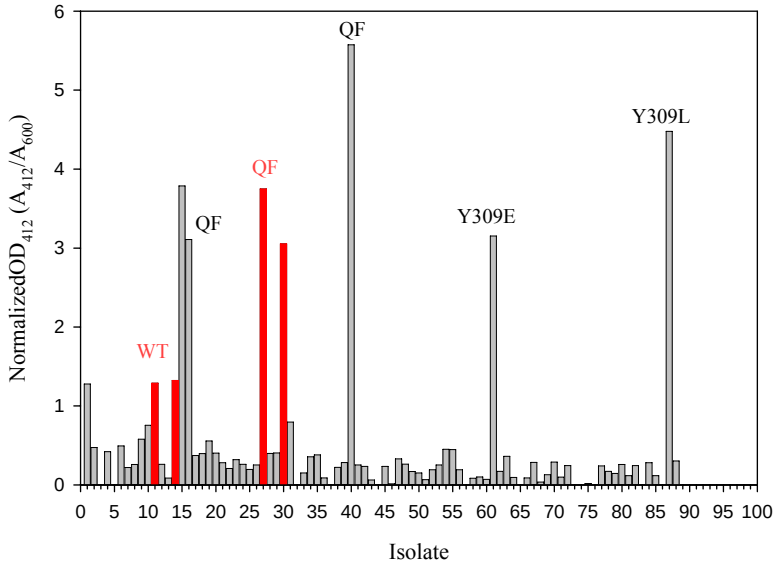

Figure 2.9. Results from the crude screen for the pZA32-QF/Y309X library, block 1 (A) and block 2 (B). The library was screened with 0.2 mM DEVX (**4**).

A

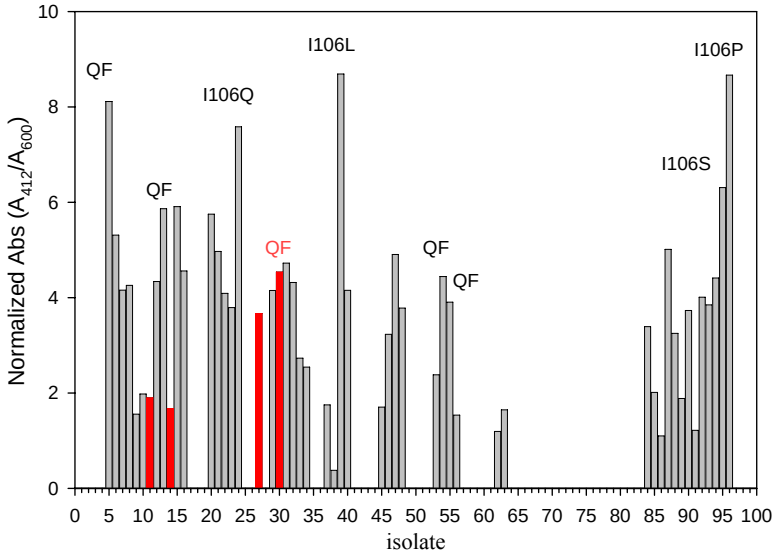

B

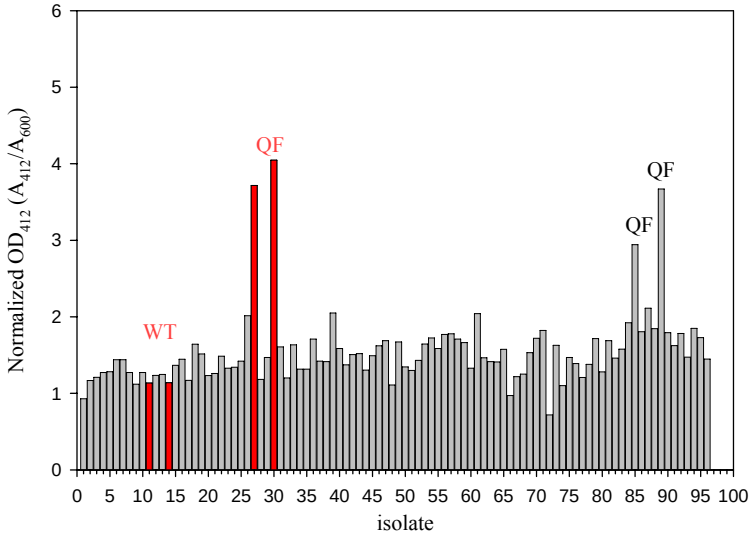

Figure 2.10. Results from the crude screen for the pZA32-QF/I106X library, block 1 (A) and block 2 (B). The library was screened with 0.2 mM DEVX (**4**).

Two growth blocks from the library pZA32-QF/L271X were similarly screened for the hydrolysis of the VX analog, DEVX (Figure 2.11A and B). The activity of the standard QF was lower in this library compared to other blocks. In block 1, the template QF was present at approximately 2% of the population. Two different wild type codons were identified by DNA sequencing, which further confirms the randomness of the library. However, that did not seem to affect the overall activity. The variants QF/L271V, QF/L271M, and QF/L271I displayed relatively similar activity to the QF control.

The results obtained from screening the library pZA32-QF/F306X for hydrolysis of DEVX are presented in Figure 2.12A and B. Similarly, the library pZA32-QF/F306X showed reasonable representation of the controls. Both codons for phenylalanine were identified by DNA sequencing, which further ensures the randomness of the mutagenesis procedure. However, no variants displayed higher rates for DEVX hydrolysis.

A

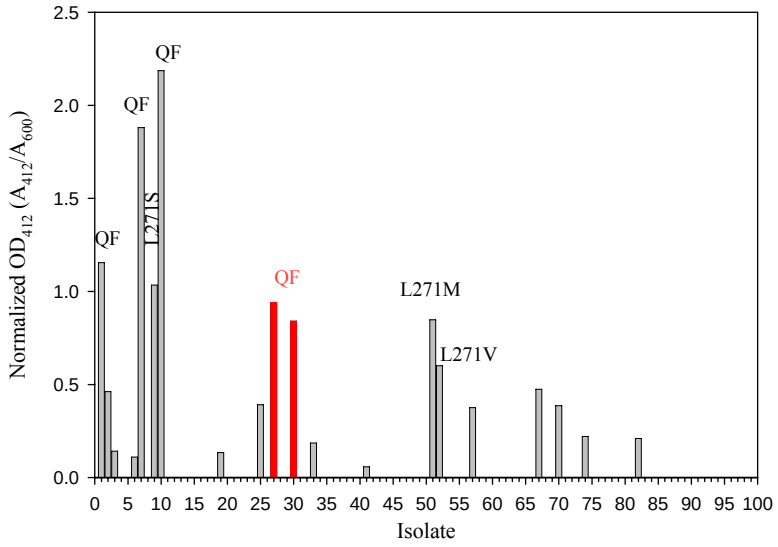

B

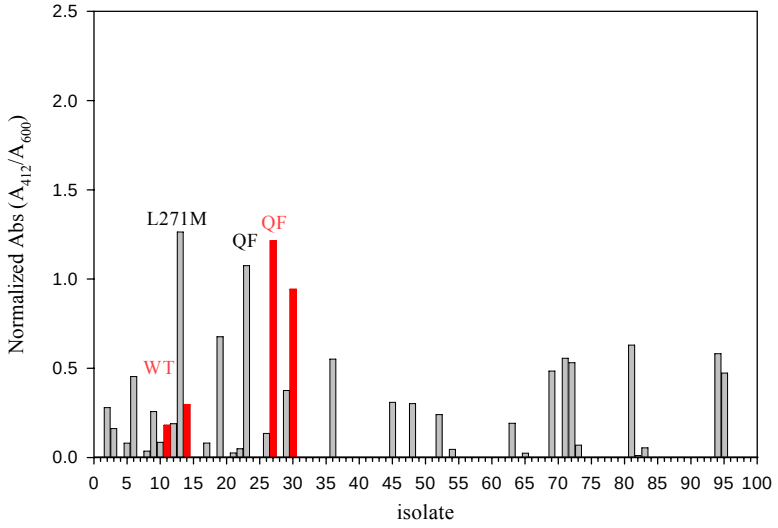

Figure 2.11. Results from the crude screen for the pZA32-QF/L271X library, block 1 (A) and block 2 (B). The library was screened with 0.2 mM DEVX (**4**).

A

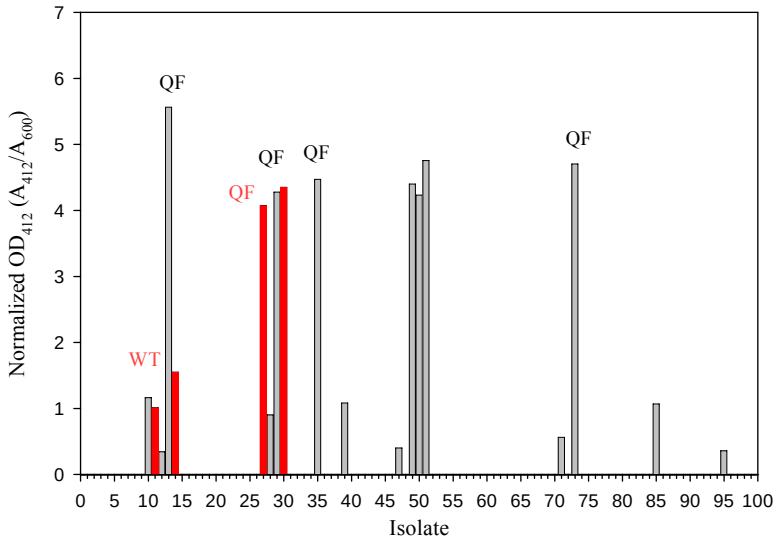

B

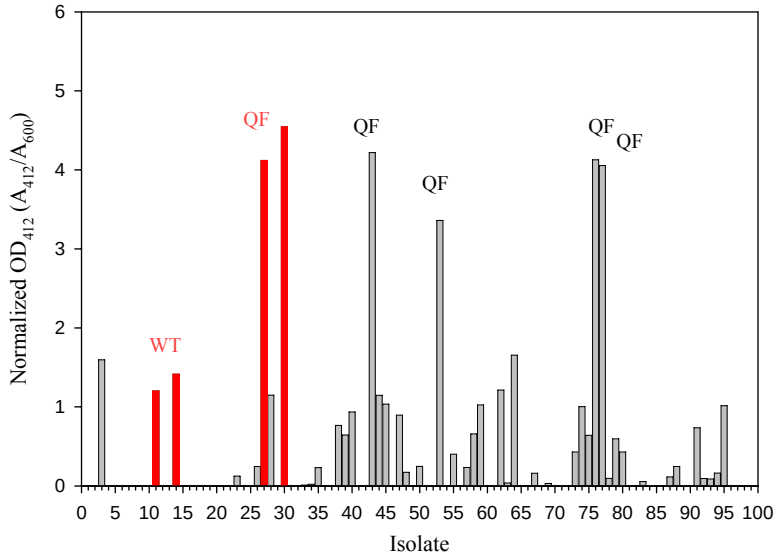

Figure 2.12. Results from the crude screen for the pZA32-QF/F306X library, block 1 (A) and block 2 (B). The library was screened with 0.2 mM DEVX (**4**).

The results for screening two blocks from the library pZA32-QF/M317X are shown in Figure 2.13A and B. The previously identified mutants; QF/M317Y and QF/M317S were inoculated in positions 1, 2 of block 1, respectively. The order of activity of the standard H254Q/H257F relative to wild type was reproducible in this library as well. In block 1, one variant had a 10-fold enhancement over wild type. However, DNA sequencing revealed that it was the template, H254Q/H257F. This could be due to variations in protein expression within the library. In block 2, the mutant QF/M317L was 2-fold higher than wild type, but remained lower than the QF standard.

In the same manner, the library pZA32-QF/S308 was screened for DEVX hydrolysis (Figure 2.14A and B). The assay background was unusually higher in this library compared to other plates. The previously sequenced CFU's; QF/S308L, S308H, S308P, wild type, S308Q, S308E, and S308V were inoculated in positions 1, 2, 3, 4, 5, 6, 7 of block 1, respectively. Block 2 contained several mutants that were isolated and sequenced for having slightly elevated activity compared to the QF control. They were identified as QF/S308A, QF/S308C, QF/308W, QF/S308N, and QF/S308K.

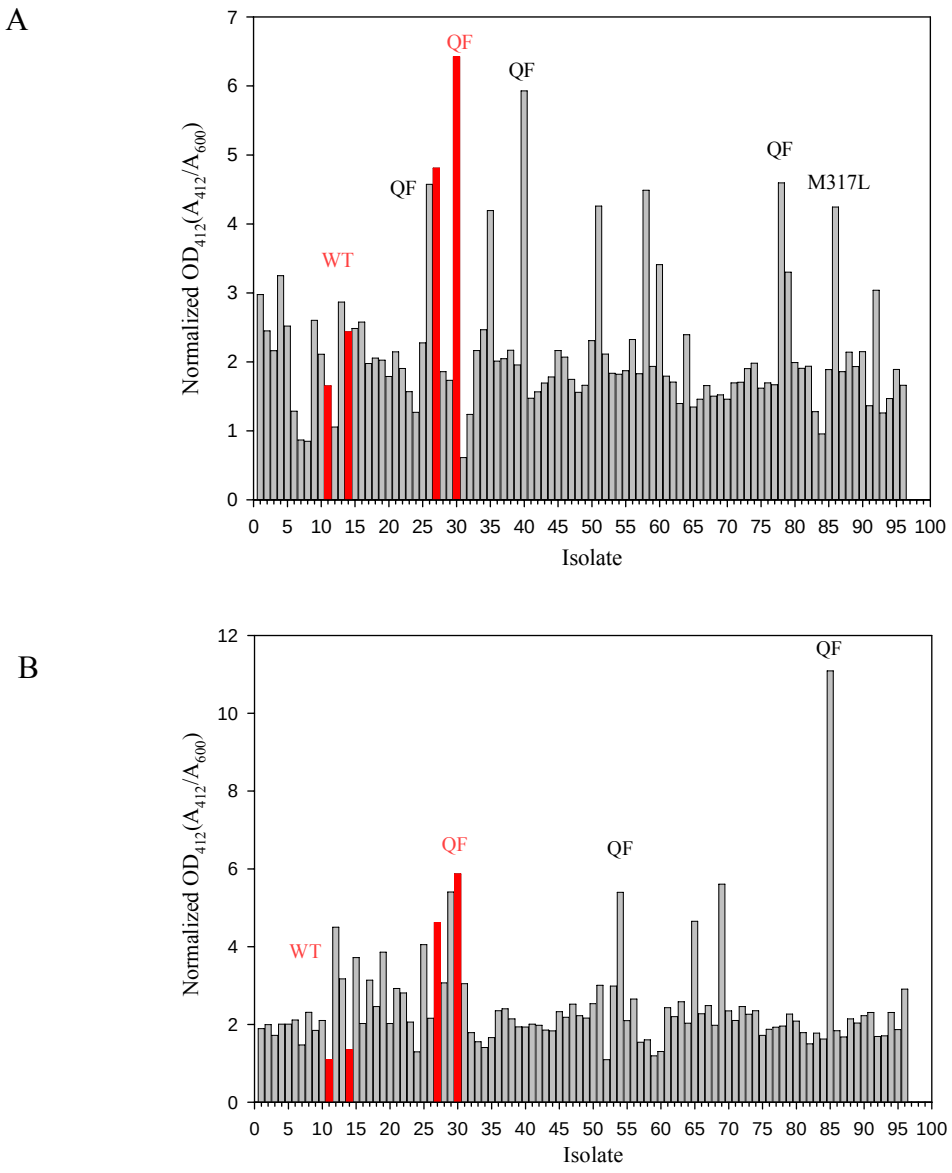

Figure 2.13. Results from the crude screen for the pZA32-QF/M317X library, block 1 (A) and block 2 (B). The library was screened with 0.2 mM DEVX (**4**).

A

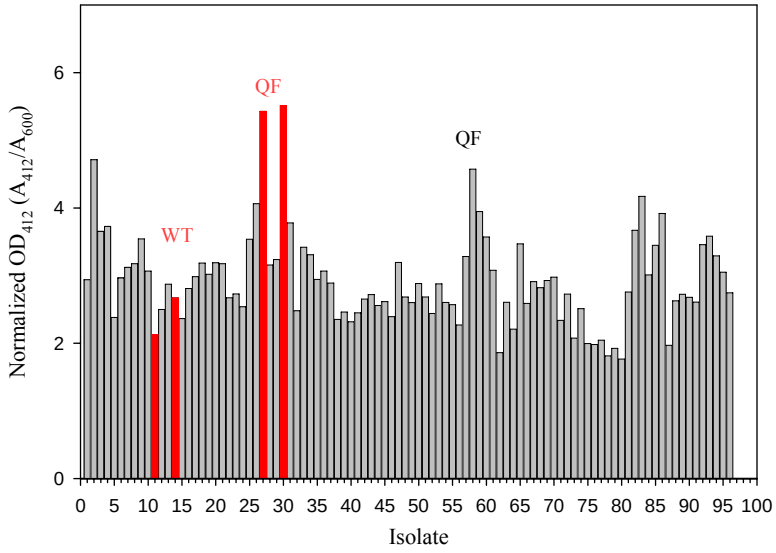

B

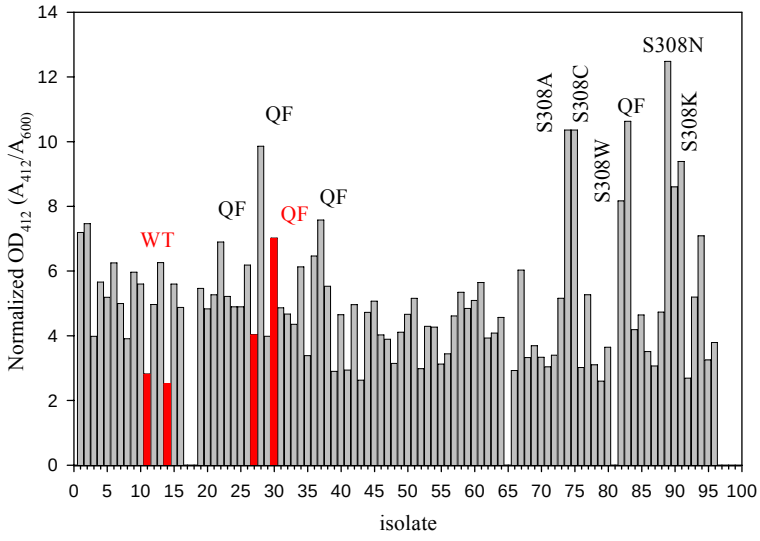

Figure 2.14. Results from the crude screen for the pZA32-QF/S308X library, block 1 (A) and block 2 (B). The library was screened with 0.2 mM DEVX (**4**).

One block from the pZA32-QF/W131 library was screened due to the lower level of PCR amplification, which resulted in fewer colonies (Figure 2.15). The background for the DEVX assay was unusually high, and no variants could be isolated for enhanced activity.

Two blocks from the QF/F132X library were screened with paraoxon and DEVX (Figure 2.16A and B). The standards included in this library were wild type in positions 11 & 14, H254A in positions 27 & 30, and QF in positions 43 & 46. The variant QF/F132L isolated from both block 1 and block 2 had slightly higher rate for DEVX hydrolysis than the QF control. Also, QF/F132I displayed the same level of activity as the standard QF.

Similarly, two blocks representing the pZA32-QF/G60X were screened for the hydrolysis of 0.2 mM DEVX. (Figure 2.17A and B). DNA sequencing of mutants selected from block 1 indicated that the background level caused by the QF parent was approximately 4-6% of the library. The mutant QF-G60A displayed a small enhancement over wild type, but not the template. The same mutation was isolated from block 2 in addition to the variant QF/G60T. It is worth mentioning that the H254Q/H257F background was caused not only by the template, but also by the mutagenesis to other glycine codons.

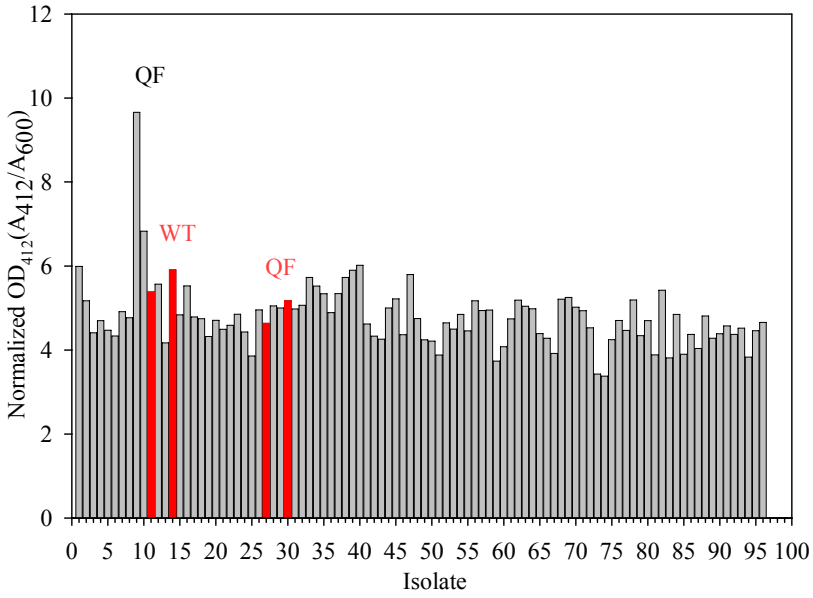

Figure 2.15. Results from the crude screen for the pZA32-QF/W131X library. The library was screened with 0.2 mM DEVX (**4**).

A

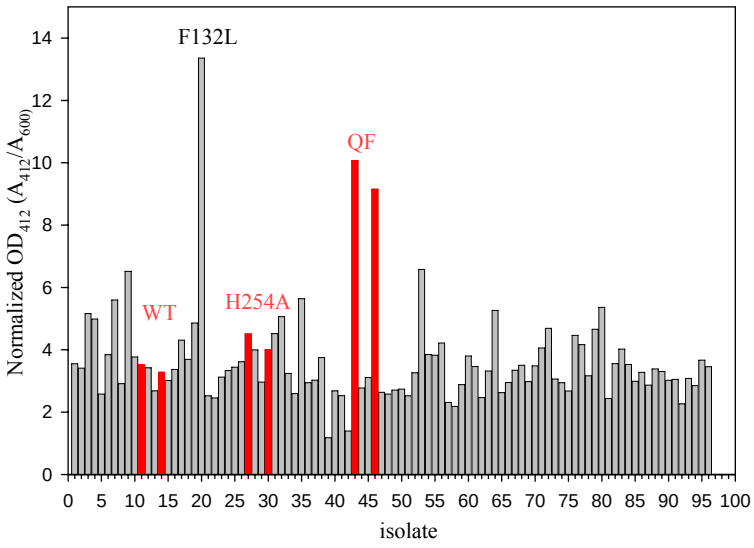

B

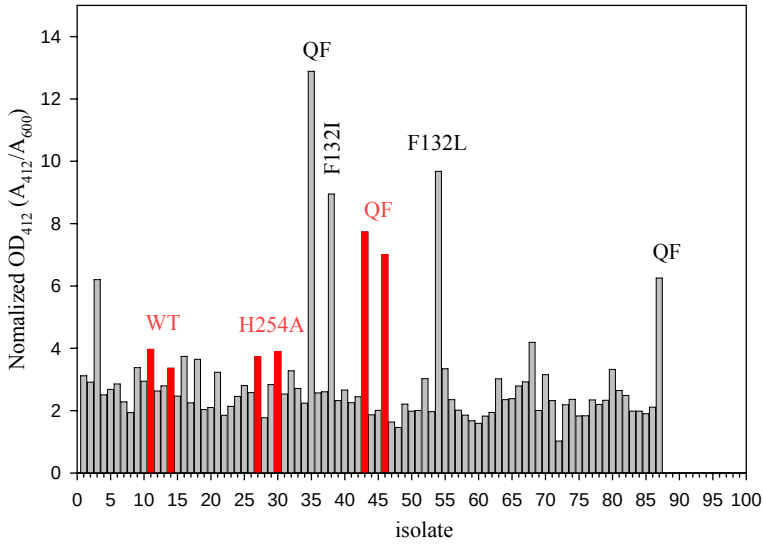

Figure 2.16. Results from the crude screen for the pZA32-QF/F132X library, block 1 (A) and block 2 (B). The library was screened with 0.2 mM DEVX (**4**).

A

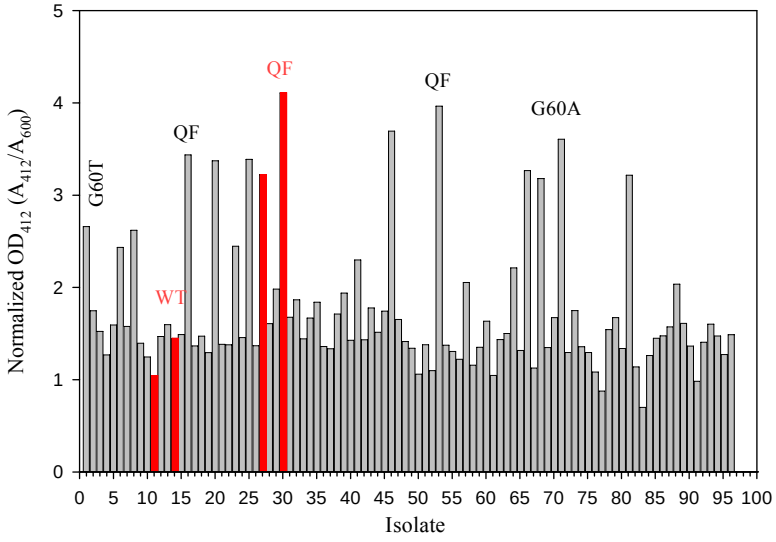

B

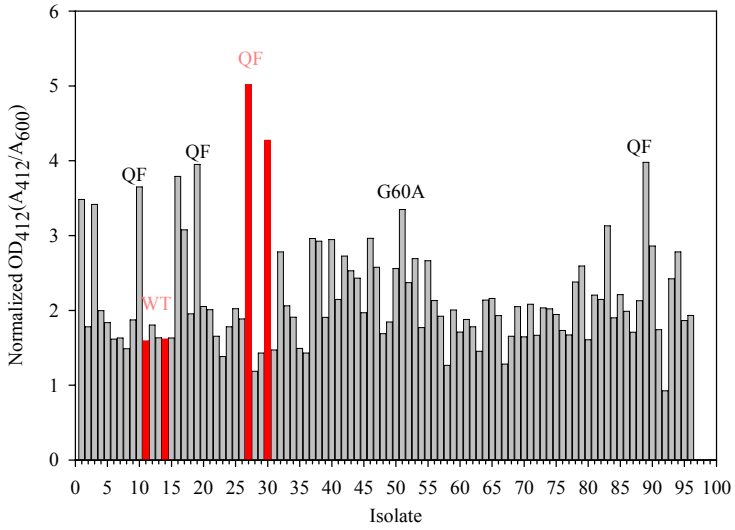

Figure 2.17. Results from the crude screen for the pZA32-QF/G60X library, block 1 (A) and block 2 (B). The library was screened with 0.2 mM DEVX (**4**).

The final third generation library screened was the pZA32-QF/L303X library. Only one block was screened from this library because of low PCR product yield. The previously identified mutants; QF/L303E, L303S, L303V, L303D, wild type are located in wells number 1, 2, 3, 4, and 5, respectively (Figure 2.18). Screening this library for DEVX hydrolysis did not result in identifying variants with enhanced activity relative to the parent H254Q/H257F.

Several mutants were isolated from the crude assay and purified for they displayed enhanced activity over wild type towards the hydrolysis of the VX analog, DEVX. The kinetic parameters are reported in Table 2.8. In addition, a comparison of H254Q/H257F to other PTE mutants that have displayed improvements for the hydrolysis of *p*-nitrophenol analogs of the nerve agents sarin and soman is shown in Figure 2.19. The assay conditions with regard to substrate concentration were similar to the crude assay, so that the rate observed is correlated to the k_{cat}/K_m values relative to wild type and QF. The comparison of the rates reported in Figure 2.19 clearly show that H254Q/H257F has highest improvement for DEVX hydrolysis.

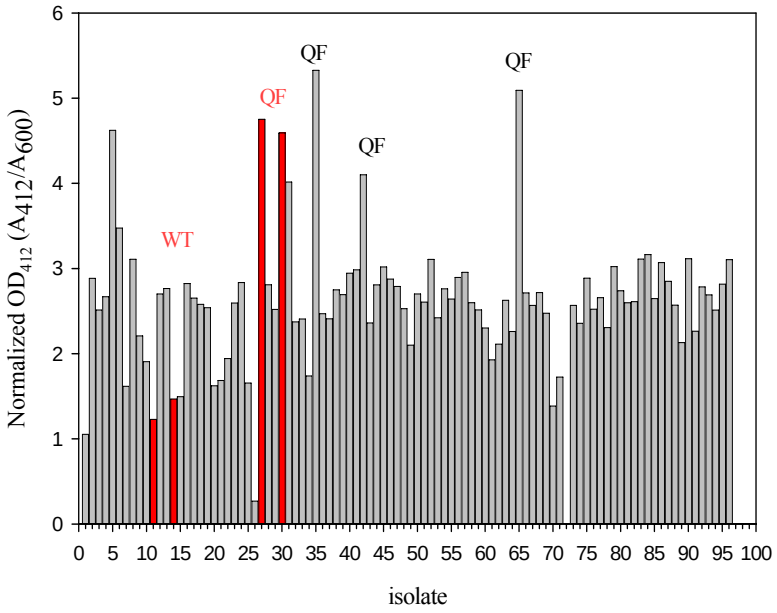

Figure 2.18. Results from the crude screen for the pZA32-QF/L303X library. The library was screened with 0.2 mM DEVX (**4**).

Table 2.8. Kinetic parameters of selected PTE mutants for the hydrolysis of DEVX.

Protein	k_{cat} (s^{-1})	K_m (mM)	k_{cat}/K_m ($M^{-1}s^{-1}$)
WT	0.8 (0.1)	0.8 (0.2)	10^3 (130)
H254G	0.2 (0.004)	0.8 (0.05)	2.5 x 10^2 (10)
H254R	0.4 (0.02)	3.5 (0.3)	120 (5)
H254Q/H257F	7.4 (0.5)	2.6 (0.3)	3.0 x 10^3 (300)
QF/I106P	ND	ND	2.8 x 10^2 (17)
QF/I106Q	1.4 (0.04)	0.4 (0.05)	3.2 x 10^3 (250)

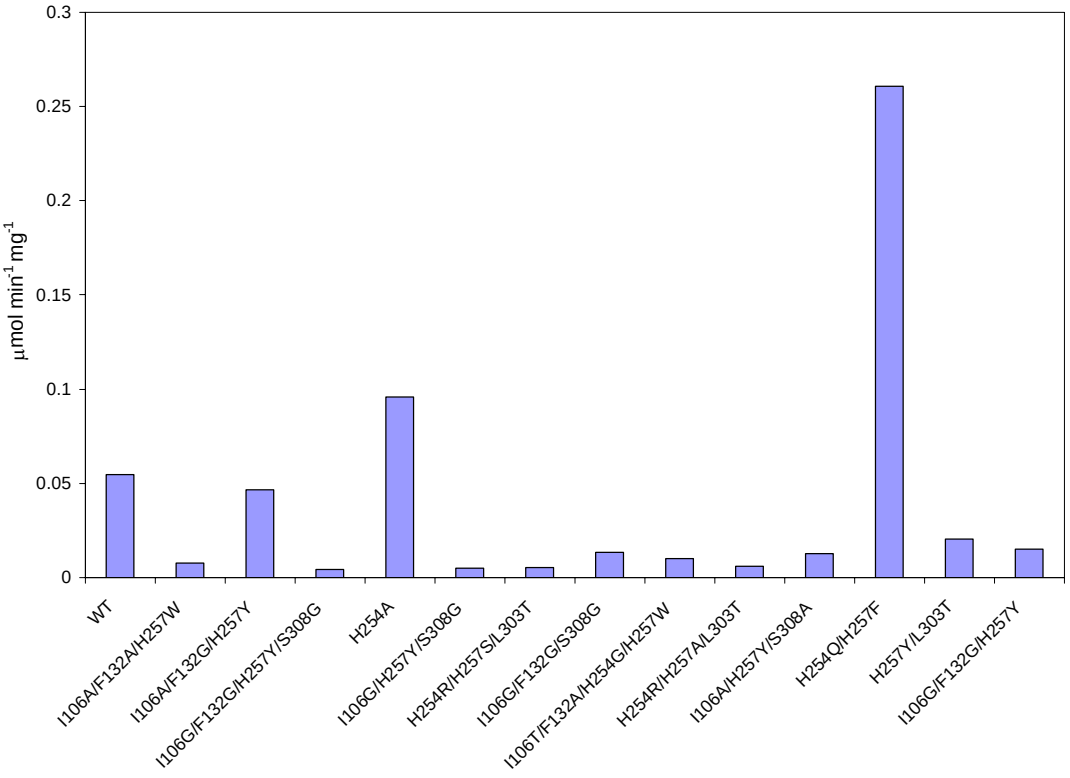

Figure 2.19. The specific activity (µmol min^{-1} mg^{-1}) of purified PTE mutants for the hydrolysis of the VX analog, DEVX. The assay contained 0.2 mM substrate, 0.3 mM DTNB, and 50 mM HEPES, pH 8.0.

Several other libraries were screened for DEVX hydrolysis, but no beneficial mutations could be identified (data not shown). Those libraries targeted primarily the substrate binding pocket of PTE. They were H254A/H257X, H254R/H257X, H254R/Y309X, H254R/I106X, and H254R/F306X.

Hydrolysis of the Pesticide Demeton-S

The H254Q /H257F mutant was tested for its ability to hydrolyze the pesticide demeton-S. Table 2.9 shows a comparison of the kinetic parameters for demeton-S by wild type PTE and selected mutants. QF displayed an 18-fold enhancement in the turnover number over wild type and a 10-fold enhancement in k_{cat}/K_m. Another mutant that showed enhancement towards demeton-S hydrolysis, H254G/H257F, had phenylalanine at position 257. H254Q/H257F was 2-fold less than the best characterized mutant for demeton-S hydrolysis, H254R/H257L.

Table 2.9. Kinetic parameters for the hydrolysis of demeton-S by wild type PTE and selected mutants.

Protein	k_{cat} (s^{-1})	K_m (mM)	k_{cat}/K_m ($M^{-1}s^{-1}$)
WT	1.0 (0.002)	3.0 (0.2)	380 (25)
H254A	2.4 (0.1)	4.3 (0.3)	560 (45)
H254R[a]	1.2 (0.03)	1.1 (0.1)	1.1×10^3 (100)
H254Q/H257F	18 (0.65)	5.0 (0.4)	3.8×10^3 (400)
H254R/H257F[a]	7.5 (0.4)	2.3 (0.3)	3.3×10^3 (460)
H254R/H257L[a]	19 (0.4)	2.3 (0.1)	8.4×10^3 (400)

[a] kinetic parameters were provided by Dr. Craig Hill (Unpublished data)

Discussion

Targeting the VX Analog within the Double Substitution Library H254X/H257X

Previous studies have indicated that PTE is a potential candidate for the detoxification of organophosphates. Engineering the substrate binding site of PTE has proven promising for altering the substrate specificity and enhancing the catalytic efficiency towards the hydrolysis of sarin and soman analogs (Li et al., 2001 and Hill et al., 2003). Both His254 and His257 are located in the *large* subsite. It has been demonstrated that beneficial mutations can be isolated by simultaneously randomizing His254 and His257. The H254X/H257X double substitution library was screened in a search for mutants with enhanced activity towards the hydrolysis of the VX analog, DEVX. The screen resulted in identifying the mutant H254Q/H257F with approximately 3-fold enhancement over wild type. Another mutant was identified with a phenylalanine at position 257, H254G/H257F. Comparison of kinetic parameters indicated that H254Q/H257F exhibited a 10-fold enhancement over wild type for k_{cat} and a 3-fold enhancement in k_{cat}/K_m.

The mutant H254Q/H257F displayed enhancement over wild type when the block containing the G60X and I106X single substitution libraries was screened for hydrolysis of the S_PR_C/S_PS_C-(1) and the S_PS_C(1) analogs of the nerve agent soman (Scheme 2.4). Purified QF exhibited a 100-fold enhancement in k_{cat}/K_m for hydrolysis of the S_PR_C-(1) and S_PS_C-(1) (Ph.D. dissertation by Karin T. Lum).

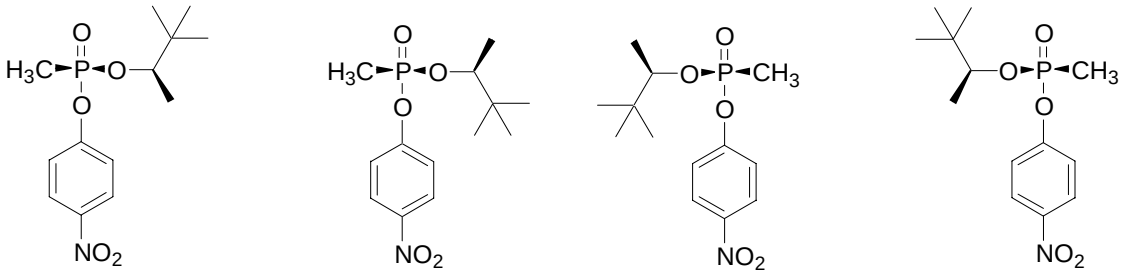

Scheme 2.4. Structures of the individual stereoisomers of the *p*-nitrophenol soman analog.

Targeting the VX Analog within the Single Substitution Libraries

Twelve single substitution libraries targeting the active site of PTE were constructed and screened for DEVX hydrolysis. Screening the block containing the G60X and I106X libraries did not result in any improvement over the control QF for DEVX hydrolysis. However, the mutant I106S displayed higher activity compared to wild type when screened for paraoxon hydrolysis. This is consistent with the findings of a directed evolution by *in vitro* compartmentalization study conducted by Tawfik and co-workers (Griffiths and Tawfik, 2003). They employed an *in vitro* screening approach using microbeads display to screen combinatorial libraries of PTE at positions Ile106, Phe132, Trp131, Ser308, and Tyr309. The variants I106S and I106T/F132L were isolated for they exhibited 1.3-fold and 1.8-fold enhancement for paraoxon hydrolysis over the wild type. No significant enhancements resulted from the single substitution libraries. The H254C, H257S, H257T, and L303F mutants displayed slight

improvement over the wild type, but remained less active than the H254Q/H257F mutant.

Targeting the VX Analog within the Third Generation Libraries in the QF Template

Ten amino acid residues within the PTE active site were randomized in the H254Q/H257F template in a search for improved variants for DEVX hydrolysis. Most mutations in the pZA32-QF/Y309X appeared to be detrimental to DEVX hydrolysis. The QF/Y309E and QF/Y309L were identified in this library for having similar activity to the QF template. There was a slight variation in the activity of the parent QF, which could be due to variations in protein expression.

Several variants were isolated from the pZA32-QF/I106X library for displaying a comparable activity to the standard QF. They were identified as QF/I106S, QF/I106P, QF/I106Q, and QF/I106L. Both QF/I106P and QF/I106Q were purified and the kinetic parameters for DEVX hydrolysis were determined. While the k_{cat}/K_m value for QF/I106Q was very similar to QF, the k_{cat}/K_m for QF/I106P was 10-fold slower (Table 2.8).

Like the PZA32-QF/Y309X library, the majority of mutations in the pZA32-QF/L271X were detrimental. Few mutations did not seem to reduce the rate of DEVX hydrolysis. They were identified as L271M, L271V, and L271I. Interestingly, one variant displayed a 10-fold increase in paraoxon hydrolysis over the parent, QF, which was identified as QF/L271G (data not shown).

No improvements for the hydrolysis of DEVX resulted from screening the pZA32-QF/F306X and pZA32-QF/M317X libraries. All variants isolated were identified as the parent QF except for the QF/M317L mutant, which had a similar activity as the standard QF. Despite the high background obtained from screening the pZA32-QF-S308X for DEVX hydrolysis, several variants were isolated for they were as active as the template QF. The isolated mutants had alanine, asparagine, valine, cysteine, or lysine at position 308. This suggests that mutating Ser308 was not as detrimental to hydrolysis of DEVX compared to other resides.

No beneficial mutations for DEVX hydrolysis resulted from mutating Trp131 in the QF template. However, the QF/W131E mutant had a 4-fold enhancement in paraoxon hydrolysis over the template QF (data not shown). Results from the F132X library constructed in the QF template have indicated that the vast majority of the mutations are detrimental to the activity against DEVX. Two mutants were identified for having beneficial mutations, the QF/F132L and QF/133I mutants. No enhancements over the standard QF were obtained from the G60X and the L303X libraries in the QF template.

Although the crude screen has shown some variations in the rates for paraoxon and DEVX hydrolysis, it was successful in the identification of variants with enhanced activity compared to wild type. In most cases, the kinetic parameters of purified mutants were in agreement with the relative activity on the crude assay. Attempts to further improve the catalytic efficiency of H254Q/H257F by constructing the third generation libraries did not result in any enhancements. However, some possibilities have not been

explored yet. One possibility is to employ the technique of DNA shuffling to recombine the beneficial mutants isolated from the crude screens.

CHAPTER III

CHARACTERIZATION OF GLYCEROPHOSPHODIESTER PHOSPHODIESTERASE FROM *E. AEROGENES:* *IN VIVO* SELECTION UTILIZING ORGANOPHOSPHATES AS THE SOLE PHOSPHORUS SOURCE

Introduction

Organophosphate diesters are utilized in biological systems as energy currency, signaling molecules, and components in cellular molecules such as nucleic acids and phospholipids. Hence, organophosphate diesters are very abundant in organisms. Phosphodiesterases are involved in regulating a range of intracellular processes. For example, cyclic AMP phosphodiesterases play a key role in regulating the intracellular level of the signal mediator cAMP.

Glycerophosphodiester phosphodiesterase (GpdQ) from *E. aerogenes* is a part of an operon homologous to the glycerol-3-phosphate (G3P) uptake operon in *E. coli* (*ugp*) (Larson et al., 1983). In *E. aerogenes*, expression of GpdQ is induced under phosphate limiting conditions. GpdQ was previously purified and the amino acid composition was determined (Gerlt et al., 1975). It is believed to be the first phosphohydrolase known to cleave alkyl diesters such as dimethyl phosphate (DMP) and diethyl phosphate (DEP). In addition, GpdQ catalyzes the hydrolysis of a broad range of phosphodiesters including

bis-*p*-nitrophenyl phosphate, gylcerophosphoethanolamine (GPE), ethylene phosphate, and cyclic AMP (Gerlt et al., 1975, and McLoughlin et al., 2004).

Multiple sequence alignment of GpdQ with glycerophosphodiester phosphodiesterases from *E. coli*, and *T. maritima,* shows low sequence homology (10%). Sequence analysis suggests that GpdQ is a member of class III 3', 5'-cyclic nucleotide phosphodiesterases (PDE's) along with *E. coli* 3', 5'-cAMP phosphodiesterase, Ser/Thr protein phosphatases, and purple acid phosphatases (Richter, 2002). Members of this family contain a binuclear metal center in their active site and share the conserved sequence motif, $DXH(X)^{n}GDXXD(X)^{n}GNHD/E$, that forms the metal ion binding site (Figure 3.1).

Ollis and co-workers demonstrated that GpdQ enables *E. coli* to utilize alkyl phosphodiesters (e.g. DMP and DEP) as the sole phosphorus source (McLoughlin et al., 2004). An *in vivo* growth assay where GpdQ was co-expressed with organophosphorus hydrolase from *Agrobacterium radiobacter* (opdA) (Horne, et al., 2002) was employed to examine the ability of *E. coli* to break down dimethyl-*p*-nitrophenyl phosphate (methyl paraoxon) to inorganic phosphate (Scheme 3.1). Their findings showed that, under phosphate limiting conditions, cells expressing only opdA were unable to utilize the phosphotriester as a source of phosphate. However, cells co-expressing GpdQ and opdA, with the triesterase being the growth limiting factor, allowed *E. coli* to grow on methyl paraoxon as the sole phosphorus source.

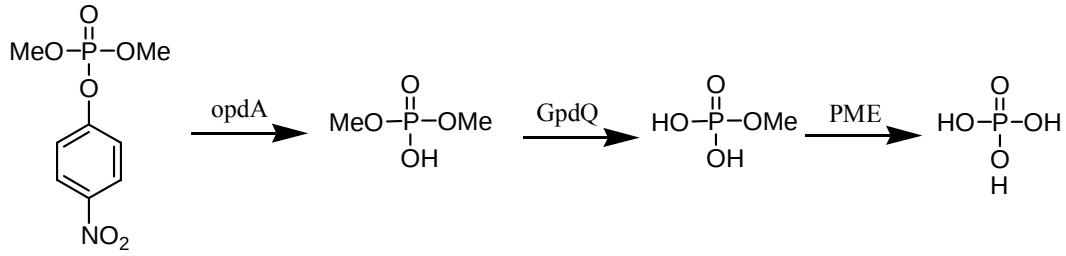

Scheme 3.1. Proposed catabolic pathway of methyl paraoxon.

In this chapter, a more detailed characterization of GpdQ with regard to substrate specificity is presented. A series of organophosphate diesters and methyl phosphonate monoesters were exploited as potential substrates. The aim of this investigation was to expand the application of the *in vivo* coupling assay to cover a number of analogs of the chemical warfare agents; GF, sarin, soman, VX, and Russian VX. In the case of methyl phosphonate monoesters, the released methyl phosphonate is degraded by the gene products of the *Phn* operon (Wanner, 1994). The *Phn* operon is only induced under phosphate starvation conditions and is known to enable *E. coli* to utilize methyl phosphonate as a phosphorus source. This would provide an alternative means to conventional screening assays in the search for improved variants of PTE for the detoxification of organophosphate triesters.

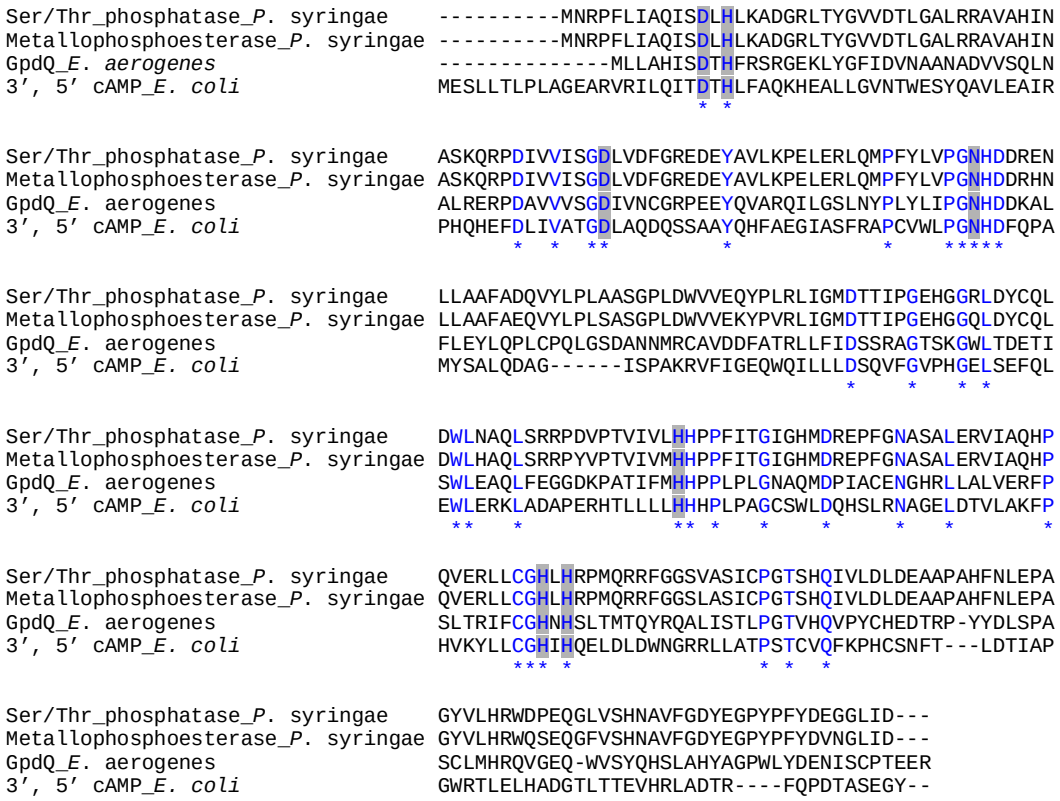

Figure 3.1. Multiple sequence alignment of the *P. syringae* Ser/Thr protein phosphatase, *P. syringae* metallophosphatase, *E. aerogenes* GpdQ, and *E. coli* 3',5'- cAMP phosphodiesterase. Residues involved in the metal ion-binding site are shaded in grey.

Materials and Methods

Materials

Plasmids and strains used in this study are listed in Table 3.1. *E. aerogenes* was purchased from ATCC (ATCC number 13048). *E. coli* BL21-DEIII and XL1-blue cells were obtained from Stratagene. The expression plasmid pET30 (a) and *Platinium pfx* DNA polymerase were purchased from Invitrogen. The Genomic DNA purification kit was obtained from Promega. Alcohol dehydrogenase and NAD^+ were purchased from Sigma. Organophosphate diesters and methyl phosphonates (Scheme 3.2) were synthesized in our laboratory by Dr. Yingchun Li and Dr. Chengfu Xu. The medium copy number expression vector, pZA32-luc was generously provided by Dr. Ryland Young, Department of Biochemistry and Biophysics. The overexpressing PTE construct, pET20b-5S was a gift from Dr. Dan Tawfik, Department of Biological Chemistry, Weizmann Institute of Science. DNA sequencing was performed in the GTL, Texas A&M University

Cloning of GpdQ

Genomic DNA from *E. aerogenes* was isolated using the Genomic DNA kit purchased from Promega, and used as the template for PCR amplification. The GpdQ gene was amplified by PCR using the primers, GpdQ (+) 5'- GGC GGC CAA GCT TGC AGG TTT AAA ATC ATA TGC TGT TAG CGC ACA TTT CCG ATA C and GpdQ (-)3'- CTA CGA ATT CTC ATC ATC ATT AGC GCT CTT CCG TTG GAC. The *NdeI* and *EcoRI* restriction sites are underlined. PCR conditions were 95 °C for 30

seconds, followed by 30 cycles of 95 °C for 1 min, 55 °C for 1 min, 68°C for 4 min. and final extension at 68°C for 10 min. The 824 bp PCR product was purified, digested with *NdeI* and *EcoR I*, and ligated in a similarly digested pET 30 (a). The ligation product was transformed in *E. coli* XL1-blue electro-competent cells for DNA sequencing.

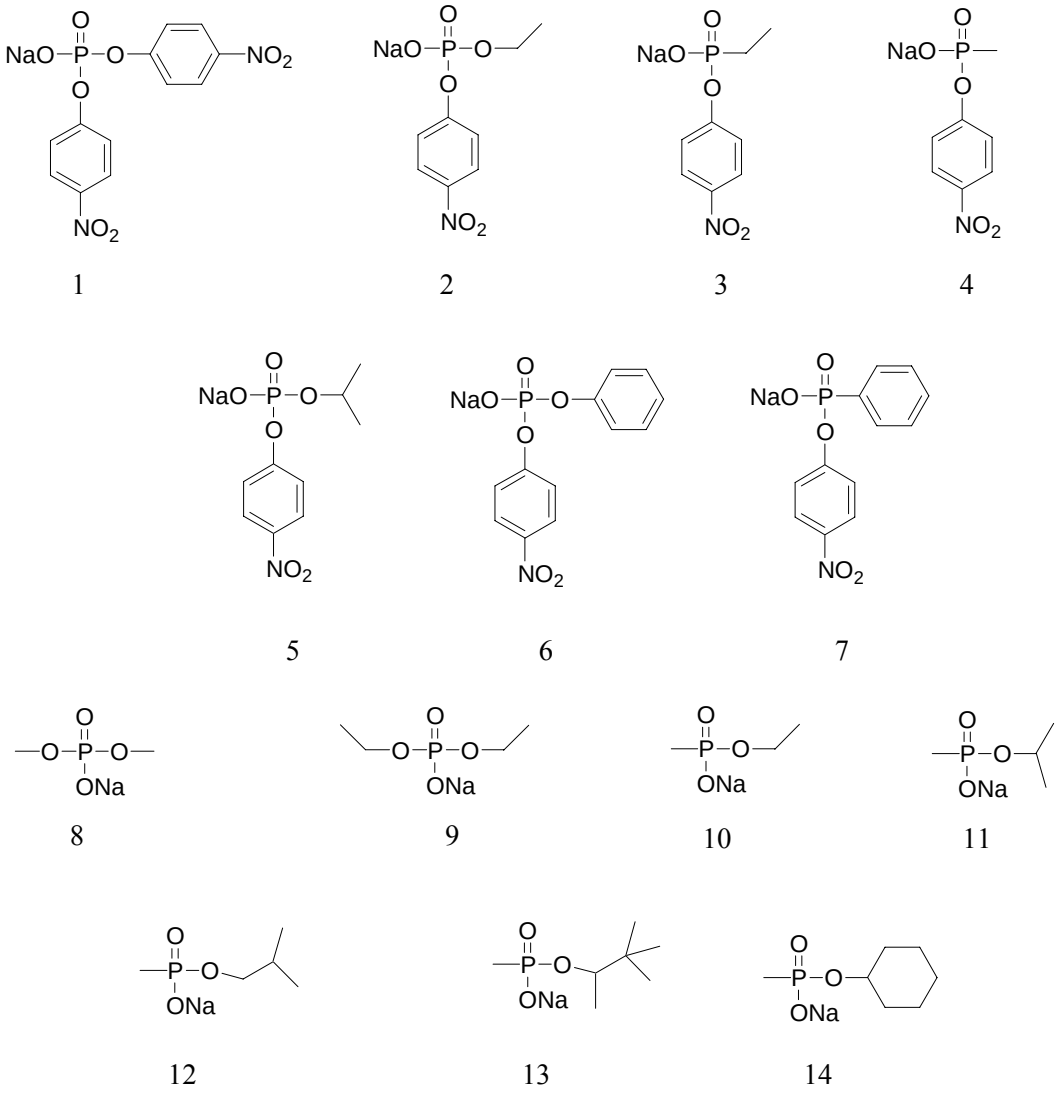

Scheme 3.2. Structures of the organophosphate diesters and methyl phosphonate monoesters used to investigate the substrate specificity of GpdQ.

Table 3.1. Description of plasmids and strains utilized in this work.

Plasmid/Strain	Description	Reference
pZA32-luc	A medium copy number *tac* promoter expression vector	Obtained from Dr. Young
pZA32-opd	Wild type PTE cloned in pZA32-luc plasmid	
GpdQ	*E. aerogenes* phosphodiesterase cloned in pET30 (a)	
GpdQ+	GpdQ transformed in BL21-DEIII competent cells	
GpdQ/PTE	GpdQ+ cells transformed with the plasmid pZA32-opd	
GpdQ/pET20b-5S	GpdQ+ cells transformed with the pET20b-5S (overexpressing PTE construct)	Roodveldt et al., 2005

Purification of GpdQ

The plasmid pET30 encoding the GpdQ gene was transformed in BL21-DEIII electro-competent cells. Cells were grown in Luria-Bertani medium supplemented with 0.05 mg/mL kanamycin and 1 mM $MnCl_2$ at 30 °C until the OD_{600} reached 0.6. Protein expression was induced by the addition of 1.0 mM isopropyl-β-thiogalactoside (IPTG) and the culture was grown for an additional 12 hours at 30 °C. Cells were harvested by centrifugation and resuspended in 20 mM Tris-HCl buffer, pH 7.6, containing 0.1 mg/mL phenylmethanesulfonyl fluoride (PMSF). All purification steps were carried out at 4 °C. Cells were disrupted by sonication, and the soluble fraction was isolated by centrifugation. The supernatant was treated with 1.5% protamine sulfate to precipitate nucleic acids. Protein was then precipitated with 60% saturation of ammonium sulfate. The ammonium sulfate pellet was resuspended in 20 mM Tris, pH 7.6 and loaded on a Superdex 200 gel filtration column (Amersham Biosciences). Fractions eluted from the Superdex column were assayed for the hydrolysis of 1.0 mM bis-*p*NPP at pH 9.0. Fractions with the highest activity were pooled and loaded on a Resource Q anion exchange column (Amersham Biosciences) and eluted with 0-1M sodium chloride gradient in 20 mM Tris-HCl buffer, pH 7.6. SDS-PAGE indicated that the protein was at least 95% pure and that the activity was associated with a band at ~ 31 kDa. Protein concentration was determined using $\varepsilon_{280} = 38{,}600\ M^{-1}cm^{-1}$. The purified protein was dialyzed against 10 mM HEPES pH 7.6 and concentrated to 10 mg/mL for crystallography purposes.

Kinetic Measurements and Data Analysis

All kinetic measurements ware performed on a SPECTRAmax-340 plate reader (Molecular Devices Inc, Sunnyvale CA). The assays contained 0.1 mM $MnCl_2$ and 25 mM CHES buffer, pH 9.0. The release of *p*-nitrophenol (ε_{400} = 17,000 $M^{-1}cm^{-1}$) was monitored at 25 °C for the enzymatic hydrolysis of compounds **1**-**7**. Hydrolysis of diethyl phosphate, dimethyl phosphate, *O*-ethyl methyl phosphonate, and *O*-isopropyl methyl phosphonate (**8, 9, 10,** and **11**) was monitored by coupling the reaction to yeast alcohol dehydrogenase (YADH). The assay contained 10 units ADH, 1.0 mM NAD^+, 25 mM CHES, pH 9.0, and 0.1 mM $MnCl_2$. The production of NADH (ε = 6.22 $mM^{-1}cm^{-1}$) was monitored at 340 nm. Hydrolysis of *O*-isobutyl methyl phosphonate, *O*-cyclohexyl methyl phosphonate, and soman analog (**12, 13,** and **14**) was monitored by coupling the reaction to liver alcohol dehydrogenase (LADH). The assay contained 5 units ADH, 4.0 mM NAD^+, 25 mM CHES pH 9.0, and 0.1 mM $MnCl_2$. Hydrolysis of diethyl phosphate, *O*-ethyl methyl phosphonate, *O*-isopropyl methyl phosphonate and *O*-isobutyl methyl phosphonate was also measured by NMR. Methyl-demeton-S and DEVX (Scheme 3.3) hydrolysis was monitored using Ellman's reagent, 5,5'-dithio-bis(2-nitrobenzoic acid) (DTNB). Release of the 2-nitro-5-thiobenzoate anion (ε_{412} = 14,150 $M^{-1}cm^{-1}$) was followed at pH 8.0. $MnCl_2$ was included in the assay in a final concentration of 0.1 mM. Total concentration of substrate was determined using the PTE mutant H254Q/H257F.

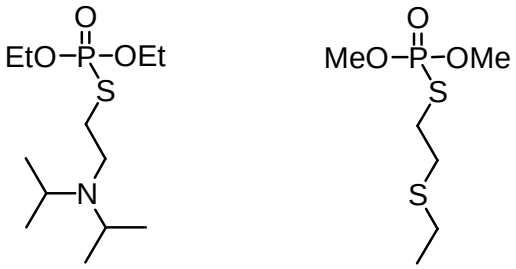

DEVX (15) Methyl-demeton-S (16)

Scheme 3.3. Structure of DEVX and methyl-demeton-S.

Kinetic parameters were obtained by fitting the data to equation 1 where *v* is the initial velocity, V_{max} is the maximal velocity, S is substrate concentration, and K_m is the Michaelis constant. Relative concentrations of the substrate and the product were calculated by integrating the NMR spectra. Rate constants for product formation and substrate decay were obtained by fitting the integration data to equations 2 and 3 respectively. In equations 2 and 3, y_0 is the y-intercept, a is the amplitude, b is the rate constant, and t is the time. Time course ratios for the GpdQ catalyzed hydrolysis of methyl demeton-s and DEVX were determined by fitting the data to equation 4, where y_0 is the y-intercept, a and c are the amplitudes of the curve, b and d are the rate constants.

$$v = V_{max}\,[S]/K_m + [S] \quad (1)$$

$$y=y_0 + a(1-e^{-bt}) \quad (2)$$

$$y=y_0 + a(e^{-bt}) \quad (3)$$

$$y=y_0 + a(1-e^{-bt}) + c(1-e^{-dt}) \quad (4)$$

In Vivo *Growth Assays*

E. coli BL21-DEIII competent cells were transformed with the GpdQ plasmid and plated on LB plates containing 0.05 mg/mL kanamycin resulting in GpdQ+ cells. Overnight cultures in LB media were inoculated from fresh transformations and washed three times with minimal media to remove any traces of rich medium. To test the ability of GpdQ+ cells grow to on organophosphate diesters and organophosphonates, the growth rate was measured under phosphate limiting conditions using liquid 1X MOPS phosphate free minimal medium, pH 7.4 (Neidhardt et al., 1974). The minimal medium was supplemented with 0.5 mM $MnCl_2$, 0.1 % glucose as carbon source and 0.1 μg/mL thiamin (vitamin B1). Cells were grown in the presence of 1.0 mM K_2HPO_4, 1.0 mM methyl phosphonate, 1.0 mM diethyl phosphate, 1.0 mM *O*-isopropyl methyl phosphonate, 1.0 mM *O*-isobutyl methyl phosphonate or 1.0 mM methyl phosphonate of soman analog. A 20 mL culture was inoculated with 1% fresh, previously washed overnight culture. As a control, $GpdQ^-$ BL21-DEIII cells were grown in the presence and absence of inorganic phosphate. Cell growth was monitored by measuring the OD_{600} for 4-5 days at 30 °C.

The choice of organophosphate triester substrates for the *in vivo* selection under phosphate limiting condition is limited to the ability of *E. coli* to survive the release of a phenol leaving group upon hydrolysis. Therefore, *E. coli* BL21-DEIII was tested for its ability to grow in the presence of various phenols (Scheme 3.4). Cells were grown in LB medium containing 1.0 mM of each phenol. Methanol was added to a final

concentration of 1.0% to enhance the solubility of some phenols. Growth rate was monitored every 20 min at 37 °C for 24 hours.

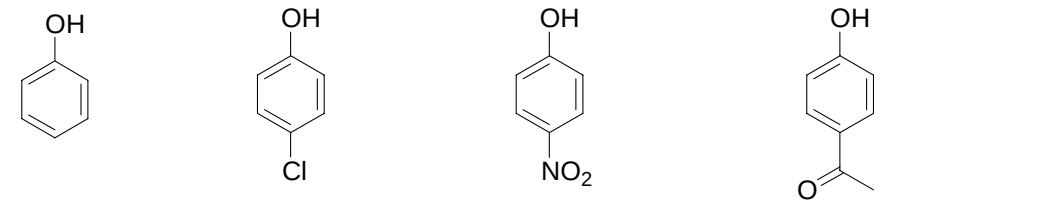

phenol *p*-chlorophenol *p*-nitrophenol *p*-hydroxyacetophenone

Scheme 3.4. Structures of various phenols tested for their effect on the growth of *E. coli.*

Cells co-expressing PTE and GpdQ were tested for their ability to grow on the paraoxon and Russian-VX analogs (Scheme 3.5) as the sole phosphorus source. Phosphate free MOPS minimal medium was supplemented with 1.0 mM of the triester, 0.1 % glucose and 0.1 μg/mL thiamin. A 20 mL culture was inoculated with 5% (v/v) from the overnight culture. Additional metal was found to have an inhibitory effect in this case.

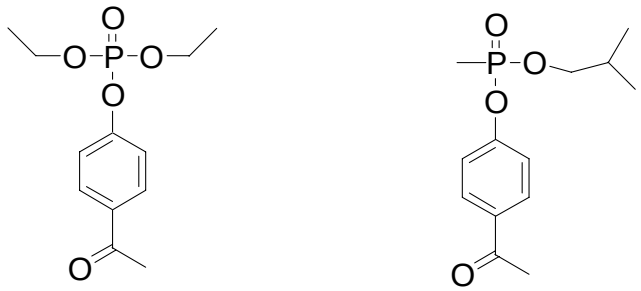

17 18

Scheme 3.5. Chemical structures of the organophosphate triesters used to test the *in vivo* selection under phosphate limiting conditions.

Results

Expression and Purification of Glycerophosphodiester Diesterase (GpdQ)

GpdQ was cloned from genomic DNA of *E. aerogenes* into the pET30 plasmid and expressed in *E. coli* BL21-DEIII. GpdQ was purified using size exclusion and anion exchange column chromatography. The overall yield obtained from a 1 liter culture was approximately 30-40 mg of purified protein (Table 3.2). The diesterase activity is associated with ~ 31 kDa band on SDS-PAGE. GpdQ elutes from an equilibrated Superdex gel filtration column at a volume equivalent to a molecular weight of 200 kDa. This suggests that the protein is a hexamer. Specific activity of GpdQ towards the hydrolysis of 1.0 mM bis-pNPP was enhanced 2-fold and 4-fold when the assay included 0.1 mM $ZnCl_2$ and $MnCl_2$, respectively. Atomic absorption analysis of the purified protein indicated that GpdQ contains 1.0 equivalents of Mn^{2+} and 0.6 equivalents of Zn^{2+}.

Table 3.2. Summary of the purification steps of GpdQ from *E. aerogenes*.

Purification step	Volume (mL)	Protein (mg/mL)	Activity (unit/mL)	Total mg	Total units	Specific activity (u/mg)
Cell lysis	30	110	113	3,300	3,400	1.3
Protamine sulfate	33	22	82	730	2,700	3.7
$(NH_4)_2SO_4$ pellet	12	32	270	384	3,200	8.4
$(NH_4)_2SO_4$ supernatant	31	6.0	0.8	186	5.0	0.1
Superdex 200	100	2.0	17.0	200	1,700	8.5
Resource Q	65	1.2	10.5	78	715	8.8
2^{nd} Superdex 200	30	1.3	12	39	360	9.2

Substrate Specificity of GpdQ

The substrate specificity of GpdQ towards the hydrolysis of various organophosphate diesters and organophosphonates was investigated using compounds listed in Scheme 3.2. This list of potential substrates included analogs of chemical warfare agents for which the corresponding triester is a substrate for PTE. For example, compounds **10, 11, 12, 13,** and **14** are potential analogs of the nerve agents VX, sarin, RVX, soman and GF, respectively. The kinetic parameters of compounds **1-7** were determined by monitoring the production of *p*-nitrophenol at pH 9.0. Hydrolysis of compounds **8-14** was monitored by coupling the reaction to alcohol dehydrogenase and monitoring the production of NADH at pH 9.0.

Kinetic parameters are summarized in Table 3.3. The best substrate for GpdQ was bis-*p*-nitrophenyl phosphate (**1**) with a k_{cat}/K_m value of 6.7×10^3 $M^{-1}s^{-1}$. The substrate specificity of GpdQ followed two major trends. Organophosphate diesters are better substrates than their corresponding phosphonates. For example, the k_{cat}/K_m for the hydrolysis of *O*-ethyl-*p*-NPP (**2**) is 2-fold higher than the corresponding ethyl-*p*NPP (**3**). This feature was more pronounced in the case of *O*-phenyl-*p*NPP (**6**) where the catalytic efficiency was 10-fold higher than phenyl-*p*NPP (**7**). The second feature that emerged from the substrate specificity profile is that the turnover number for organophosphate diesters with a *p*-nitrophenol leaving group is significantly higher than the turnover number for the corresponding aliphatic diester. However, the K_m values are lower for alkyl diesters. For example, the k_{cat}/K_m for the hydrolysis of *O*-ethyl-*p*-NPP (**2**) is 400-fold higher than the k_{cat}/K_m value for diethyl phosphate (**9**).

Nuclear magnetic resonance (NMR) was employed to monitor the hydrolysis of four GpdQ substrates—diethyl phosphate, *O*-isobutyl methyl phosphonate, *O*-isopropyl methyl phosphonate, and *O*-ethyl methyl phosphonate (**9, 10, 11, 12**). In the *O*-isopropyl methyl phosphonate reaction, the concentration of GpdQ was 54 μM. The decrease in the signal intensity at 25.9 ppm was accompanied by an increase in the methyl phosphonate signal at 20.9 ppm. The NMR spectra for the reaction time course are shown in Figure 3.2A. The area under both resonances was integrated and the product/substrate ratio was plotted against time to obtain the second order rate constant k_{cat}/K_m (Figure 3.2B). The k_{cat}/K_m value was calculated as 0.83 ± 0.03 $M^{-1}s^{-1}$. Similarly, the reduction of the *O*-isobutyl methyl phosphonate signal at 27.1 ppm was accompanied by an increase in the methyl phosphonate signal intensity at 21.2 ppm. The concentration of GpdQ was 9.3 μM and the k_{cat} value was calculated as 0.22 ± 0.008 s^{-1} (Figure 3.3A and B). The rates obtained from the NMR assay are in agreement with the rates obtained using the alcohol dehydrogenase coupling assay.

Table 3.3. Kinetic parameters for the hydrolysis of organophosphate diesters and methyl phosphonate monoesters by GpdQ.

Substrate	k_{cat} (s^{-1})	K_m (mM)	k_{cat}/K_m ($M^{-1}s^{-1}$)
1	6.0 (0.2)	0.9 (0.11)	6.7×10^3 (500)
2	2.0 (0.05)	0.9 (0.08)	2.1×10^3 (10^2)
3	0.5 (0.006)	0.4 (0.03)	1.2×10^3 (92)
4	1.6 (0.04)	1.3 (0.1)	1.2×10^3 (74)
5	1.0 (0.04)	6.5 (0.5)	169 (15)
6	4.0 (0.1)	1.8 (0.1)	2.2×10^3 (178)
7	2.8 (0.29)	13 (2.1)	215 (42)
8	5.0×10^{-4} (1.2×10^{-5})	0.006 (0.001)	82 (14)
9	1.0×10^{-3} (5.0×10^{-5})	0.2 (0.04)	5.0 (1.0)
10	ND	ND	2.2 (0.15)
11	0.01 (7×10^{-4})	19.0 (2.1)	0.51 (0.02)
12	0.1 (6×10^{-3})	3.3 (0.56)	33 (4.3)
13	ND	ND	ND
14	0.3 (0.02)	27 (3.0)	11 (0.54)

A

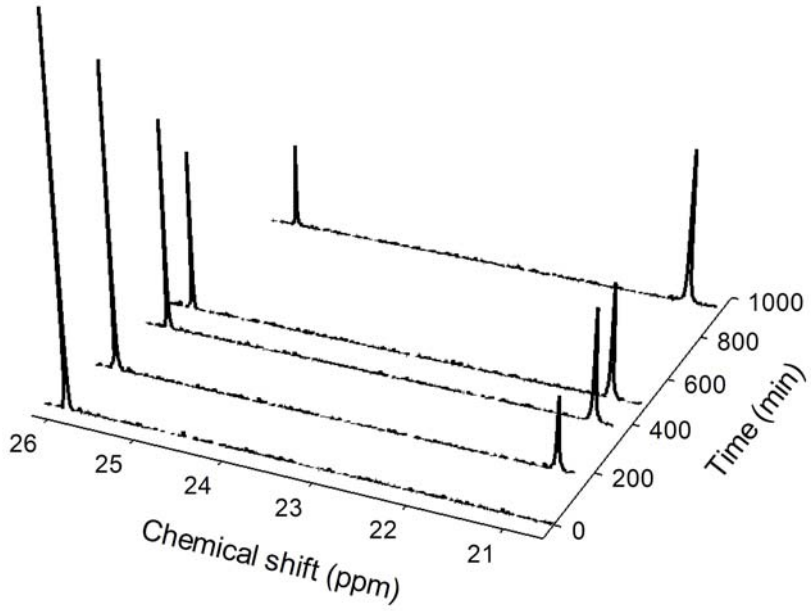

B

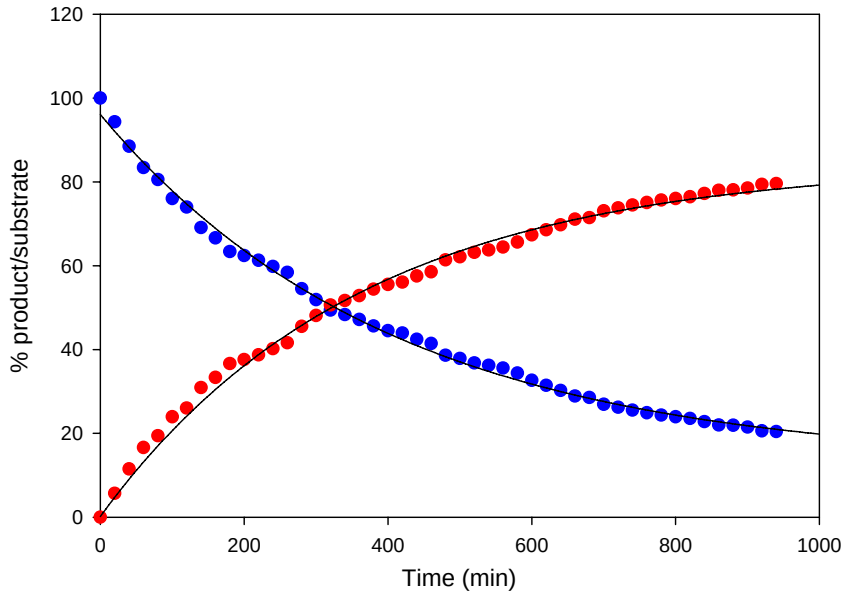

Figure 3.2. GpdQ-catalyzed hydrolysis of *O*-isopropyl methyl phosphonate (10 mM) monitored by NMR (A). The amount of protein used was 54 μM and k_{cat}/K_m was calculated as 0.83 ± 0.03 $M^{-1}s^{-1}$ (B).

A

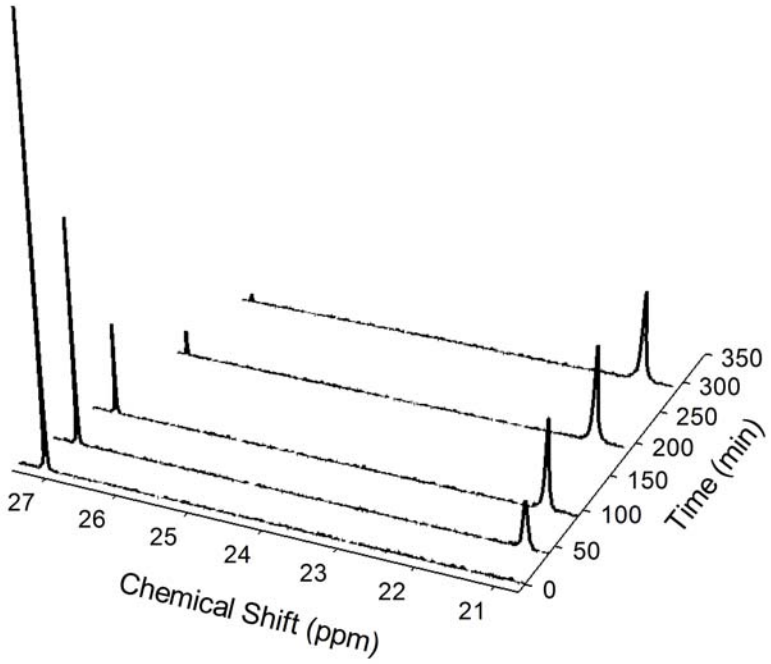

B

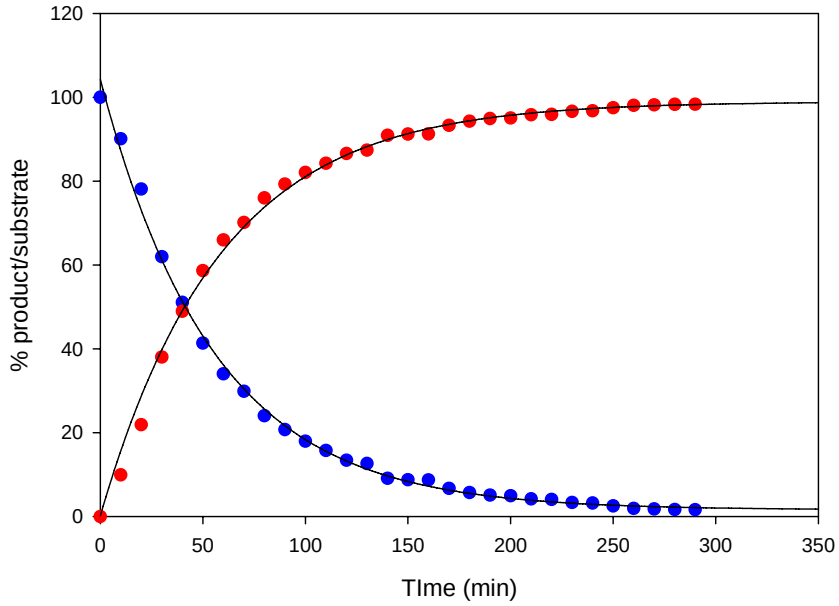

Figure 3.3. GpdQ-catalyzed hydrolysis of *O*-isobutyl methyl phosphonate (10 mM) monitored by NMR (A). The amount of protein used was 9.3 μM and the turnover number was calculated as 0.22 s^{-1} ± 0.008 (B).

In a similar experiment, the enzymatic hydrolysis of diethyl phosphate (**10**) was also monitored by NMR. The reaction mixture contained 10 mM substrate and 73 μM enzyme. The turnover number obtained for diethyl phosphate (**9**) hydrolysis is 0.015 ± 0.002 s^{-1} (Figure 3.4A). GpdQ catalyzed hydrolysis of *O*-ethyl methyl phosphonate (**10**) was monitored by NMR using 45 μM enzyme. The k_{cat}/K_m value for substrate decay over time was calculated as 2.2 ± 0.25 $M^{-1}s^{-1}$ (Figure 3.4B).

GpdQ did not exhibit any measurable activity for the soman analog monoester (**14**). Based on NMR spectra, less than 10% of the substrate was hydrolyzed after five-day incubation with 48 μM enzyme. This was further confirmed by the alcohol dehydrogenase coupling assay.

Hydrolysis of Organophosphate Triesters

It has been previously reported that GpdQ has the ability to hydrolyze organophosphate triesters such as methyl paraoxon and methyl demeton-S (McLoughlin et al., 2004). Figure 3.5A shows the time course for the hydrolysis of paraoxon by 77 μM GpdQ. The total concentration of paraoxon (20 μM) was determined using KOH hydrolysis and the turnover number was calculated as 8.7 x 10^{-6} s^{-1}. This is approximately 10^5-fold lower than the rate obtained for the corresponding diester, *O*-ethyl-*p*-nitrophenyl phosphate.

A

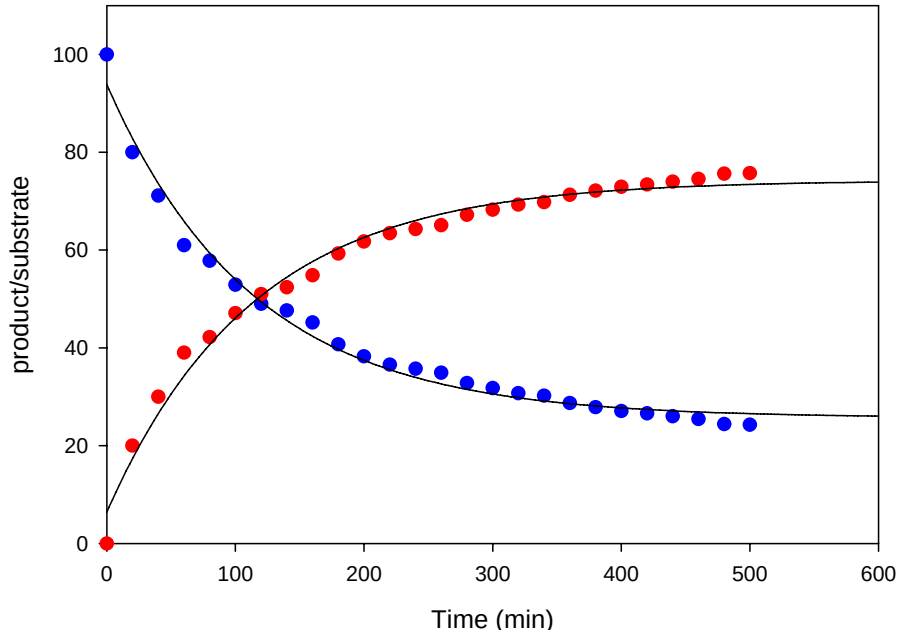

B

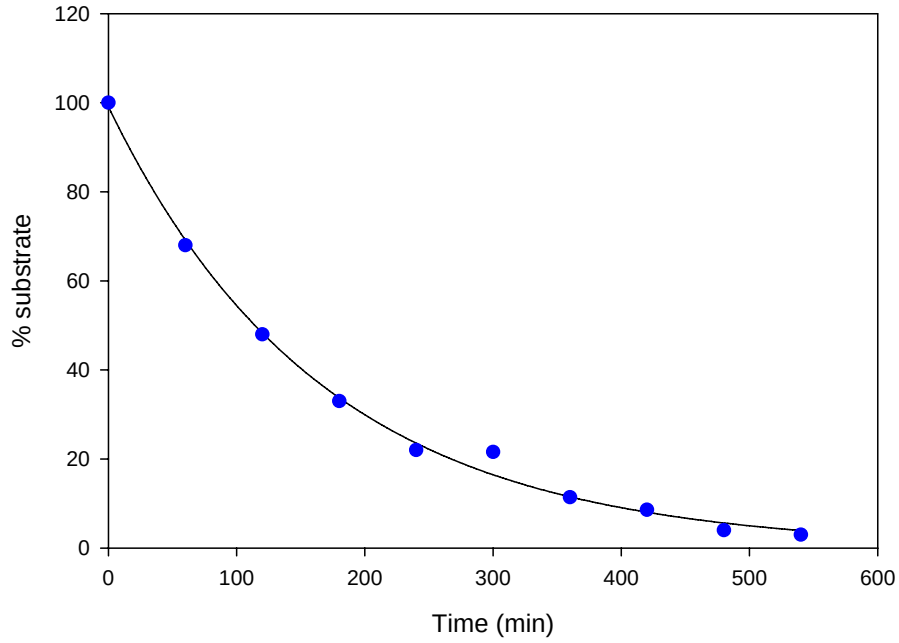

Figure 3.4. Hydrolysis of 10 mM DEP using 73 µM GpdQ (A) and 10 mM *O*-ethyl methyl phosphonate using 45 µM GpdQ (B).

GpdQ was further tested for its ability to hydrolyze a racemic mixture of *O*-methyl-*O*-ethyl-*p*-nitrophenyl phosphate (Figure 3.5B). The turnover number obtained for this compound is 6.8 x 10^{-5} s^{-1}, which is 10-fold higher than k_{cat} value for paraoxon hydrolysis. The initial fast phase shown in Figure 3.5B could be due to a diester contaminant in the racemic mixture.

Hydrolysis of Organophosphate Monoesters

In comparison to the rates obtained for the hydrolysis of organophosphate diesters, the activity of GpdQ toward the hydrolysis of 28 μM *p*-nitrophenyl phosphate was measured using 11 μM enzyme. The turnover number was 1.3x 10^{-4} s^{-1}, which is 10^5-fold lower than the turnover number for the corresponding diester. This is consistent with the previously reported activity profile of GpdQ (Gerlt et al., 1975).

Hydrolysis of Methyl-demeton-S and DEVX

GpdQ catalyzed hydrolysis of methyl-demeton-s was monitored using NMR and the spectrophotometeric Ellman assay. Figure 3.6A shows the NMR spectra of 10 mM methyl-demeton-s incubated with 52 μM GpdQ and 10 mM DTNB at pH 8.0. At time zero there is one major resonance at 35.2 ppm that corresponds to the substrate. The substrate resonance was diminishing as a second resonance at 4.7 ppm was increasing. Integration of the area under both resonances indicated that after 7.5 hours, 30% of the substrate was hydrolyzed.

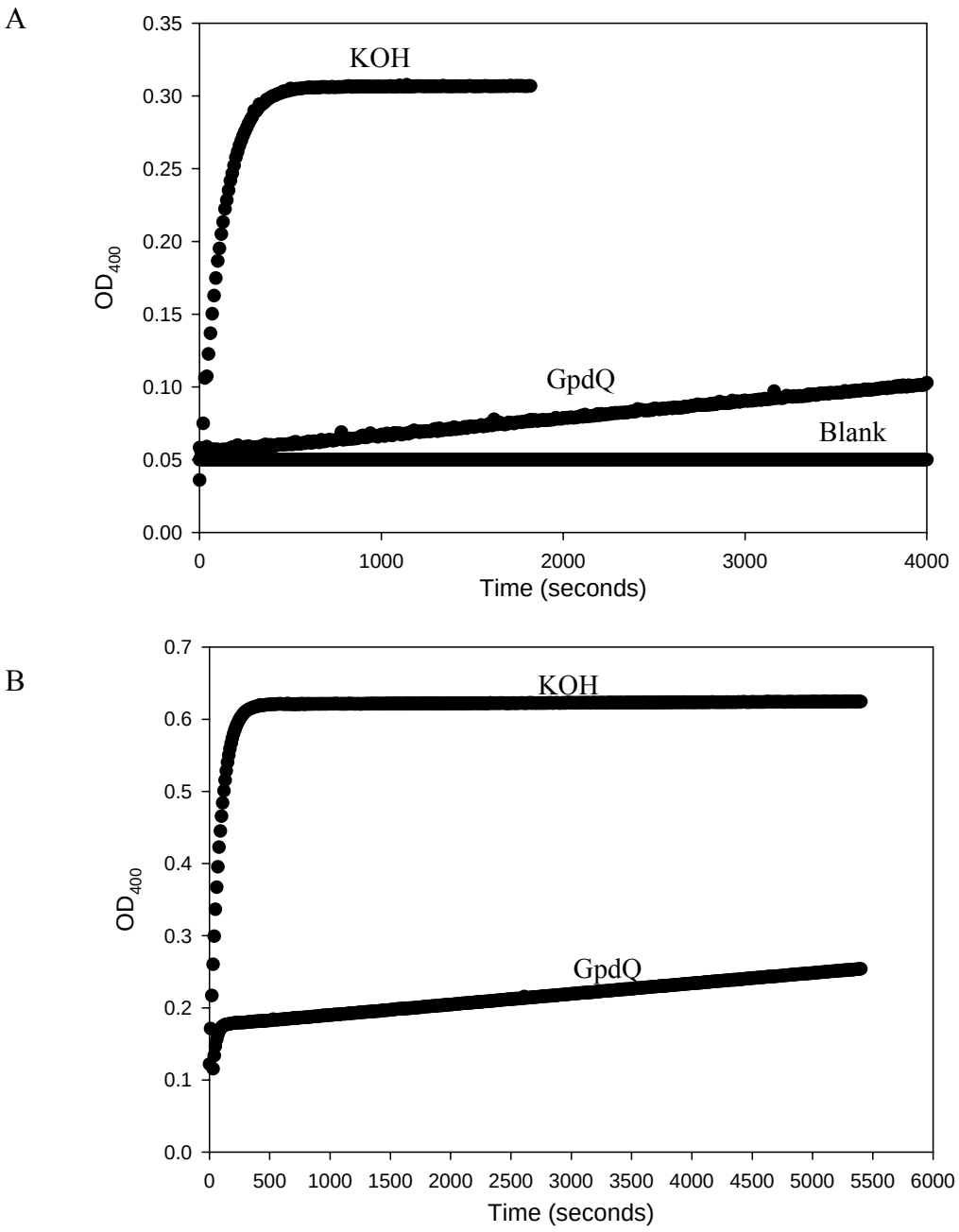

Figure 3.5. Hydrolysis of organophosphate triesters by GpdQ. (A)Time course for GpdQ-catalyzed hydrolysis of paraoxon. The total concentration of paraoxon (20 uM) was determined using KOH. The enzyme concentration was 77 μM and the turnover number was calculated as 8.7x 10^{-6} s^{-1}. (B) Hydrolysis of 40 μM racemic mixture of *O*-methyl, *O*-ethyl-*p*NPP using 13 μM GpdQ. The k_{cat} was calculated as 6.8x 10^{-5} s^{-1}.

In a parallel experiment, the GpdQ catalyzed hydrolysis of methyl-demeton-S was monitored spectrophotometrically using the DTNB coupling assay. Figure 3.6B shows the time course for the hydrolysis of 36 μM methyl-demeton using 23 μM GpdQ. A fit of the data to equation 4 provides two first order rate constants. The observed rate constant for the initial fast phase was 0.002 (1.0×10^{-5}) s^{-1} with an amplitude of 0.128 (3.0×10^{-4}). Dividing the observed rate constant by the enzyme concentration yields a k_{cat}/K_m value of 89 $M^{-1}s^{-1}$. The observed rate constant for the second phase was 0.0002 (2.2×10^{-6}) s^{-1} with an amplitude of 0.08 (2.0×10^{-4}). This provides a k_{cat}/K_m value of 9.0 $M^{-1}s^{-1}$. Based on the final absorbance determined by the PTE mutant H254Q/H257F, the reaction was approximately 50% completed. Figure 3.7 shows the hydrolysis of 36 μM methyl-demeton using 25 μM GpdQ presented in terms of concentration of product released. After 60 minutes, an additional 25 μM enzyme was added, which drove the reaction to completion. It appears that the enzyme is inhibited after a single turnover of the substrate.

A similar inhibitory effect was observed for DEVX hydrolysis. Shown in Figure 3.8, is the time course for the hydrolysis of 29 μM DEVX using 16 μM GpdQ. A fit of the time course to equation 4 provided two first order rate constants; 0.0027 (7.2×10^{-6}) s^{-1} and 0.0004 (2.3×10^{-6}) s^{-1} with an amplitude of 0.154 and 0.04, respectively. This corresponds to k_{cat}/K_m values of 169 $M^{-1}s^{-1}$ and 25 $M^{-1}s^{-1}$ for the fast and slow phase, respectively.

A

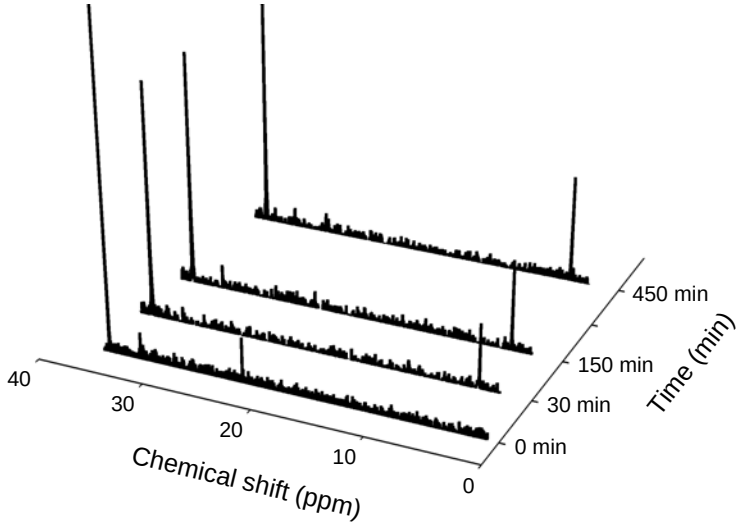

B

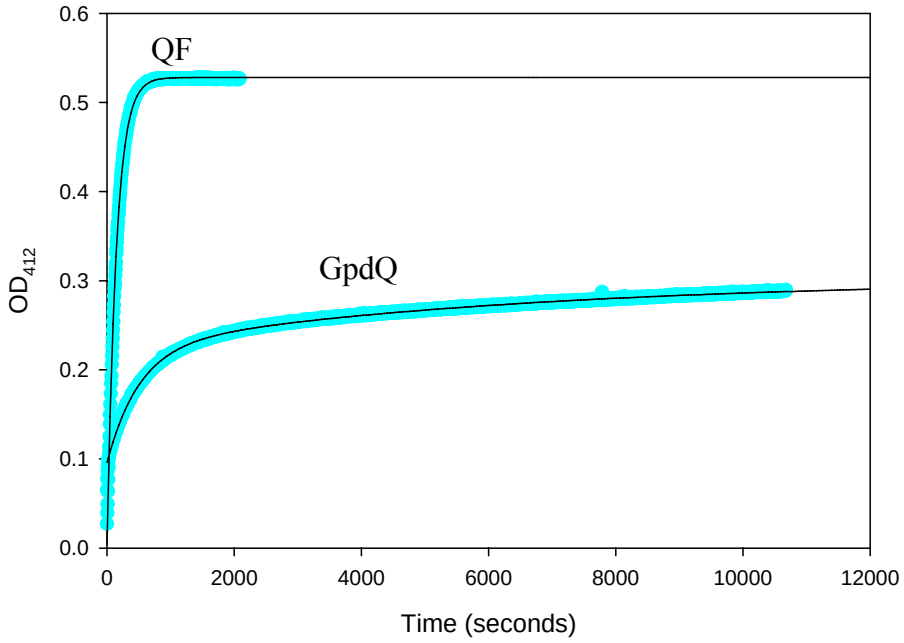

Figure 3.6. Hydrolysis of methyl-demeton-S by GpdQ. (A) NMR spectra for the hydrolysis of methyl-demeton-S by GpdQ. (B) time course for the DTNB coupling assay. Concentration of GpdQ was 23 µM and the rates calculated as 89 $M^{-1}s^{-1}$ and 9 $M^{-1}s^{-1}$ resulting in 10-fold difference.

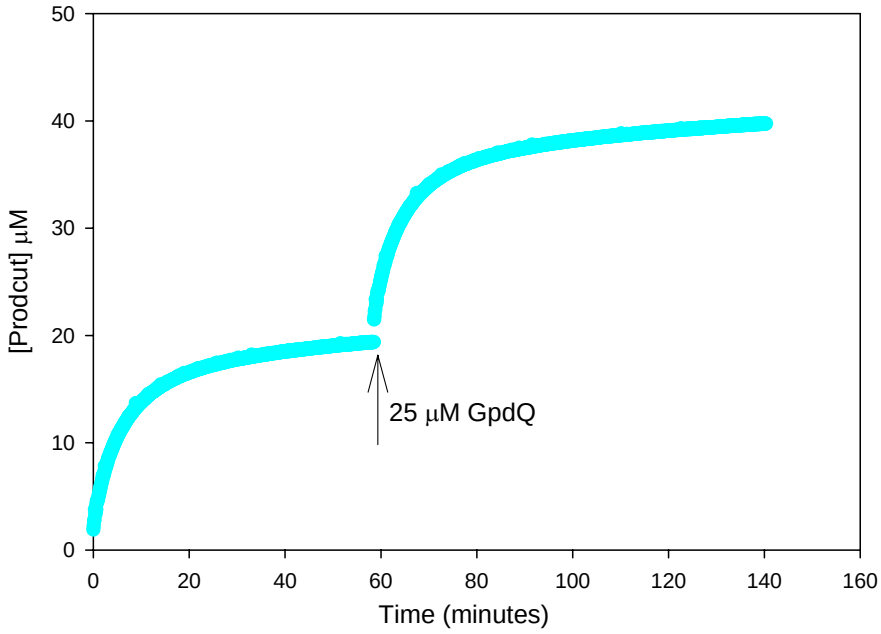

Figure 3.7. Hydrolysis of 36 μM methyl-demeton-S presented in terms of concentration of product released. GpdQ concentration was 25 μM.

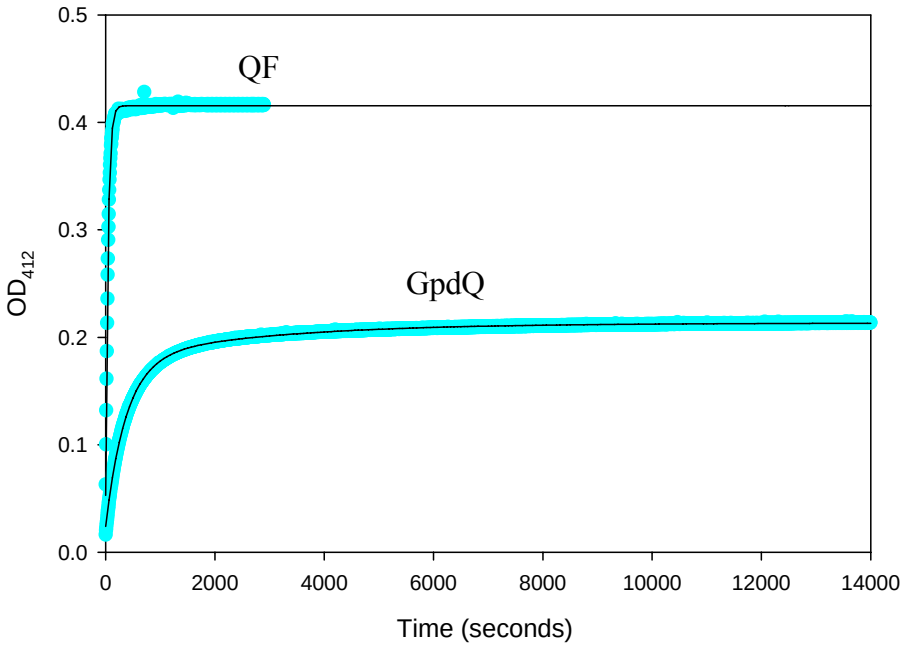

Figure 3.8. GpdQ-catalyzed hydrolysis of DEVX. The amount of enzyme used was 16 μM. The rates were caluculated as 169 $M^{-1}s^{-1}$ and 25 $M^{-1}s^{-1}$ resulting in 7-fold difference.

Growth of GpdQ+ Cells on Organophosphates/phosphonates

Cells expressing GpdQ were tested for their ability to grow on several organophosphate diesters and organophosphonate monoesters under inorganic phosphate limiting conditions. Substrates tested were diethyl phosphate, *O*-isopropyl methyl phosphonate, *O*-isobutyl methyl phosphonate, and the soman analog (**9, 11, 12**, **13,** and **14** in Scheme 2). Figures 3.9 and 3.10 show a graphical representation of the growth of GpdQ- and GpdQ+ cells in the presence of 1.0 mM substrate. As positive and negative controls, GpdQ- and GpdQ+ cells were grown in the presence and absence of 1.0 mM potassium phosphate, respectively. *E. coli* cells lacking the diesterase gene were unable to utilize any of the substrates as a source of phosphorus, and were able to grow only when the minimal medium was supplemented with inorganic phosphate or methyl phosphonate. The methyl phosphonate time course was obtained on a different day using the same number of cells to inoculate the 20 mL culture. On the other hand, GpdQ+ cells were able to grow on three of the four substrates tested. As anticipated, growth rate was proportionally related to the catalytic efficiency of GpdQ towards each substrate. For example, cells growing on *O*-isopropyl methyl phosphonate as the phosphorus source experienced a lag time of nearly three days, which corresponds to the k_{cat}/K_m value of 0.5 $M^{-1}s^{-1}$. In contrast, cells growing on *O*-isobutyl methyl phosphonate displayed a lag phase of approximately 30 hours corresponding to a k_{cat}/K_m value of 33 $M^{-1}s^{-1}$. Unsurprisingly, the soman analog did not support the growth of GpdQ+ cells which is consistent with the results obtained from the *in vitro* assays.

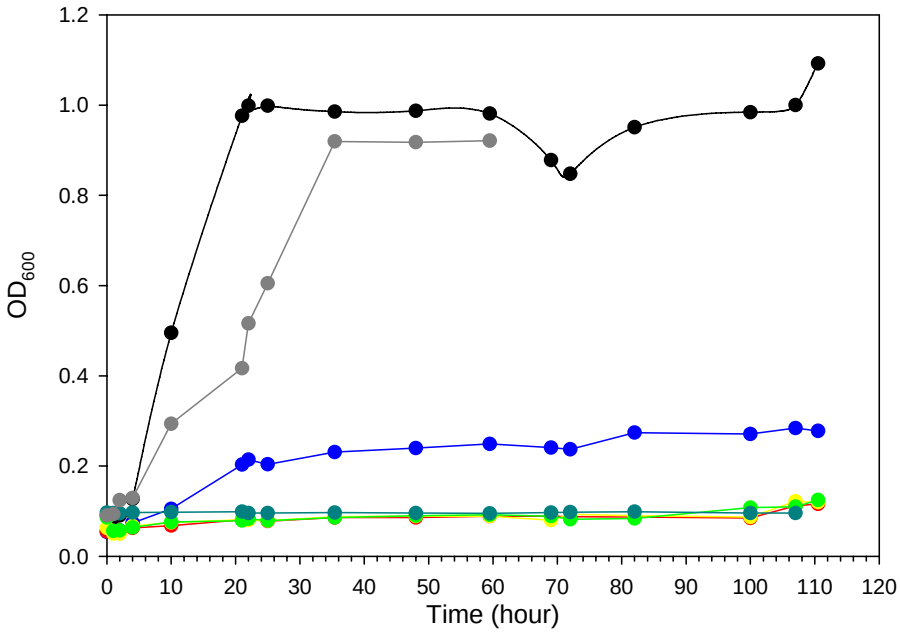

Figure 3.9. Growth of BL21–DEIII (GpdQ-) cells in the presence of organophosphates as the sole phosphorus source. Substrates that were tested included: inorganic phosphate (●), diethyl phosphate **9** (●), isoproyl methyl phophonate **11** (●), isobuty methyl phosphonate **12** (●), mono-ester of soman analog **13** (●), methyl phosphonate (●) and no phosphate source (●). Substrate concentration was 1.0 mM in 1X phosphate free MOPS minimal media, pH 7.4.

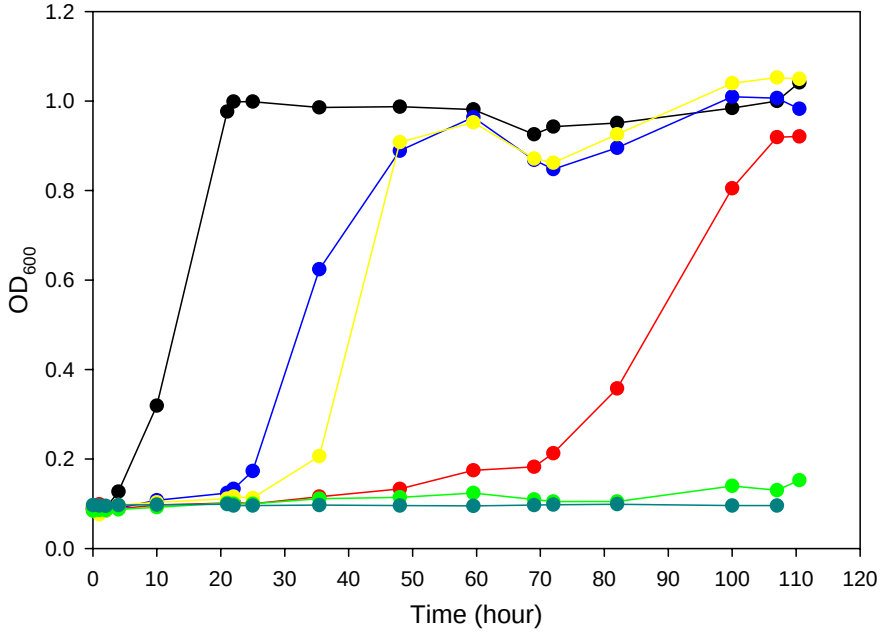

Figure 3.10. Growth of GpdQ+ cells in the presence of organophosphates as the sole phosphorus source. Substrates that were tested included: inorganic phosphate (●), diethyl phosphate **9** (●), isoproyl methyl phophonate **11** (●), isobuty methyl phosphonate **12** (●), mono-ester of soman analog **13** (●), and no phosphate source (●). Substrate concentration was 1.0 mM in 1X phosphate free MOPS minimal media, pH 7.4.

Effect of Various Phenols on the Growth Rate of E. coli

Since the *in vivo* hydrolysis of organophosphate triesters releases a phenol leaving group in the growth culture, *E. coli* was tested for its growth tolerance to the presence of different phenols (Figure 3.11). Of the three phenols tested, *p*-nitrophenol was the most toxic to *E. coli* and significantly inhibited its growth. In contrast, *p*-chlorophenol and *p*-hydroxyacetophenone displayed a slight inhibitory effect, that could possibly be due to the prsence of 1.0% methanol. Therefore, organophosphate triesters with a *p*-hydroxyacetophenone leaving group are more suitable for *in vivo* selection compared to substrates containing *p*-nitrophenol.

Growth of E. coli Co-expressing PTE and GpdQ on Organophosphate Triesters as the Sole Phosphorus Source

The goal of this experiment was to test the ability of E. coli cells co-expressing PTE and GpdQ to grow on the organophosphate triesters, shown in Scheme 5, as the sole phosphorus source. The rate constant kcat/Km for the hydrolysis of 18 (Scheme 3.5) by wild type PTE is 2 x 106 M-1s-1.

Time course for the hydrolysis of the RVX analog (**19**) by wild type PTE showed two phases with k_{cat}/K_m values of 6 x 10^5 $M^{-1}s^{-1}$ and 1.3 x 10^4 $M^{-1}s^{-1}$ for the fast and slow phase, respectively. GpdQ+ electro-competent cells were transformed with wild type PTE and the PTE construct provided by Dr. Tawfik, pET20b-5S. A graphical representation of the growth rate is shown in Figure 3.12.

The results from this growth assay are promising. The length of the lag time for *E. coli* growing under phosphate starvation is dependent on the hydrolysis of the triester substrate by PTE. The 10-fold difference in expression level between the wild type PTE and the pET20b-5S construct was very recognizable in the growth assay as the GpdQ+/pET20b-5S cells growing on the paraoxon analog (**18**) experienced a lag time as short as 5 hours. In addition, the 10-fold difference in the k_{cat}/K_m values between the **18** and **19** influenced the bioavailability of the diester in the culture. GpdQ+/pET20b-5S cells growing on the RVX analog exhibited a 2-fold longer lag time than the cells utilizing the DE substrate as a phosphate source.

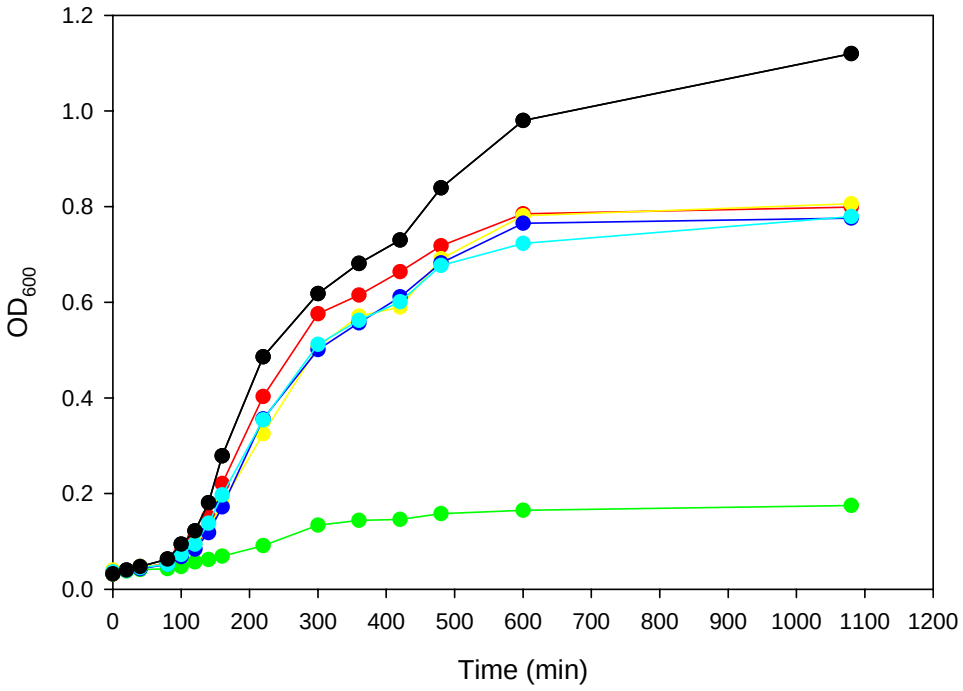

Figure 3.11. Time course for the growth of *E. coli* BL21-DEIII in the presence of various phenol leaving groups. Leaving groups that were tested included: phenol (●), *p*-nitrophenol (●), *p*-chlorophenol (●), and *p*-hydroxy acetonphenone (●). As control, cells were grown in the absence of any phenols (●) and in the presence of 1% methanol (●). Phenol concentration was 1.0 mM.

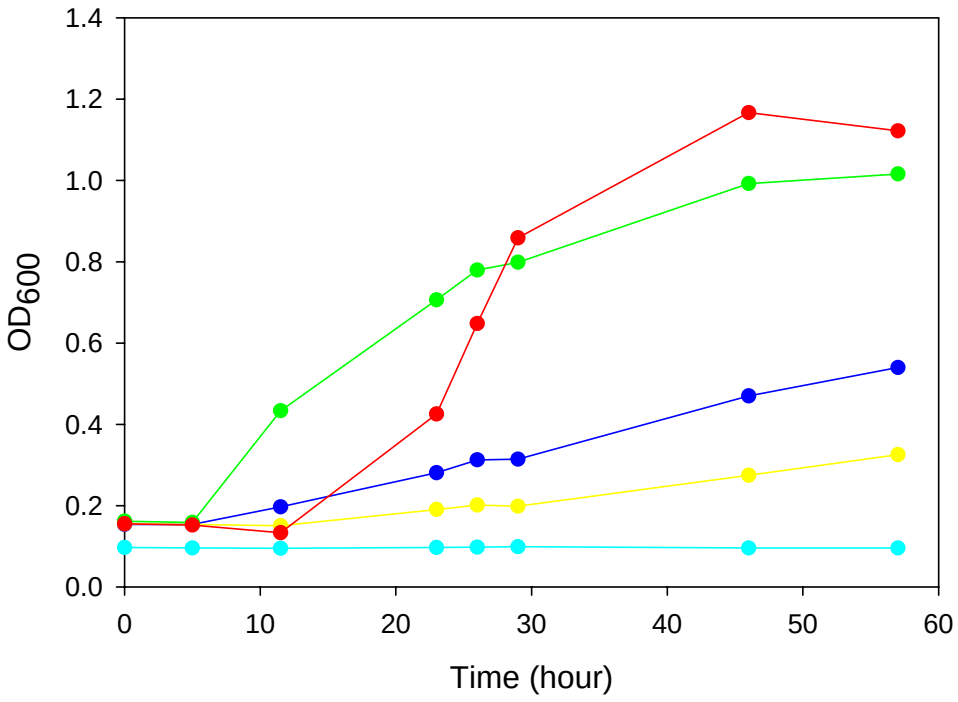

Figure 3.12. Time course for the growth of *E. coli* co-expressing PTE and GpdQ in the presence of organophosphate triesters as the sole phosphorus source. Strains that were tested included: GpdQ+/WT PTE on the paraoxon analog **18** (●), GpdQ+/WT PTE on the RVX analog **19** (●), GpdQ+/pET20b-5S on the paraoxon analog **18** (●), GpdQ+/pET20b-5S on the RVX analog **19** (●), and GpdQ+ cell with no substrate (●). Substrate concentration was 1.0 mM in 1X phosphate free MOPS minimal medium, pH 7.4.

Discussion

Substrate Specificity of GpdQ

When applicable, *in vivo* selection is a powerful tool for identifying interesting mutants in a directed evolution experiment. The use of PTE co-expressed with GpdQ to enable *E. coli* to utilize organophosphate triesters as the sole phosphorus source is limited to the substrate promiscuity of the diesterase. Therefore, the substrate specificity of GpdQ was examined using a series of structurally diverse organophosphate diesters and phosphonate monoesters. Consistent with previously published data (Gerlt et al., 1975, and McLoughlin et al., 2004), GpdQ predominantly exhibits a diesterase activity and minimal monoesterase activity. GpdQ displayed the highest activity towards the hydrolysis of bis-*p*NPP with a k_{cat}/K_m value of 6.7×10^3 $M^{-1}s^{-1}$. It is not unusual for bacterial diesterase to be able to hydrolyze bis-*p*NPP (Vogel et al., 2002, Shenoy et al., 2005). A comparison of the k_{cat}/K_m values for *p*-nitrophenyl phosphates with their corresponding *p*-nitrophenyl phosphonates shows that GpdQ preferentially hydrolyzes the phosphate diesters over the phosphonate monoesters. For example, the k_{cat}/K_m value for the hydrolysis of *O*-phenyl-*p*-nitrophenyl phosphate is an order of magnitude higher than the k_{cat}/K_m for phenyl-*p*-nitrophenyl phosphonate. The same trend was observed when comparing the k_{cat}/K_m values for *O*-ethyl-*p*-nitrophenyl phosphate with ethyl-*p*-nitrophenyl phosphonate.

The catalytic efficiency for the hydrolysis of alkyl phosphodiesters and phosphonate monoesters is significantly lower compared to the substrates containing the *p*-nitrophenol leaving group. For example, the k_{cat}/K_m for the hydrolysis of diethyl

phosphate (DEP) is 5 $M^{-1}s^{-1}$. However, it is sufficient to support the growth of *E. coli* under phosphate limiting conditions. GpdQ is thought to be the first enzyme isolated with the ability to hydrolyze alkyl diesters. A second enzyme that was isolated from *Delftia acidovorans* was shown to enable *E. coli* to utilize DEP as the sole phosphorus source as well (Tehara et al., 2003). No catalytic parameters for DEP hydrolysis has been published for this enzyme yet.

GpdQ was also able to utilize methyl phosphonate monoesters as substrate to support the growth of *E. coli* under phosphate starvation conditions. This is the first reported activity of GpdQ with this class of compounds. The highest catalytic efficiency obtained (k_{cat}/K_m = 33 $M^{-1}s^{-1}$) was for *O*-isobutyl methyl phosphonate, which is a monoester analog for the nerve agent Russian-VX. GpdQ did not display any measurable activity towards the hydrolysis of the soman analog (**13**, Scheme 3.2).

Hydrolysis of Methyl-demeton-s and DEVX

Initial characterization by Ollis and colleagues indicated that GpdQ hydrolyzes methyl-demeton-S with a 10-fold less specific activity than bis-*p*NPP at pH 8.0 (McLoughlin et al., 2004). GpdQ was tested for its ability to hydrolyze the phosphotriester thiolates, methyl-demeton-s and DEVX. The time course for the hydrolysis of methyl-demeton-S showed an initial fast phase followed by a slower phase with a rate ratio of 10. The final OD_{412} indicates that approximately 50% of the substrate remains unhydrolyzed. Similarly, the NMR spectra revealed that 30% of the substrate was hydrolyzed after 7.5 hours and the product observed at 4.7 ppm is not

dimethyl phosphate (DMP). To determine the identity of the resonance at 4.7 ppm, 10 mM DMP (chemical shift is 3.0 ppm) was hydrolyzed using 32 μM GpdQ at pH 8.0. After an overnight incubation, the DMP was completely hydrolyzed to methyl phosphate, which resonates at 4.7 ppm. Therefore, the product resonance observed in the NMR of methyl-demeton-S hydrolysis corresponds to methyl phosphate. There are two possible scenarios for generating methyl phosphate from me-demeton (Scheme 3.6). Since no diester intermediate is observed in the current NMR spectra, it is not possible to determine if methyl phosphate is generated via route A or B in Scheme 3.6.

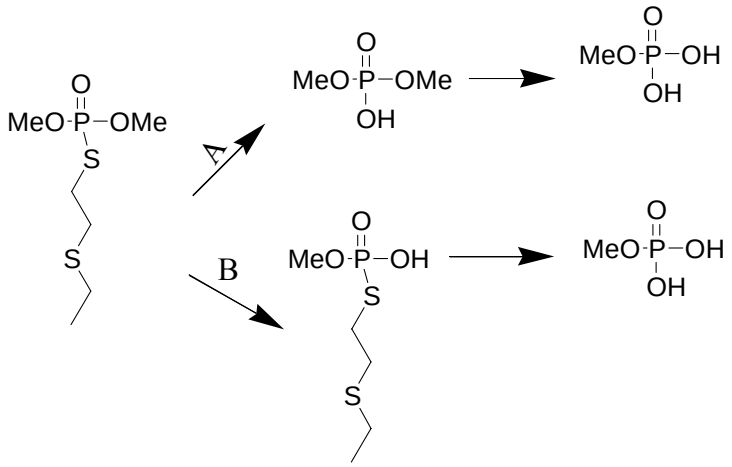

Scheme 3.6. Two possible routes for generating the dimethyl phosphate observed in the NMR spectra of GpdQ catalyzed hydrolysis of methyl-demeton-S.

The apparent inhibition of methyl-demeton hydrolysis when monitored by NMR is probably due to the inhibition of GpdQ by the free thiol liberated from DTNB hydrolysis. Similar to methyl-demeton-S, the time course for the hydrolysis of DEVX with GpdQ also resulted in two phases with a rate ratio of approximately 7-fold. The

second order rate constants for the fast and slow phase were calculated as 168 $M^{-1}s^{-1}$, and 25 $M^{-1}s^{-1}$ respectively, that is slightly higher than the rated obtained for methyl-demeton-S.

In Vivo *Growth Assays*

E. coli BL21-DEIII cells expressing GpdQ were examined for their ability to utilize various organophosphate diesters and methyl phosphonate monoesters as a source for inorganic phosphate. As anticipated, the observed growth rate was faster for substrates with higher rates of hydrolysis. For example, cells growing on *O*-isopropyl methyl phosphonate showed a longer lag time than cells growing on DEP or *O*-isobutyl methyl phosphonate. Similarly, the soman analog **13** did not support the growth of *E. coli* since it is not a substrate for GpdQ.

The results from the *in vivo* assays for cells co-expressing GpdQ with PTE appear promising. Two variables were considered: i) the intracellular concentration of PTE, and ii) the specific activity of PTE towards the hydrolysis of the substrates tested. When GpdQ was co-expressed with PTE, it was clear that a faster growth rate was obtained for the faster substrate, paraoxon analog **17**. In the case of pET20b-5S, the over-expression of PTE is enhanced approximately 10-fold. This difference in the intracellular concentration of PTE was evident as a significantly shorter lag time for the paraoxon analog was observed. A comparison of the growth rates for GpdQ+/pET20b-5S cells using the paraoxon analog and the Russian-VX analog **18** suggests that the lag phase is clearly dependent on the activity of PTE. However, as the diesters are

produced, the 6-fold difference in k_{cat}/K_m for DEP and *O*-isobutyl methyl phosphonate can be noticed in the exponential phase as the cell growing on RVX analog appear to be growing slightly faster.

Potential Applications and Future Direction

Based on the results obtained from the *in vivo* growth assays, co-expression of PTE and GpdQ appears to be a promising approach for directed evolution of PTE. Under the current conditions, the growth rate is limited by PTE activity. Since the stereoselectivity of sarin, soman, VX, and R-VX hydrolysis by PTE is a critical issue for efficient detoxification, this approach could be applied for the selection of variants with enhanced catalytic efficiency towards the hydrolysis of the most toxic stereoisomer. The employment of *in vivo* selection for variants with enhanced activity towards the hydrolysis of phosphorothiolates is dependent upon further investigations with regard to the inhibition of GpdQ during the time course of the reaction.

CHAPTER IV

CELLULAR LOCALIZATION OF PHOSPHOTRIESTERASE: CAN PTE BE TRANSLOCATED TO THE PERIPLASM OF *ESCHERICHIA COLI* ?

Introduction

Directed evolution strategies have been widely employed to mimic natural evolution for developing enzymes with enhanced catalytic efficiency, altered substrate specificity, improved thermostability or enantioselectivity. A combination of ep-PCR and saturation mutagenesis was utilized to enhance the enantioselectivity of a bacterial lipase from *P. aeruginosa* (Liebeton et al., 2000). The best variant contained five amino acid substitutions and displayed a 25-fold enhancement in enantioselectivity over the wild type enzyme. Another remarkable example that demonstrated the power of directed evolution is the evolution of a glyphosate tolerance gene (Castle et al., 2004). The catalytic efficiency of the enzyme glyphosate *N*-acetyltransferase (GAT) was improved 10^4-fold after eleven rounds of DNA shuffling. In addition to enhanced activity, the evolved GAT displayed higher thermostability compared to the wild type.

The success of a directed evolution experiment is dependent on the size of the library and the choice of a suitable selection and/or screening approach to identify desired variants (Soumillion et al., 2001). Unlike high throughput screening techniques where every clone must be tested, *in vivo* selection links the survival of a host to the desired function. Therefore, selection is very powerful for isolating interesting variants from large size random libraries. The power of *in vivo* selection was illustrated by

Kagamiyama and co-workers in a study aimed at evolving the *E. coli* aspartate aminotransferase (ApsAT) to a valine aminotransferase (Yano et al., 1998). Their work relied on using the *ΔilvE::kan* strain for which the gene for branched chain amino acids aminotransferase was knocked out. After five rounds of mutagenesis and selection, they isolated an AspAT variant with five orders of magnitude improvement in the catalytic efficiency for valine and 2-oxovaline compared to the native enzyme.

This chapter aims at the potential use of *in vivo* selection to identify variants of phosphotriesterase with enhanced activity towards the hydrolysis of phosphorothiolates. The selection strategy is based on utilizing a substrate that releases cysteine upon hydrolysis by PTE (Scheme 4.1).

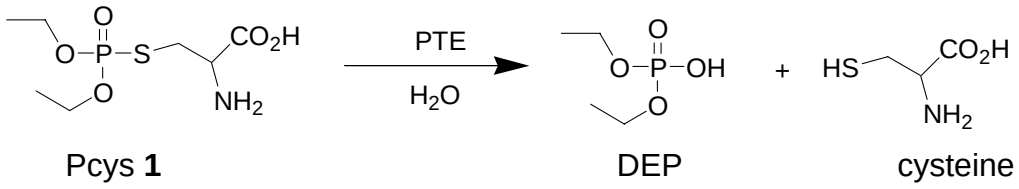

Scheme 4.1. The hydrolysis of Pcys **1** to liberate cysteine and diethyl phosphate.

A major requirement for this system is an *E. coli* strain that cannot synthesize cysteine, a cysteine auxotroph. The *E. coli* cysteine biosynthesis pathway is shown in Scheme 4.2. It starts with the acetylation of L-serine to *O*-acetyl serine by the *cycE* gene product, serine acetyl transferase. *O*-acetyl serine is then converted to cysteine by the gene products of *cysE* and *cysK*.

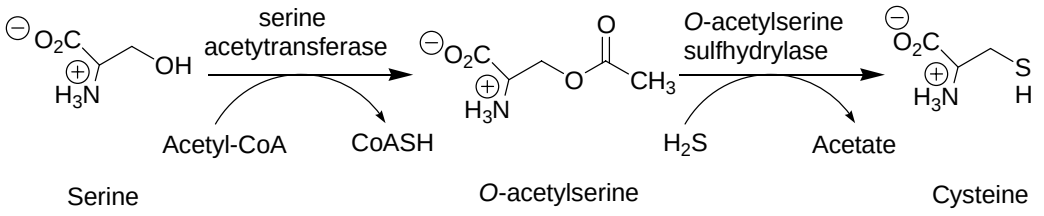

Scheme 4.2. The biosynthesis of cysteine in *E. coli* K12.

The first reaction in cysteine biosynthesis cannot take place in the *E. coli* RY1633 strain in which the *cysE* gene has been deleted. Hence, the survival of RY1633 cells expressing PTE will be linked to the hydrolysis of Pcys **1**. One of the *in vivo* selection limitations is the intercellular availability of the substrate of interest. To overcome this constraint, the export of PTE into the periplasmic space of *E. coli* is discussed.

Materials and Methods

Materials

Restriction enzymes and T4 DNA ligase were purchased from New England Biolabs. Wizard Plus SV miniprep DNA Purification System was obtained from Promega. *Flavobacterium sp.* was purchased from ATCC (ATCC 27551). Proteinase K and egg white lysozyme were purchased from Sigma-Aldrich. *Pfx platinum* DNA polymerase was obtained from Invitrogen. The cysteine leaving group containing VX analog (Pcys **1**) was synthesized in our laboratory by Dr. YingChung Li. The medium copy number expression vector, pZA32-luc, and the cysteine auxotroph *E. coli* strain, RY1633 (Table 4.1) were generously provided by Dr. Ryland Young, Department of

Biochemistry and Biophysics. DNA sequencing was performed in the GTL, Texas A&M University. Oligonucleotides were obtained from the Integrated DNA Technologies (IDT). Antibodies against PTE were raised in rabbits at the Alpha Diagnostic Intl. Inc., San Antonio, TX. The serum collected was used as the primary antibody for all Western blot experiments.

Kinetic Measurements

All kinetic measurements ware performed on a SPECTRAmax-340 plate reader (Molecular Devices Inc, Sunnyvale CA). Paraoxon hydrolysis was measured by monitoring the release of *p*-nitrophenol (ε_{400} = 17,000 $M^{-1}cm^{-1}$) at pH 9.0. The DTNB coupling assay was utilized to monitor the hydrolysis of Pcys **1** at pH 8.0. The reaction of glucose-6-phosphate dehydrogenase was used to monitor the spheroplast formation. The enzymatic assay contained 3.0 mM glucose-6-phosphate, 2.0 mM $NADP^+$, 3.0 mM $MgCl_2$. The production of NADPH (ε_{340} = 6.22 $mM^{-1}cm^{-1}$) was monitored at pH 8.0. The kinetic parameters were obtained by fitting the data to equation 1, where *v* is the initial rate, V_{max} is the maximal velocity, K_m is the Michaelis constant, and [S] is the substrate concentration.

$$v = V_{max}\,[S]/K_m + [S] \qquad (1)$$

Cloning of the PPTE and the PhoA::PTE Constructs

Flavobacterium sp. strain ATCC 27551 was grown in LB medium at 30 °C for 24 hours. The plasmid containing the *opd* gene was isolated and used as the template for the PCR amplifictaion using *pfx platinum* DNA polymerase. The PPTE was cloned using the primers, opd-5'-*KpnI* and opd-3'-*AvrII* (Table 4.2). PCR conditions were 95 °C for 30 seconds, followed by 30 cycles of 95 °C for 1 min, 55 °C for 1 min, 68 °C for 4 min. and final extension at 68 °C for 10 min. The 1,100 bp PCR product was purified, digested with *KpnI* and *AvrII*, and ligated into a similarly digested pZA32-luc. The ligation product was transformed in *E. coli* XL1-blue electro-competent cells for DNA sequencing. The plasmid pJK01 served as a template for constructing the phoA::PTE fusion protein using the primers phoA-ss-linker and opd-3'-*AvrII* (Table 4.2).

Growth Conditions for the Cysteine Selection

The *E. coli* RY1633 cys^- strain was transformed with wild type PTE and the H254A mutant. An overnight culture was grown in Luria-Bertani medium containing 0.05 mg/mL kanamycin at 37 °C and 0.025 mg/mL Chloramphenicol. Cells were washed 3 times with sterile MQ water before inoculation in the minimal medium. The M9 based minimal medium was supplemented with 0.4 % glucose, 0.01 mg/mL thymine, 0.05 μg/mL thiamin, 20 μg /mL Pcys **1,** 0.05 mg/mL kanamycin, and 0.025 mg/mL chloramphenicol. All amino acids, except for cysteine and methionine, were added to the minimal medium to a final concentration of 0.02-0.1 mg/mL. The OD_{600} was monitored at 30 °C for 48 hours.

Table 4.1. Description of plasmids and strains used in chapter IV.

Plasmid/Strain	Description	Reference
pZA32-Luc	A medium copy number, chloramphenicol resistant, *tac* promoter expression vector	Obtained from Dr. Young
pZA32-opd	Wild type PTE cloned in pZA32-luc plasmid	
pZA32-PPTE	Full length PTE cloned from *Flavobacterium sp.* into the pZA32-luc vector	
PhoA::PTE	Wild type PTE fusion to the phoA signal peptide	
RY1633	cycE::TN5, cyc^-, thy^-, thi^-, kan r, P1 from CBK 286	Obtained from Dr. Young

Table 4.2. Sequence of the primers used in chapter IV.

Primer	Sequence (5'-3')
opd-5'-*KpnI*	CCC GGC CAC GGT ACC ATG CAA ACG AGA AGG GTT GTG CTC
opd-3'-*AvrII*	CCG GGT ACC CCT AGG TCA TCA TCA TGA CGC CCG CAA GGT C
phoA-ss-linker	GCC CGC GAC GGT ACC ATG AAA CAA AGC ACT ATT GCA CTG GCA CTC TTA CCG TTA CTG TTT ACC CCT GTG ACA AAA GCA AGC CTG GCA TCG ATC GGC ACA GGC GAT CGG ATC

Spheroplast Formation

Spheroplasts from RY1633 cells expressing PTE were formed according to the previously published procedure (Broome-Smith et al., 1986). Cells from a 30 mL culture were harvested by centrifugation at 7000 rpm at 4 °C. Cells were then resuspended in 250 μL of 30 mM Tris-HCl, pH 8.0 containing 25% sucrose. EDTA and egg white lysozyme were added to final concentration of 5 mM and 100 μg/mL, respectively. Finally, 250 μL MQ water were added and the cells were incubated at room temperature for 3 minutes. The periplasmic contents were isolated by centrifugation at 12,000 x g for 10 minutes. Cytoplasmic contents were extracted by treating the spheroplasts with the Bugbuster reagent. 50 μL spheroplast aliquots were incubated with and without proteinase K and incubated at room temperature for 30 minutes. The proteinase K digestion was quenched by the addition of PMSF to a final concentration of 1 mM. Cellular fractions were analyzed by SDS-PAGE and western blotting.

Results

Growth of RY1633 at Different Concentrations of Cysteine

The cysteine auxotroph RY1633 strain was tested for its ability to grow on different concentrations of cysteine. Figure 4.1 shows a graphical representation of the growth of RY1633 in the presence of 0, 1, 2, 4, 8, and 10 μg/mL cysteine in 1X M9 minimal medium. While the optimum concentration of cysteine required to complement the auxotroph strain was 8-10 μg/mL, a slow growth rate was observed at concentrations

as low as 1 μg/mL cysteine. In addition, growth of RY1633 in minimal medium supplemented with 10 μg/mL was not affected by the presence of 20 μg/mL Pcys **1**, which indicates that Pcys did not exert any toxicity on *E. coli*.

Growth of RY1633 Expressing PTE Utilizing Pcys as a Source of Cysteine

To examine the feasibility of the cysteine auxotroph based *in vivo* selection, the kinetic parameters for the hydrolysis of Pcys **1** by wild type PTE and the H254A mutant were determined using the DTNB coupling assay (Table 4.3). Although the turnover number is very similar for both proteins, the K_m for H254A was 22-fold lower resulting in a 30-fold enhancement in k_{cat}/K_m over wild type.

The RY1633 cells expressing wild type PTE and the H254A mutation were tested for their ability to utilize Pcys **1** as a source of cysteine. The growth curve of the cys^- strain in minimal medium supplemented with 20 μg/mL Pcys **1** is shown in Figure 4.2. As can be seen in Figure 4.2, the cys- cells expressing PTE were able to grow only when the medium was supplemented with cysteine, and could not use Pcys **1** to complement the cysteine deficiency. The 30-fold enhancement in catalytic efficiency that H254A displayed over wild type did not seem to enhance the growth rate. This observation has raised the question regarding the bioavailability of the substrate, Pcys **1**, and whether it is able to permeate the cellular membrane to the cytoplasm where PTE is expressed.

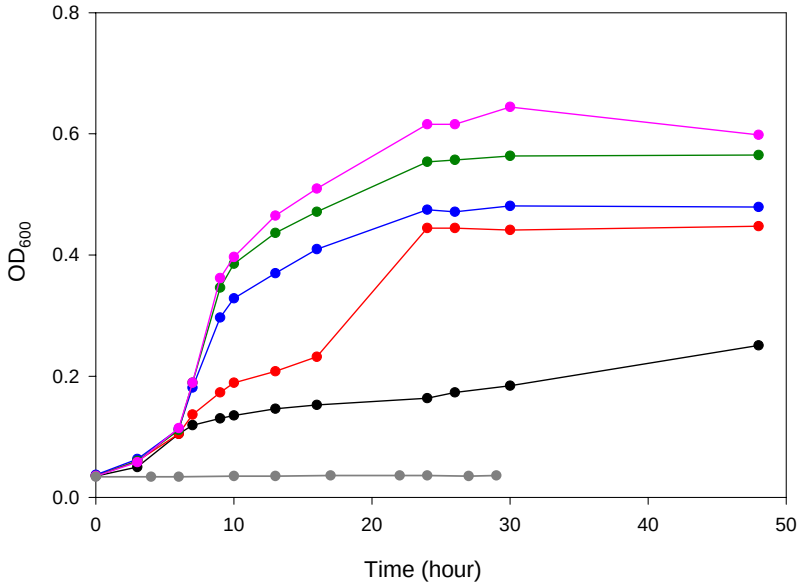

Figure 4.1. Growth curve of the RY1633 cys$^-$ strain in 1X M9 based minimal medium. The culture was supplemented with; 0 (●), 1.0 (●), 2.0 (●), 4.0 (●), 8.0 (●), and 10.0 (●) µg/mL cysteine. OD_{600} was monitored at 30 °C for 48 hours.

Table 4.3. Kinetic parameters for the hydrolysis of Pcys **1** by wild type PTE and the H254A mutant.

Protein	k_{cat} (s^{-1})	K_m (mM)	k_{cat}/K_m ($M^{-1}s^{-1}$)
Wild type	0.1 (0.006)	6.1 (0.9)	16.4 (0.5)
H254A	0.14 (0.006)	0.27 (0.04)	504 (50)

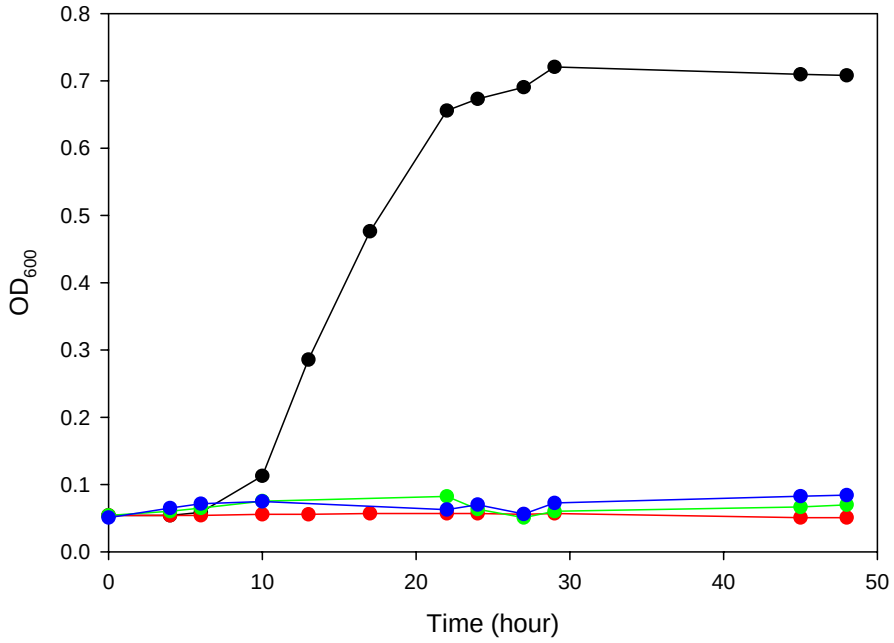

Figure 4.2. Growth of RY1633 expressing PTE in the presence of Pcys as a source of cysteine. Cells were transformed with wild type PTE (●) and the H254A (●) mutant in 1X M9 minimal medium supplemented with 20 μg/mL Pcys. As control, cells were grown in the absence of cysteine (●) and in the presence of 10 μg/mL cysteine (●). Cells were incubated at 30 °C and growth was monitored by measuring the change in OD_{600}.

The native PTE is expressed in *Flavobacterium sp.* with a leader sequence that enables the protein to be translocated to the periplasmic space (Mulbry et al., 1989). In an attempt to express PTE in the periplasm of *E. coli*, the full length *opd* gene was cloned from *Flavobaterium sp*. into the expression vector, pZA32-Luc resulting in the construct pZA32-PPTE. The cellular location of PTE was determined by spheroplast formation followed by SDS-PAGE fractionation and detection by Western blot. To ensure that no serious spheroplast lysis occurred during the extraction, the activity of the cytoplasmic enzyme, glucose-6-phosphate dehydrogenase, was measured using 3.0 mM glucose-6-phosphate. Figure 4.3A shows that wild type PTE expressed in the cytoplasm was, in fact, retained in the spheroplast fraction. The majority of the PPTE protein was also present in the spheroplast fraction despite the fact that it was processed to the mature length PTE. A small fraction of PPTE remained in the spheroplast fraction without being digested with the signal peptidase. Table 4.4 shows the total units measured for PTE and glucose-6-phosphate dehydrogenase in the periplasmic fraction and in the spheroplast. The cellular location of PTE was verified by testing its susceptibility to digestion by proteinase K. Figure 4.3B shows that neither wild PTE nor PPTE was susceptible to proteinase K in the spheroplast. Purified PTE (2.5 μg) was completely digested with 1.0 mg/mL proteinase K after 10 min incubation at room temperature (data not shown).

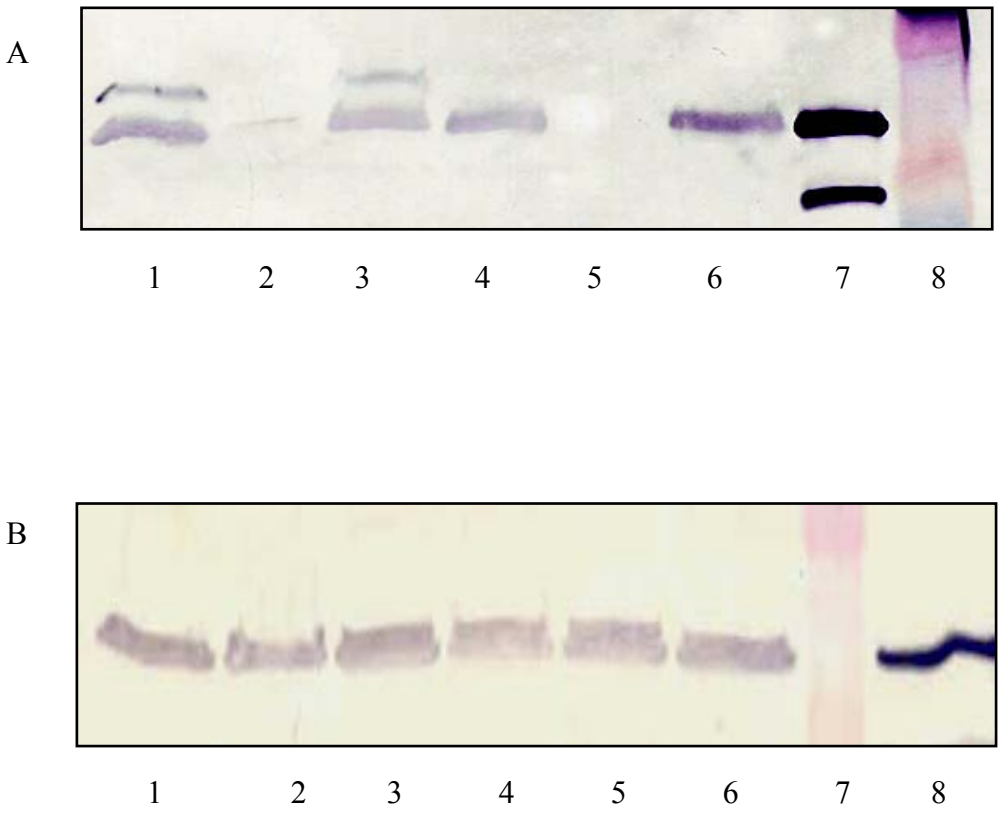

Figure 4.3. Cellular fractionation of *E. coli* expressing the PTE and PPTE constructs. (A) Western blot analysis of subcellular fractions of cells expressing PTE and PPTE. 1) PPTE spheroplast 2) PPTE periplasmic fraction 3) PPTE total cellular fraction 4) PTE spheroplast 5) PTE periplasmic fraction 6) PTE total cellular fraction 7) Purified PTE 8) Molecular weight marker. (B) Sensitivity of PTE and PPTE to proteinase K 1) PPTE, no proteinase K 2) PPTE 0.2 mg/mL proteinase K 3) PPTE 1.0 mg/mL proteinase K 4) PTE, no proteinase K 5) PTE, 0.2 mg/mL proteinase K 6) PTE, 1.0 mg/mL proteinase K 7) Molecular weight marker 8) Purified PTE.

Table 4.4. Activity (total units) of PTE and glucose-6-phosphate dehydrogenase in the periplasmic fraction and the spheroplast of PTE and PPTE. The PTE assay contained 1.0 mM paraoxon and 50 mM CHES buffer, pH 9.0. The glucose-6-phosphate dehydrogenase contained 3.0 mM G-6-P, 2.0 mM NAD^+, 3.0 mM $MgCl_2$, and 50 mM HEPES buffer, pH 8.0.

	Wild type PTE Total units (μmol min^{-1})		PPTE Total units (μmol min^{-1})	
Enzyme	Periplasmic fraction	Spheroplast fraction	Periplasmic fraction	Sheroplast fraction
PTE	0.2	8.5	0.06	3.8
Glucose-6-phosphate dehydrogenase	0.023	3.5	0.01	3.0

Cloning and Expression of the PhoA::PTE Construct

Since PTE was not translocated to the periplasm using its native signal peptide, the 21 amino acids leader sequence of alkaline phosphatase (PhoA) was utilized in an attempt to express PTE in the periplasmic space. The phoA::PTE construct was expressed in RY1633 cells using the pZA32-Luc expression vector. The first construct did not contain a linker between the phoA signal sequence and PTE. Expression of that construct and western blot analysis indicated that the leader sequence of phoA was not processed (data not shown). The second construct contained the ser-leu-ala linker. It was suggested that a short linker is required for recognition by the signal peptidase (Dodt et al., 1986). Cellular fractionation of RY1633 cells expressing the phoA::PTE construct indicated that both the full length and the processed forms of PTE remained soluble in the spheroplast (Figure 4.4). The cytoplasmic fraction was concentrated 10-fold in this experiment. Table 4.5 shows that most of the PTE activity was in the cytoplasmic fraction.

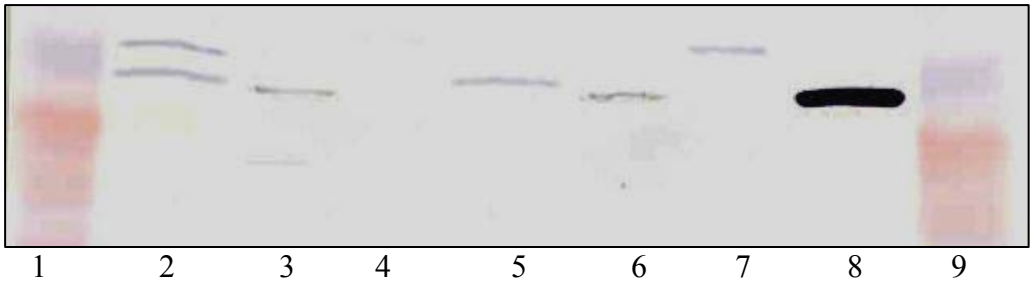

Figure 4.4. Cellular localization of wild type PTE and the phoA::PTE construct. Lanes 1 and 9) Molecular weight marker 2) PhoA::PTE, insoluble fraction 3) phoA::PTE, cytoplasmic fraction. 4) PhoA::PTE, periplasmic fraction 5) PTE, insoluble fraction 6) PTE, cytoplasmic fraction 7) PTE, periplasmic fraction 8) Purified PTE.

Table 4.5. Activity (total units) of PTE and glucose-6-phosphate dehydrogenase in the periplasmic, cytoplasmic, and spheroplast fractions of PTE and phoA::PTE. The PTE assay contained 1.0 mM paraoxon and 50 mM CHES buffer, pH 9.0. The glucose-6-phosphate dehydrogenase contained 3.0 mM G-6-P, 2.0 mM NAD^+, 3.0 mM $MgCl_2$, and 50 mM HEPES buffer, pH 8.0.

Enzyme	Wild type PTE Total units (μmol min^{-1})			phoA::PTE Total units (μmol min^{-1})		
	Periplasmic fraction	Cytoplasmic fraction	Insoluble fraction	Periplasmic fraction	Cytoplasmic fraction	Insoluble Fraction
PTE	0.12	7.0	0.2	0.02	1.8	0.01
G-6-P dehydrogenase	0.018	3.6	ND	0.04	3.0	ND

Discussion:

In Vivo *Selection using the cys⁻ RY1633 Strain*

In Chapter III of this dissertation, *in vivo* selection based on a deficiency of a vital chemical element, phosphorus, in the growth medium was discussed. In this chapter, a different *in vivo* selection approach where cysteine is required for the genetic complementation of a cys⁻ strain was investigated. The *E. coli* K12 strain, RY1633, is not capable of synthesizing the amino acid cysteine due to a deletion in the *cycE* gene. Therefore, this strain was used to test the ability of wild type PTE and the H254A mutant to complement the cysteine deficiency via hydrolysis of the substrate Pcys **1**. The results obtained from the growth experiments showed that the RY1633 cells transformed with PTE were able to survive only when the minimal medium was supplement with cysteine. Although the catalytic efficiency of H254A is 30-fold higher than the wild type enzyme for the hydrolysis of Pcys **1**, RY1633 cells expressing H254A were not able to grow in the absence of cysteine.

In vivo selection based on genetic complementation of an amino acid deficiency has been previously described. Penicillin amidase from *E. coli*, an enzyme involved in the production of semi-synthetic antibiotics, was subjected to random mutagenesis to isolate mutants for enhanced hydrolysis of glutaryl-L-leucine, which is not a substrate for the wild type enzyme (Forney et al., 1989). Desired variants were isolated based on the growth of a leucine auxotroph *E. coli* in minimal medium supplemented with glutaryl-L-leucine as the sole source of leucine. More recently, the gene encoding glutaryl acylase from *Pseudomonas* SY-77 was a target for saturation mutagenesis

experiments to identify variants with enhanced activity for the hydrolysis of adipyl-7-ADCA, an intermediate in the semi-synthesis of cephalosporin antibiotics (Sio et al., 2004). This system utilized a serine derivative, which upon hydrolysis, liberates serine and, therefore, supports the growth of a serine auxotrophic bacterial strain.

In both examples, the target enzyme was translocated across the cytoplasmic membrane to the periplasmic space of the bacterial host, which enhanced the bioavailability of the substrate. In the case of PTE, the enzyme is expressed in the cytoplasm. Since the Pcys substrate is expected to carry a negative and a positive charge at the experimental pH, it is unlikely for the substrate to be able to pass through the cellular membrane to the cytoplasm where PTE is located. Therefore, attention was drawn to secretion of PTE into the periplasmic space of *E. coli*.

Cloning and Expression of Full Length PTE (PPTE) from Flavobaterium sp.

Initial characterization of PTE indicated that the protein is expressed with an N-terminal domain that functions as a signal sequence for protein transport in *Flavobacterium sp*. Since the deletion of that signal peptide has enhanced the specific activity of PTE, the protein has been routinely expressed in the cytoplasm. For the selection purposes, it is preferred to have the target protein secreted into the periplasmic space. Therefore, full length PTE (PPTE) was cloned into the pZA32-luc expression vector and expressed in *E. coli*. However, cellular fractionation showed that both the PPTE and wild type PTE forms were retained soluble in the cytoplasm and were not exported. The paraoxonase activity of both the periplasmic fraction and the spheroplast

was in agreement with the majority of PTE retained in the cytoplasm, although the activity of the PPTE form was approximately 2-fold less than the wild type PTE. This is consistent with the results obtained from a study conducted in the Wild's Lab. Their findings indicated that the leader sequence of PTE was able to secrete alkaline phosphatase into the periplasm, but it was not successful in exporting PTE (Dave et al., 1993)

Cloning and Expression of the PhoA::PTE Construct

In another attempt to translocate PTE into the periplasm, the 21 amino acid signal peptide of the periplasmic protein, alkaline phosphatase (PhoA), was used to construct the phoA::PTE fusion. The fusion protein was expressed in the RY1633 strain under the *ptac* promoter. Western blot analysis of subcellular fractionation of the phoA::PTE fusion indicated that the signal sequence of approximately 50% of the protein was digested, while the protein remained soluble in the spheroplast. The rest of the protein was in the full length form and also remained in the spheroplast.

Based on the results of this investigation, it was not possible to translocate PTE into the periplasmic space using its native signal sequence or the alkaline phosphatase signal peptide. Thus far, the reason for this is not clear. A possible explanation might be that PTE is not recognized by the *E. coli* SecB and, therefore, the newly synthesized polypeptide chain is folded into its native conformation without being exported. Sec B, a component of the *E. coli* Sec machinery, is an anti-folding molecular chaperone which binds to the unfolded protein precursor and delivers it to the SecY/E protein for

translocation (Wicker et al., 1991). This limitation can be circumvented by *in vivo* co-overexpression of Sec B. Overexpression of molecular chaperones such as SecB or DnaK was successful in enhancing the export of human cytokines into the periplasmic space of *E. coli* (Bergès et al., 1996).

Using a different signal peptide could be beneficial in targeting PTE to the periplasm. Cha and co-workers have demonstrated that a fraction of PTE was exported to the periplasm of *E. coli* using the pelB signal sequence (Kang et al., 2006). Although the activity for paraoxon hydrolysis of the pelB::PTE::His_6 fusion was 10-fold lower than the cytosolic PTE, they showed that approximately 67% of total cellular activity was associated with the periplasmic fraction.

A more recently characterized export pathway is the Tat pathway (DeLisa et al., 2002). Unlike the Sec pathway, the Tat-dependent pathway is specific for partially folded or folded proteins. Proteins translocated via the Tat pathway contain a signal peptide with the conserved sequence motif, S/TRRXFLK at the N-region and a positively charged amino acid at the C-region of the leader sequence. The leader peptide of PTE contains the signature sequence, MQTRRVVLKS, but it does not contain any positively charged residues at the C-region. To target PTE to the periplasm via the Tat pathway, the leader sequence can be slightly modified for better recognition by the Tat machinery.

CHAPTER V

SUMMARY AND CONCLUSIONS

Phosphotriesterase has displayed a great potency in hydrolyzing a wide range of the extremely toxic organophosphate pesticides and nerve agents. In addition, PTE is the only enzyme known to hydrolyze the V-series nerve agents including VX and Russian-VX. However, the catalytic efficiency for the hydrolysis of phosphorothiolates and phosphonothiolates like VX is significantly lower. Chapter II of this dissertation aimed at modifying the active site of PTE for enhanced hydrolysis of the VX analogs, diisopropyl amiton (DEVX) and demeton-S. Previous investigations of the substrate binding pocket of PTE have demonstrated that the substrate specificity can be altered by simultaneously randomizing the residues His245 and His257. Screening the double substitution library H254X/H257X for the hydrolysis of DEVX led to the identification of two variants with enhanced activity compared to wild type. They were identified as H254G/H257F and H254Q/H257F. The double mutant H254Q/H257F displayed a 10-fold enhancement in k_{cat} and a 3-fold enhancement in k_{cat}/K_m over wild type PTE for the hydrolysis of DEVX. When tested for the hydrolysis of demeton-S, H254Q/H257F exhibited an 18-fold and a 10-fold improvement in k_{cat} and k_{cat}/K_m compared to the wild type.

The substrate binding site of PTE was the target for the first round of random mutagenesis. Twelve single substitution libraries were constructed and screened for the hydrolysis of DEVX. From the H254X library, the mutant H254A showed a 2-fold

enhancement over wild type. The H257S and H257T mutations from the H257X library displayed a slight enhancement compared to wild type for the hydrolysis of DEVX. From the L303X single substitution library, the L303F mutation was approximately 2-fold higher than the wild type. None of the isolated mutations displayed enhancement over the H254Q/H257F control.

The double mutation H254Q/H257F served as a template for constructing the third generation random libraries targeting the active site of PTE. Most mutations in the pZA32-QF/Y309X appeared to be detrimental to DEVX hydrolysis. The QF/Y309E and QF/Y309L were isolated from this library as they displayed similar activity to the QF template. Several variants were isolated from the pZA32-QF/I106X library for displaying a comparable activity to the standard QF. They were identified as QF/I106S, QF/I106P, QF/I106Q, and QF/I106L. The k_{cat}/K_m value for QF/I106Q was very similar to the QF parent, but the k_{cat}/K_m for QF/I106P was 10-fold lower than QF (Table 2.8). Similar to the PZA32-QF/Y309X library, the majority of mutations in the pZA32-QF/L271X were detrimental. Few mutations did not seem to lower the rate of DEVX hydrolysis. They were identified as L271M, L271V, and L271I. No improvements for the hydrolysis of DEVX resulted from screening the pZA32-QF/F306X and pZA32-QF/M317X libraries. All variants isolated were identified as the parent QF except for the QF/M317L mutant, which had a similar activity as the standard QF. From the pZA32-QF/S308X library, variants with valine, cysteine, or lysine at position 308 were isolated for displaying similar activity to the QF template. Results from the F132X library constructed in the QF template have indicated that the vast majority of the

mutations are detrimental to the activity against DEVX. Only two mutants were identified for having beneficial mutations, the QF/F132L and QF/133I mutants. Thus far, H254Q/H257F has the highest improvement for DEVX hydrolysis.

In chapter III of this dissertation, the feasibility of utilizing the phosphodiesterase isolated from *E. aerogenes* (GpdQ) to enable *E. coli* to grow on organophosphate diesters as the sole phosphorus source was discussed. The substrate specificity of GpdQ was investigated using a small library of organophosphate diesters and phosphonate monoesters. The best substrate tested was bis-*p*-nitrophenyl phosphate with a k_{cat}/K_m value of 6.7×10^3 $M^{-1}s^{-1}$. Kinetic measurements indicated that GpdQ preferentially hydrolyzes *p*-nitrophenyl phosphates over their corresponding phosphonates. For example, the k_{cat}/K_m value for the hydrolysis of *O*-phenyl-*p*-nitrophenyl phosphate is 10-fold higher than the k_{cat}/K_m for phenyl-*p*-nitrophenyl phosphonate. The catalytic efficiency for the hydrolysis of alkyl phosphodiesters and phosphonate monoesters is significantly lower compared to the substrates containing the *p*-nitrophenol leaving group.

Results obtained from the *in vivo* growth assays indicated that *E. coli* BL21-DEIII cells could not survive on organophosphate diesters as a source for inorganic phosphate. However, cells expressing GpdQ were able to utilize organophosphate diesters and phosphonate monoesters as the sole phosphorus source with a growth rate comparable to the catalytic efficiency. Based on the findings from the *in vivo* growth assays for *E. coli* cells co-expressing PTE with GpdQ, it was clear that the growth rate is

limited by the intercellular concentration and the catalytic efficiency of PTE rather than the activity of the diesterase GpdQ.

Experiments presented in chapter IV of this dissertation focused on the translocation of PTE into the periplasmic space as a tool for the PTE-aided genetic complementation of cysteine deficiency in the cysteine auxotroph RY1633. Protein export into the periplasm was proven beneficial for the *in vivo* selection experiments which are based on genetic complementation of an amino acid deficiency (Forney et al., 1989 and Sio et al., 2002). The selection scheme is based on the hydrolysis of the Pcys substrate, an analog of phosphorothiolates, by PTE to liberate cysteine. Based on the results obtained from the growth assays using wild type PTE and the H254A mutant, it is thought that the substrate is not able to cross the inner membrane to the cytoplasm where PTE is expressed. It is generally believed that charged molecules will not pass through cell membranes. Since the cysteine auxotroph RY1633 cells expressing wild type PTE and the H254A mutation were not able to utilize the Pcys substrate as a source for cysteine, several attempts were made to export PTE to the periplasm. The full length PTE (containing the native leader sequence) was cloned from *Flavobacterium sp*. and expressed in *E. coli*. Cellular fractionation showed that most of the PTE activity remained in the cytoplasm. Furthermore, expression of PTE with the signal peptide of the periplasmic protein alkaline phosphatase did not facilitate the translocation of PTE across the inner membrane. Currently, two more strategies are being considered. The first is to clone PTE with the signal peptide of pelB which is commercially available.

The second choice is to modify the leader sequence of PTE to make use of the Tat-dependent export pathway.

REFERENCES

Aubert, S.D., Li, Y., Raushel, F.M., 2004. Mechanism for the hydrolysis of organophosphates by the bacterial phosphotriesterase. Biochemistry 43, 5707-5715.

Beckman, R.A., Mildvan, A.S., Loeb, L.A., 1985. On the fidelity of DNA replication: manganese mutagenesis *in vitro*. Biochemistry 24 (21), 5810-5817.

Benning, M.M., Kuo, J.M., Raushel, F.M., Holden, H.M., 1994. Three-dimensional structure of phosphotriesterase: An enzyme capable of detoxifying organophosphate nerve agents. Biochemistry 33, 15001-15007.

Benning, M.M., Hong, S.B., Raushel, F.M., Holden, H.M., 2000. The binding of substrate analogs to phosphotriesterase. J. Biol. Chem. 275, 30556-30560.

Benning, M.M., Shim, H., Raushel, F.M., Holden, H.M., 2001. High resolution X-ray structures of different metal-substituted forms of phosphotriesterase from *Pseudomonas diminuta*. Biochemistry 40, 2712-2722.

Benschop, H.P., Konings, C.A.G., Genderen, J.V., De Jong, L.P.A., 1984. Isolation, anticholinesterase properties, and acute toxicity in mice of the four stereoisomers of the nerve agent soman. Toxicol. Appl. Pharmacol. 72, 61-74.

Benschop, H.P., De Jong, L.P.A., 1988. Nerve agent stereoisomers: Analysis, isolation and toxicology. Acc. Chem. Res. 21, 368-374.

Bergès, H., Joseph-Liauzun, E., Fayet, O., 1996. Combined effects of the signal sequence and the major chaperone proteins on the export of human cytokines in *E. coli*. Appl. Environ. Microbiol. 62, 55-60.

Berman, H.A., Decker, M.M., 1986. Kinetic, equilibrium, and spectroscopic studies on dealkylation ("Aging") of alkyl organophosphonyl acetylcholinesterase. J. Biol. Chem. 261, 10646-10652.

Broome-Smith, J.K., Spratt, B.G., 1986, A vector for the construction of translational fusions to TEM β-lactamase and the analysis of protein export signals and membrane protein topology. Gene 49, 341-349.

Chae, M.Y., Postula, J.F., Raushel, F.M., 1994. Stereospecific enzymatic hydrolysis of phosphorus-sulfur bonds in chiral organophosphate triesters. Bioorg. Med. Chem. Lett. 4, 1473-1478.

Cadwell, R.C., Joyce, G.F., 1992. Randomization of genes by PCR mutagenesis. PCR Methods Appl. 2, 28-33.

Caldwell, S.R., Raushel, F.M., 1991a. Detoxification of organophosphate pesticides using an immobilized phosphotriesterase from *Pseudomonas diminuta.* Biotechnol. Bioeng. 37, 103-109.

Caldwell, S.R., Raushel, F.M., 1991b. Detoxification of organophosphate pesticides using a nylon based immobilized phosphotriesterase from *Pseudomonas diminuta.* Appl. Biochem. Biotech. 31, 59-73.

Castle, L.A., Siehl, D.L., Gorton, R., Patten, P.A., Chen, Y.H., Bertain, S., Cho, H., Duck, N., Wong, J., Liu, D., Lassner, M.W., 2004. Discovery and directed evolution of a glyphosate tolerance gene. Science 304, 1151-1154

Cheng, T.C., Harvey, S.P., Chen, G.L., 1996. Cloning, expression and nucleotide sequence of a bacterial enzyme for decontamination of organophosphorus nerve agents. Appl. Environ. Microbiol. 62, 1636-1641.

Cheng, T.C., DeFrank, J.J., Rastogi, V.K., 1999. *Alteromonas* prolidase for organophosphorus G-agent decontamination. Chem. Biol. Interact. 119-120, 455-462.

Chen-Goodspeed, M., Sogorb, M.A., Wu, F., Hong, S.B., Raushel, F.M., 2001a. Structural determinants of the substrate and stereochemical specificity of phosphotriesterase. Biochemistry 40, 1325-1331.

Chen-Goodspeed, M., Sogorb, M.A., Wu, F., Raushel, F.M., 2001b. Enhancement, relaxation, and reversal of the stereoselectivity for phosphotriesterase by rational evolution of active site residues. Biochemistry 40, 1332-1339.

Cho, C.M., Mulchandani, A., Chen, W., 2002. Bacterial cell surface display of organophosphorus hydrolase for selective screening of improved hydrolysis of organophosphate nerve agents. Appl. Environ. Microbiol. 68, 2026-2030.

Crameri, A., Raillard, S., Bermudez, E., Stemmer, W.P.C., 1998. DNA shuffling of a family of genes from diverse species accelerates directed evolution. Nature 391, 288-291.

Dave, K.I., Miller, C.E., Wild, J.R., 1993. Characterization of organophosphorus hydrolases and the genetic manipulation of the phosphotriesterase from *P. diminuta*. Chem. Biol. Interact. 87, 55-68.

DeLisa, M.P., Samuelson, P., Palmer, T., Georgiou, G., 2002. Genetic analysis of the twin arginine translocator secretion pathway in Bacteria. J. Biol. Chem. 277, 29825-29831.

Di Sioudi, B.D., Miller, C.E., Lai, K., Grimsley, J.K., Wild, J.R., 1999. Rational design of organophosphorus hydrolase for altered substrate specificities. Chem. Biol. Interact. 119-120, 211-223.

Dodt, J., Schmitz, T., Schafer, T., Bergmann, C., 1986. Expression, secretion and processing of hirudin in *E. coli* using the alkaline phosphatase signal sequence. FEBS Lett. 202, 373-377.

Donarski, W.J., Dumas, D.P., Heitmeyer, D.P., Lewis, V.E., Raushel, F.M., 1989. Strucure-activity relationships in the hydrolysis of substrates by the phosphotriesterase from *Pseudomonas diminuta.* Biochemistry 28, 4650-4655.

Dumas, D.P., Caldwell, S.R., Wild, J.R., Raushel, F.M., 1989. Purification and properties of the phosphotriesterase from *Pseudomonas diminuta*. J. Biol. Chem. 264, 19659-19665.

Dumas, D.P., Wild, J.R., Raushel, F.M., 1990a. Expression of *Pseudomonas* phosphotriesterase activity in the Fall Armyworm confers resistance to insecticides. Experientia 46, 729-731.

Dumas, D.P., Durst, H.D., Landis, W.G., Raushel, F.M., Wild, J.R., 1990b. Inactivation of organophosphorus nerve agents by the phosphotriesterase from *Pseudomonas diminuta.* Arch. Biochem. Biophys. 277, 155-159.

Ecobichon, D.J., 2001. Toxic effects of pesticides. In: Casarett & Doull's Toxicology: The Basic Science of Poisons, 6th ed. C.D. Klaassen (McGraw-Hill, New York, 2001) pp. 763-810.

Forney, L.J., Wong, D.C.L., Ferber, D.M., 1989. Selection of amidases with novel substrate specificities from penicillin amidase of *Escherichia coli.* Appl. Environ. Microbiol. 55, 2550-2555

Gerlt, J.A., Whitman, G.J.R., 1975. Purification and properties of a phosphohydrolase from *Enterobacter aerogenes*. J. Biol. Chem. 250, 5053-5058.

Gill, I., Ballesteros, A., 2000. Degradation of organophosphorous nerve agents by enzyme-polymer nanocomposites: efficient biocatalytic materials for personal protection and large-scale detoxification. Biotechnol. Bioeng. 70, 400-410.

Griffiths, A.D., Tawfik, D.S., 2003. Directed evolution of and extremely fast phosphotriesterase by *in vitro* compartmentalization. EMBO J. 22, 24-35.

Hartleib, J., Rüterjans, H., 2001. Insights into the reaction mechanism of the diisopropyl fluorophosphatase from *Loligo vulgaris* by means of kinetic studies, chemical modification and site-directed mutagenesis. Biochim. Biophys. Acta. 1546, 312-324.

Hill, C.M., Wu, F., Cheng, T.C., DeFrank, J.J., Raushel, F.M., 2000. Substrate and stereochemical specificity of the organophosphorus acid anhydrolase from

Alteromonas sp. JD6.5 toward p-nitrophenyl phosphotriesters. Bioorg. Med. Chem. Lett. 10, 1285-1288.

Hill, C.M., Li, W.S., Cheng, T.C., DeFrank, J.J., Raushel, F.M., 2001. Stereochemical specificity of organophosphorus acid anhydrolase toward *p*-nitrophenyl analogs of soman and sarin. Bioorg. Chem. 29, 27-35.

Hill, C.M., Li, W.S., Thoden, J.B., Holden, H.M., Raushel, F.M., 2003. Enhanced degredation of chemical warfare agents through molecular engineering of the phosphotriesterase active site. J. Am. Chem. Soc.125, 8990-8991.

Holm, L., Sander, C., 1997. An evloutionary treasure: unification of a broad set of amidohydrolases related to urease. Proteins 28, 72-78.

Hong, S.B., Raushel, F.M., 1996. Metal-substrate interactions facilitate the catalytic activity of the bacterial phosphotriesterase. Biochemistry 35, 10904-10912.

Hong, S.B., Raushel, F.M., 1999a. Stereochemical constraints on the substrate specificity of phosphotriesterase. Biochemistry 38, 1159-1165.

Hong, S.B., Raushel, F.M., 1999b. Stereochemical preference for chiral substrates by the bacterial phosphotriesterase. Chem. Biol. Interact. 119-120, 225-234.

Horne, I., Sutherland, T.D., Harcourt, R.L., Russell, R.J., Oakeshott, J.G., 2002. Identification of an *opd* (organophosphate degradation) gene in an *Agrobacterium* isolate. Appl. Environ. Microbiol. 68, 3371-3376.

Jabri, E., Carr, M.B., Hausinger, R.P., Karplus, P.A., 1995. The crystal structure of urease from *Klibsiella aerogenes*. Science 268, 998-1004.

Jao, S.C., Huang, L.F., Tao, Y.C., Li, W.S., 2004. Hydrolysis of organophosphate triesters by *Escherichia coli* aminopeptidase P. J. Mol. Catal. B Enzym. 27, 7-12.

Kaliste-Korhonen, E., Ylitalo, P., Hanninen, O., Raushel, F.M., 1993. Phosphotriesterase decreases paraoxon toxicity in mice. Toxicol. Appl. Pharmacol. 121, 275-278.

Kang, D.G., Choi, S.S., Cha, H.J., 2006. Enhanced biodegradation of toxic organophosphate compounds using recombinant *E. coli* with Sec pathway-driven periplasmic secretion organophosphorus hydrolase. Biotechnol. Prog. 22, 406-410.

Koca, J., Zhan, C.G., Rittenhouse, R.C., Ornstein, R.L., 2001. Mobility of the active site bound paraoxon and sarin in zinc-phosphotriesterase by molecular dynamics simulation and quantum chemical calculation. J. Am. Chem. Soc. 123, 817- 826.

Kolakowski, J.E., DeFrank, J.J., Harvey, S.P., Szafraniec, L.L., Beaudry, W.T., Lai, K., Wild, J.R., 1997. Enzymatic hydrolysis of the chemical warfare agent VX and its neurotoxic analogues by organophosphorus hydrolase. Biocatalysis Biotransform. 15, 297-312.

Larson, T.J., Ehrmann, M., Boos, W., 1983. Periplasmic glycerophosphodiester phosphodiesterase of *E. coli*, a new enzyme of the *glp* regulon. J. Biol. Chem. 258, 5428-5432.

Liebeton, K., Zonta, A., Schimossek, K., Nardini, M., Lang, D., Dijkstra, B.W., Reetz, M.T., Jaeger, K., 2000. Directed evolution of an enantioselective lipase. Chem. Biol. 7, 709-718.

LeJeune, K.E., Russell, A.J., 1999. Biocatalytic nerve agent detoxification in fire fighting foams. Biotechnol. Bioeng. 62, 659-665.

Lewis,V.E., Donarski, W.J., Wild, J.R., Raushel, F.M., 1988. Mechanism and stereochemical course at phosphorus of the reaction catalyzed by a bacterial phosphotriesterase. Biochemistry 27, 1591-1597.

Li, W.S., Lum, K.T., Chen-Goodspeed, M., Sogorb, M.A., Raushel, F.M., 2001. Stereoselective detoxification of chiral sarin and soman analogues by phosphotriesterase. Bioorg. Med. Chem. 9, 2083-2091.

Lum, K.T., 2004. Ph.D. dissertation, Directed evolution of phosphotriesterase: towards the efficient detoxification of sarin and soman. Department of Chemistry, Texas A& M University.

Lum, K.T., Huebner, H.J., Li, Y., Phillips, T.D., Raushel, F.M., 2003. Organophosphate nerve ngent toxicity in *Hydra attenuata*. Chem. Res. Toxicol. 16, 953-957.

McLoughlin, S.Y., Jackson, C., Liu, J.W., Ollis, D.L., 2004. Growth of *E. coli* coexpressing phosphotriesterase and glycerophosphodiester phosphodiesterase, using paraoxon as the sole phosphorus source. Appl. Environ. Mirobiol. 70, 404-412.

Millard, C.B., Kryger, G., Ordentlich, A., Greenblatt, H.M., Harel, M., Raves, M.L., Segall, Y., Barak, D., Shafferman, A., Silman, I., Sussman, J.L., 1999. Crystal structures of aged phosphorylated acetylcholinesterase: Nerve agent reaction product at the atmoic level. Biochemistry 38, 7032-7039.

Mulbry, W.W., Karns, J., 1989. Purification and characterization of three parathion hydrolases from Gram-negative bacterial strains. Appl. Environ. Microbiol. 55, 289-293.

Mulchandani, P., Mulchandani, A., Kaneva, I., Chen, W., 1999a. Biosensor for direct determination of organophosphate nerve agents. 1. Potentiometric enzyme electrode. Biosens. Bioelectron. 14, 77-85.

Mulchandani, A., Pan, S., Chen,W., 1999b. Fiber-optic enzyme biosensor for direct determination of organophosphate nerver agents. Biotechnol. Prog. 15, 130-134.

Mulchandani, A., Mulchandani, P., 1999c. Amperometric thick-film strip electrodes for monitoring organophosphate nerve agents based on immobilized organophosphorus hydrolase. Anal. Chem. 71, 2246-2249.

Mulchandani, P., Chen, W., Mulchandani, A., Wang J., Chen, L., 2001. Amperometric microbial biosensor for direct determination of organophosphate pesticides using recombinant microorganism with surface expressed organophosphorus hydrolase. Biosens. Bioelectron. 16, 433-437.

Neidhardt, F.C., Bloch, P.L., Smith, D.F., 1974. Culture medium for *Enterobacter*. J. Bacteriol. 119,736-747.

Omburo, G.A., Kuo, J.M., Mullins, L.S., Raushel, F.M., 1992. Characterization of the zinc binding site of bacterial phosphotriesterase. J. Biol. Chem. 267, 13278-13283.

Pei, L., Omburo, G. McGuinn, W.D., Petrikovics, I., Dave, K., Raushel, F.M., Wild, J.R., DeLoach, J.R., Way, J.L., 1994. Encapsulation of phosphotriesterase within murine erythrocytes. Toxicol. Appl. Pharmacol. 124, 296-301.

Petrikovics, I., Hong, K., Omburo, G., Hu, Q.Z., McGuinn, W.D., Sylvester, D., Tamulinas, C., Papahadjopouls, D., Jaszberenyi, J.C., Way, J.L., 1999. Antagonism of paraoxon intoxication by recombinant phosphotriesterase encapsulated within sterically stabilized liposomes. Toxicol. Appl. Pharmacol. 156, 56- 63.

Rainina, E.I., Efremenco E.N., Varfolomeyev, S.D., Simonian, A.L., Wild, J.R., 1996. The development of a new biosensor based on recombinant *E. coli* for the direct detection of organophosphorus neurotoxins. Biosens. Bioelectron. 11, 991-1000.

Raushel, F.M., Holden, H.M., 2000. Phosphotriesterase: An enzyme in search for its natural substrate. Adv. Enzymol. Relat. Areas Mol. Biol.74, 51-93.

Raveh, L., Grauer, E., Grunwald, J., Cohen, E., Ashani, Y., 1997. The stoichiometry of protection against soman and VX toxicity in monkeys pretreated with human butyrylcholinesterase. Toxicol. Appl. Pharmacol. 145, 43-53.

Richter, W., 2002. 3',5'-cyclic nucleotide phosphodiesterases class III: members, structure, and catalytic mechanism. Proteins 46, 278-286.

Roger, K.R., Wang, Y., Mulchandani, A., Mulchandani, P., Chen, W., 1999. Organophosphorus hydrolase-based fluorescence assay for organophosphate pesticides. Biotechnol. Prog. 15, 517-522.

Saxena, A., Maxwell, D.M., Quinn, D.M., Radic, Z., Taylor, P., Doctor, B.P., 1997.

Mutant acetylcholinesterase as potential detoxification agents for organophosphate poisoning. Biochem. Pharmcol. 54, 269-274.

Scharff, E.I., Lucke, C., Fritzsch, G., Koepke, J., Hartleib, J., Dierl, S., Ruterjans, H., 2001. Crystal structure of diisopropylfluorophosphatase from *Loligo vulgaris.* Structure 9, 493-502.

Schrader, G., 1950. Organische phosphor-verbindungen als neuartige insektizide (auszug). Angew. Chem. 62, 471-473.B

Shenoy, A.R., Sreenath, N., Podobnik, M., Kovačevič, M., Visweswariah, S.S., 2005. The Rv0805 gene from *Mycobacterium tuberculosis* encodes a 3',5'-cyclic nucleotide phosphodiesterase: biochemical and mutational analysis. Biochemistry 44, 15695-15704.

Sio, C.F., Riemens, A.M., Laan, J., Verhaert, R.M., Quax, W., 2002. Directed evolution of a glutaryl acylase into an adipyl acylase. Eur. J. Biochem. 269, 4495-4504.

Soumillion, P., Fastrez, J., 2001. Novel concepts for selection of catalytic activity. Curr. Opin. Biotechnol. 12, 387-394.

Stemmer, W.P.C., 1994. DNA shuffling by random fragmentation and reassembly: *in vitro* recombination for molecular evolution. Proc. Natl. Acad. Sci. 91, 10747-10751.

Tehara, S.K., Keasling, J.D., 2003. Gene cloning, purification and characterization of a phosphodiesterase from *Delftia acidovorans*. Appl. Environ. Microbiol. 69, 504-508.

Thoden, J.B., Phillips, G.N., Neal, T.M., Raushel, F.M., Holden, H.M., 2001. Molecular structure of dihydroorotase: A paradigm for catalysis through the use of a binuclear metal center. Biochemistry 40, 6989-6997.

Tuovinen, K., Kaliste-Korhonen, E., Raushel, F.M., Hanninen, O., 1994. Phosphotriesterase: a promising candidate for use in detoxification of organophosphates. Fundam. Appl. Toxicol. 23, 578-584.

Tuovinen, K., Kaliste-Korhonen, E., Raushel, F.M., Hanninen, O., 1996a. Protection of organophosphate-inactivated esterases with phosphotriesterase. Fundam. Appl. Toxicol. 31, 210-217.

Tuovinen, K., Kaliste-Korhonen, E., Raushel, F.M., Hanninen, O., 1996b. Eptastigmine-Phosphotriesterase combination in DFP intoxication. Toxicol. Appl. Pharmacol. 140, 364-369.

Tuovinen, K., Kaliste-Korhonen, E., Raushel, F.M., Hanninen, O., 1996c. Phosphotriesterase, pralidoxime-2-chloride (2-PAM), and eptastigmine treatments and their combinations in DFP intoxication. Toxicol. Appl. Pharmacol. 141, 555-560.

Tuovinen, K., Kaliste-Korhonen, E., Raushel, F.M., Hanninen, O., 1999. Success of pyridostigmine, physostigmine, eptastigmine and phosphotriesterase treatments in acute sarin intoxication. Toxicology 134, 169-178.

Vanhooke, J.L., Benning, M.M., Raushel, F.M., Holden, H.M., 1996. Three-dimensional structure of the zinc-containing phosphotriesterase with the bound substrate analog diethyl 4-methylbenzylphosphonate. Biochemistry 35, 6020-6025.

Vogel, A., Schilling, O., Niecke, M., Bettmer, J., 2002. *ElaC* encodes a novel binuclear zinc phosphodiesterase. J. Biol. Chem. 277, 29078-29085.

Wanner, B.L., 1994. Molecular genetics of carbon-phosphorus bond cleavage in bacteria. Biodegradation 5, 175-184.

Wilce, M.C.J., Bond, C.S., Dixon, N.E., Freeman, H.C., Guss, J. M., Lilley, P.E., Wilce, J.A., 1998. Structure and mechanism of a proline-specific aminopeptidase from *Escherichia coli.* Proc. Natl. Acad. Sci. USA 95, 3472-3477.

Wu, F., Li, W.S., Chen-Goodspeed, M., Sogorb, M.A., Raushel, F.M., 2000. Rationally engineered mutants of phosphotriesterase for preparative scale isolation of chiral organophosphates. J. Am. Chem. Soc. 122, 10206-10207.

Yano, T., 1998. Directed evolution of an aspartate aminotransferase with new substrate specificity. Proc. Natl. Acad. Sci. 95, 5511-5515.

Zhang, Y.X., Perry, K., Vinci, V.A., Powell, K., Stemmer, W.P.C., Cardayré, S.P., 2002. Genome shuffling leads to rapid phenotypic improvement in bacteria. Nature 415, 644-646.

VITA

Name:	Eman Mohamed Ghanem
Address:	7924 Telegraph Rd. Bloomington, MN 55438
Email Address:	eman_ghanem@yahoo.com
Education:	B.S., Biochemistry & Nutrition, Ain Shams University, 1994 M.S., Chemistry, Eastern Illinois University, 1999 Ph.D. Chemistry, Texas A&M University, 2006